A Photoswitchable Ru *cis*-Dihydride Catalyst Accessed through Atypical Metal-Ligand Cooperative H_2 Activation: Photo-Enhanced Acceptorless Alcohol Dehydrogenation

Paul M. Fanara†, Vipulan Vigneswaran†, Parami S. Gunasekera†, Samantha N. MacMillan‡, and David C. Lacy†*

†Department of Chemistry, University at Buffalo, State University of New York; Buffalo, New York 14260, United States

‡Department of Chemistry and Chemical Biology, Cornell University; Ithaca, New York 14853, United States.

ABSTRACT: Dehydrohalogenation of pyridine-derived pincer ruthenium complexes often lead to dearomatized moieties, such as in Milstein's PNN-Ru(CO)(Cl)(H) (**1Py**) catalyst. Thus, we were surprised to find an aromatized κ^3-*N,C,P* binding mode in the lutidine-derived bidentate analog [{LutP`}Ru(CO)(H)(PPh_3)] (**2**), instead of a dearomatized compound, upon dehydrohalogenation of [{LutP}Ru(CO)(Cl)(H)(PPh_3)] (**1**). The reaction of **2** with H_2 results in formation of a *cis*-dihydride [{LutP}Ru(CO)($H)_2$(PPh_3)] (**3**) and labeling studies confirm cooperative metal-ligand activation. **3** exhibits reversible photochemistry, forming another *cis*-dihydride isomer (**4**). The lability of **4** toward ligand substitution was leveraged to demonstrate a unique example of photoswitchable H_2 production *via* acceptorless alcohol dehydrogenation. Labeling studies implicate metal-ligand cooperative (MLC) processes during the photocatalytic reaction, but they appear to be off-path processes based on our mechanistic study of the system. The latter emphasizes that aromatization/dearomatization may not be necessary for acceptorless transformations, which is generally consistent with several contemporary studies on analogous Ru catalysts.

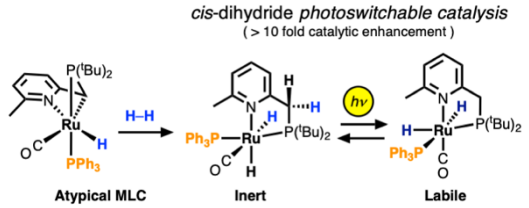

INTRODUCTION

Transition metal hydrides (TMH) have rich photochemical properties.[1] In some cases, these enable photo-assisted catalysis. Examples of these key properties include light-induced M–H homolysis,[2] reductive elimination of H_2 from *cis*-dihydrides,[3] altered chemical properties (e.g., pK_a, hydricity, etc.),[4] and photoisomerization (e.g., photoswitch).[5] When these processes are chemically reversible, it benefits the system in several ways, one of which is preventing the formation of off-path photogenerated thermodynamic sinks. However, designing reversibility into a TMH photocatalyst is not always predictable or straightforward. Phenomenologically, the *cis*-dihydride motif is best suited to this end because they tend to exhibit said properties.[1]

During the course of our studies,[6] we discovered a Ru alcohol dehydrogenation precatalyst (**1**) with a nominally on-path *cis*-dihydride complex (**3**) exhibiting reversible photochemical reactivity. The *cis*-motif was accessed through an atypical mode of metal-ligand cooperative H_2 activation by the key intermediate (**2**) that has unusual coordination chemistry that adds to the developing story of aromatization/dearomatization metal-ligand cooperativity (MLC) in catalytic cycles (Figure 1).[7,8,9] Furthermore, the reversible photochemistry from **3** enabled photoswitchable H_2 production from various alcohols using very mild reagents and conditions (r.t., $\lambda > 345$ nm). The mechanism and catalysis is a unique example of a photoswitchable H_2 generation strategy with demonstrated application in the important area of acceptorless MLC alcohol dehydrogenation.[10–13]

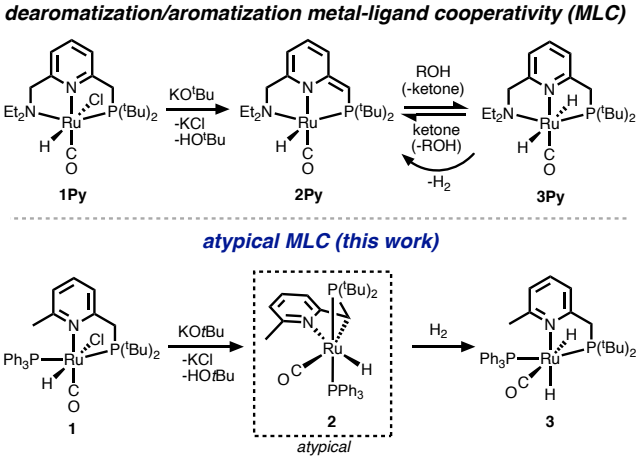

Figure 1. (top) Conventional metal-ligand cooperativity (MLC) with non-Noyori type pyridine-based Ru(II) catalysts. (bottom) Atypical MLC described in this study.

RESULTS AND DISCUSSION

In an earlier report detailing the synthesis and characterization of [{LutP}Ru(CO)(H)(Cl)(PPh_3)] (**1**), we briefly investigated its reaction with KO*t*Bu and initially hypothesized a prototypical dearomatized bidentate binding mode for the product **2b** analogous to **2Py** (Scheme 1).[6] However, the product exhibited unusual sensitivity to water and we did not pursue it further at the time. Since this initial study, we discovered that activation of **1** with 1 eq. K[$N(SiMe_3)_2$] in cold (-35 °C) and very dry

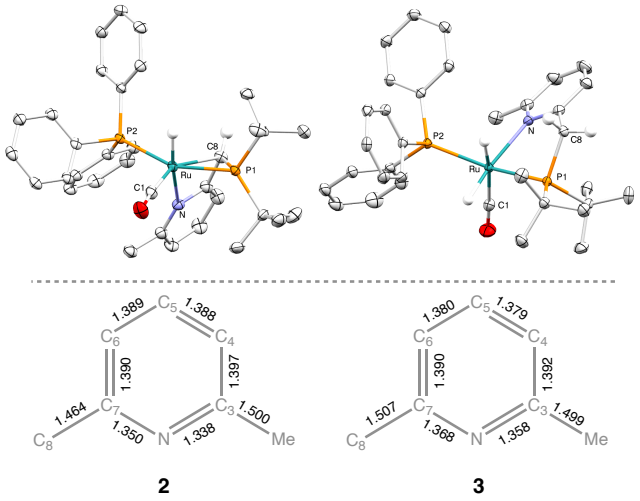

2 **3**

Figure 2. XRD molecular structure of **2** (left) and **3** (right) with ellipsoids 50% probability. Except for the RuH and methine/methylene CH atoms, hydrogen atoms have been removed for clarity. Selected bond distances (Å) and angles (°) for **2**: Ru–N = 2.196(2); Ru–C8 = 2.309(2); Ru–P1 = 2.2684(6); Ru–P2 = 2.3419(7); Ru–C1 = 1.845(3); Ru–H = 1.53(3); C1–Ru–C2 = 150.4°; P1–Ru–P2 = 149.9°; C1–Ru–N = 61.8°. Selected bond distances (Å) and angles (°) for **3**: Ru–N = 2.277(2); Ru–P2 = 2.3133(4); Ru–P1 = 2.2960(4); Ru–C1 = 1.887(2); P1–Ru–P2 = 154.8°; C1–Ru–N = 103.4°. (bottom) distances in pyridine ring for **2** and **3**.

THF, or KO*t*Bu in very dry benzene, results in formation of a highly moisture-sensitive amber-colored species (**2**) (Figure 1) whose X-ray crystal structure contains a unique NCP κ^3-*N,C,P* binding mode (Figure 2). Importantly, the κ^3-*N,C,P* binding mode remains intact in solution as evidenced from ^{1}H-^{1}H ROESY NMR correlations and ^{1}H/^{13}C coupled HSQC NMR spectroscopy (Figures S1–S8). Analogous bindings modes and spectroscopic features have been observed in other systems,[14–17] but not for ruthenium pincer complexes with pyridine-derived ligands. Ru complexes with pyridine-derived pincer ligands have dearomatized modes such as in **2Py** (Figure 1).[18] The atypical binding mode in **2** imparted unique coordination chemistry and reactivity which we explore herein.

Scheme 1. 2b, and Reaction of 2 with Excess KO*t*Bu

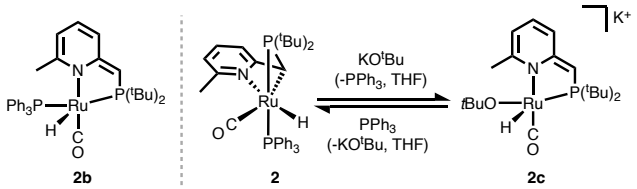

*Reaction of **2** with excess KO*t*Bu.* If excess KO*t*Bu was used to prepare **2** from **1** in THF, we noted that free PPh_3 was formed along with a new species whose ^{1}H and ^{31}P{^{1}H} NMR characterization is consistent with a LutP-bound Ru-O*t*Bu anionic complex (**2c**) (Figures S9–S10, Scheme 1). The addition of 8 equiv. of KO*t*Bu is required to achieve complete conversion to **2c** and formation of free PPh_3. The ligand substitution is reversible and solvent dependent, as removal of THF from **2c** reforms **2** in essentially quantitative yield. The nature of the [Ru-O*t*Bu]$^-$ complex (**2c**) is not explored in detail here and has not been isolated or fully characterized as of yet, but the lability of PPh_3 is an important factor in the catalysis described later.

*Reaction of **2** with H_2.* The unusual binding mode of **2** was of interest to us as we hypothesized that the Ru–C bond would be highly reactive toward H_2 and H_2 donors such as 2-propanol. Indeed, when a benzene solution of **2** was exposed to an atmosphere of H_2, an immediate color change from amber to light yellow occurred and NMR analysis demonstrated a *cis*-dihydride, **3**, quantitatively formed (Scheme 2). Similarly, **2** reacts quantitatively with 2-propanol to form **3** and equimolar acetone. X-ray crystallographic characterization revealed the *cis*-dihydride motif and 2D NMR and ^{1}H-^{1}H ROESY spectroscopic characterization confirms its solution-state structure is identical (Figures S11–S15). Subjecting **3** to vacuum at elevated temperatures (60 °C) or excess acetone (r.t.) resulted in no conversion to **2**. More forcing conditions (110 °C) resulted in trace formation of **2** along with [(CO)(PPh_3)$_3$Ru(H)$_2$] and other unidentified byproducts (Figure S16).[19] This stability toward ketones and the inability to lose H_2 is in contrast to previous reports with Milstein's dihydride complex, **3Py**, which spontaneously converts to **2Py** with loss of H_2 at room temperature.[6,7,18]

Scheme 2. Reaction of 2 with H_2

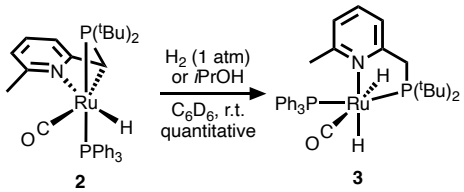

When D_2 was used to prepare **3**, deuterium incorporation occurs at both ruthenium and the ligand, consistent with an MLC activation of H_2 (Scheme 3). The mixture of isotopomers is best represented pictorially in Scheme 3 (^{2}H NMR, Fig. S17) and is generally consistent with what others have observed.[20] Notably, H_2 and HD were observed in the ^{1}H NMR spectrum when **2** was treated with D_2 indicating exchange with free dihydrogen (Figure S18). While not completely eliminated, the presence of H_2 and HD was significantly reduced when light was rigorously excluded (Figures S19–S20). As such, we hypothesized that photochemical processes are responsible.

Scheme 3. Reaction of 2 with D_2

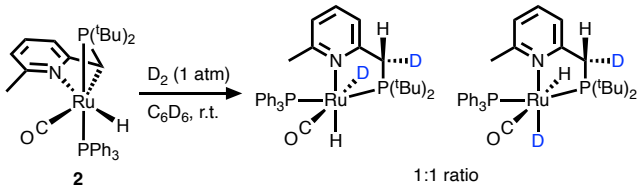

*Photochemistry of **3**.* We tested this hypothesis with broadband irradiation of **3** with a Xe arc lamp (100 W) which caused a color change of the solution to orange/red. ^{1}H NMR reveals a new dihydride species (**4**) that slowly coverts back to **3** in a few hours (Scheme 4). The ^{1}H NMR spectrum of **4** contains two hydride resonances at -5.13 ppm (dd, J = 101, 25 Hz) and -6.09 (dd, J = 92, 17 Hz), consistent with a phosphine *trans* and *cis* to each hydride (Figure S25). The ^{31}P{^{1}H} NMR spectrum indicates a *cis* conformation of the P*t*Bu$_2$ and PPh_3 ligands, as the resonances at 77.3 ppm and 42.7 ppm are doublets with J_{PP} = 10 Hz and 11 Hz, respectively (Figure S26). A ^{1}H-^{1}H ROESY NMR of **4** shows exchange coupling between the two hydride resonances. Additionally, the hydride resonance at -6.09 ppm has a through-space coupling to one of the P*t*Bu$_2$ resonances at 1.30 ppm. Meanwhile the hydride resonance at -5.13 ppm has through-space coupling to the PPh_3 and methyl resonances at 7.72 ppm and 2.56 ppm, respectively (Figure S27). Together with FTIR-ATR spectroscopy (Figure S28), the NMR data

enables confident assignment of the structure of **4** as shown in Scheme 4.

The stability of **4** was monitored with ^{1}H NMR spectroscopy and it quantitatively decayed with $t_{1/2}$ = 1.90 ± 0.04 h (r.t.) back to **3** under N_2 (Figures S21–S22). The decay was unaffected by static vacuum $t_{1/2}$ = 1.80 ± 0.14 h (r.t.) (Figures S23–S24). When the photolysis of **3** was carried out under an atmosphere of H_2, the same process occurred, except that the decay of **4** to **3** was slower ($t_{1/2}$ = 3.38 ± 0.08 h) (Figures S29–S30). Additionally, when excess (10 eq) PPh_3 was added to **3** prior to irradiation, no reaction occurred by ^{1}H and ^{31}P {^{1}H} NMR. After a 2 h irradiation, **3** and **4** are the major products along with byproducts [(CO)(PPh_3)$_3$Ru(H)$_2$] (**6**), [(PPh_3)$_3$Ru(H)$_4$], **8** (*vide infra*), free ligand, and other unidentified species (Figure S36) (Scheme 5). This result will be discussed later in the context of catalysis.

Scheme 4. Reversible Photochemistry of 3

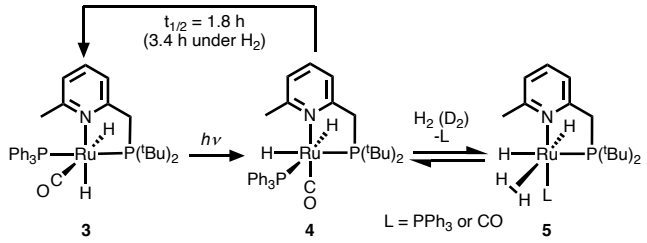

Scheme 5. Summary of Decomposition Reactions of 4

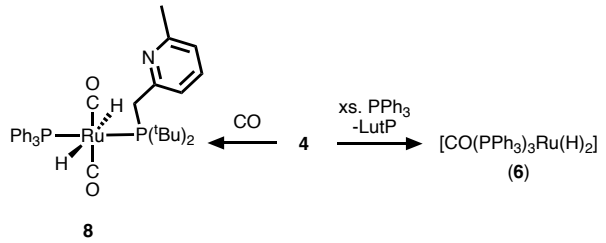

The photoisomerization of **3** into **4** is unaffected by vacuum, so the conversion must be a direct photoisomerization. We can also use the results described above to determine the mechanism of isomerization of **4** back into **3**. Several possibilities include a trigonal "twist", dissociation of CO or PPh_3 (or other ligand), or elimination of H_2. We rule out CO loss and elimination of H_2 because the rate of isomerization is unaltered when the irradiation and isomerization is performed under static vacuum. In addition, when CO is included in irradiations of **3**, **4** does not form and instead a carbonylated product **8** is formed (Scheme 5, Figure S49-S51); since we do not see this byproduct in conversions between **3** and **4**, the process unlikely involves CO photolysis/dissociation. For the same reasons, the loss of PPh_3 is unlikely since (*i*) free phosphine is not observed and (*ii*) addition of free phosphine gave other byproducts for an otherwise clean conversion of **4** to **3**. As such, we propose the isomerization is a unimolecular trigonal "twist", but other isomerization mechanisms are plausible.[21]

Exchange of H_2 with the hydrides of 4. Irradiation of a sample of **3** under an atmosphere of D_2 results in the hydride resonances washing out in the ^{1}H NMR spectrum and reappearance in the ^{2}H NMR spectrum. D-incorporation into the ligand was *not* observed (Figures S31–S32). These results suggest an exchange is taking place between the hydrides of **4** and free D_2. A ^{1}H-^{1}H ROESY NMR spectrum of **4** under H_2 confirms the exchange between both hydride resonances and free H_2 (Figure S27). Variable temperature NMR and line broadening analysis furnished activation parameters of $\Delta H^{\ddagger}$ = 24.0 ± 1.2 kcal·mol^{-1} and $\Delta S^{\ddagger}$ = 22.9 ± 3.4 cal·K^{-1}·mol^{-1} (Figures S34–S35), consistent with a ligand interchange substitution between H_2 and PPh_3 to form proposed complex **5** (Scheme 4).

The proposed presence of **5** explains two important observations. First, the appearance of both HD and H_2 when **3** or **2** was treated with D_2 and exposed to light cannot be easily explained without the presence of a tetra- or tri-hydride intermediate, which are known to mediate the H_2 isotope exchange reaction.[22] Secondly, it also explains how the isomerization of **4** to **3**, although not affected by vacuum, is slowed by the presence of H_2: the off-path equilibrium between **4** and H_2 allows for this to happen. We propose that the reaction is a ligand substitution between **4** and H_2 *via* interchange because the broadening in the NMR spectrum is uniquely from the peaks associated with **4** and H_2; although a dissociation mechanism is possible. The dissociating ligand is likely PPh_3 or CO. Since we see some of the carbonylated byproduct **8** during these experiments, CO is a likely candidate.

We suspect there also a thermal reaction between H_2 and **3** because if **3** and D_2 are left to stand in the dark for several days, the hydride resonances eventually wash out and reappear in the ^{2}H spectrum (Figure S33). The ligand exchange between **4** and H_2 is rapid (as evidenced from the line broadening) compared to the ligand exchange between **3** and H_2. This enhanced lability of **4** is important for enabling the photoswitchable catalysis.

Photoswitchable catalysis. Our previous investigation with **1** involved testing different ligand variants in alcohol dehydrogenation.[6] In that case, and also most others,[13] catalytic behavior was not achieved unless reactions are carried out at elevated temperatures. However, we intuited that complexes like **3** having reversible photochemistry might be amenable to r.t. photocatalytic alcohol dehydrogenation akin to what has been observed in certain cases.[23] We tested several simple alcohols using **3** with irradiation from a Xe arc lamp (100 W, 345 nm cutoff filter) and achieved catalytic turnover at r.t. (Figure 3). Under the same conditions but with the exclusion of light, only substoichiometric H_2 was formed (e.g., 27% H_2 relative to **3** from 2-propanol; Table 1 Entry 5). A larger scale photolysis reaction was conducted open to a bubbler and resulted in comparable conversions to the closed system.

As noted, [CO(PPh_3)$_3$Ru^{II}(H)$_2$] (**6**) was observed as a product when **3** was irradiated in the presence of free PPh_3, and since **6** is a known alcohol dehydrogenation catalyst,[24] we performed a control reaction but found that it was not the active catalyst. Namely, a control reaction with **6** gave 10% H_2 in the dark, and

Table 1. Results of photocatalysis.

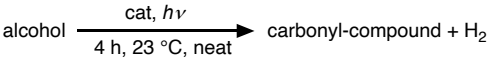

entry	alcohol	cat	product	H_2 relative to cat[a] (after 12 h)
1	MeOH	**3**	H_2CO[b]	270% (400%)
2	EtOH	**3**	ethyl acetate	640% (1000%)
3	1PhEtOH	**3**	acetophenone	640% (1100%)
4	*i*PrOH	**3**	acetone	300% (510%)
5	*i*PrOH	**3**[(c)]	acetone	27%
6	*i*PrOH	**1**	acetone	78%
7	*i*PrOH	**6**	acetone	33%
8	*i*PrOH	**7**	acetone	28%

Conditions: 2 mL of alcohol, 0.02-0.04 mol% catalyst, 200 µL benzene, under N_2, irradiation with a Xe-arc lamp (100 W) with a 345 nm cutoff filter for 4 h. Yield of H_2 was determined by GC. (a) average of three runs. (b) trace CO observed. (c) dark. **6** = [CO(PPh_3)$_3$Ru^{II}(H)$_2$]; **7** = [(Cl)(CO)(PPh_3)$_3$Ru(H)]. 1PhEtOH = 1-phenylethanol.[25]

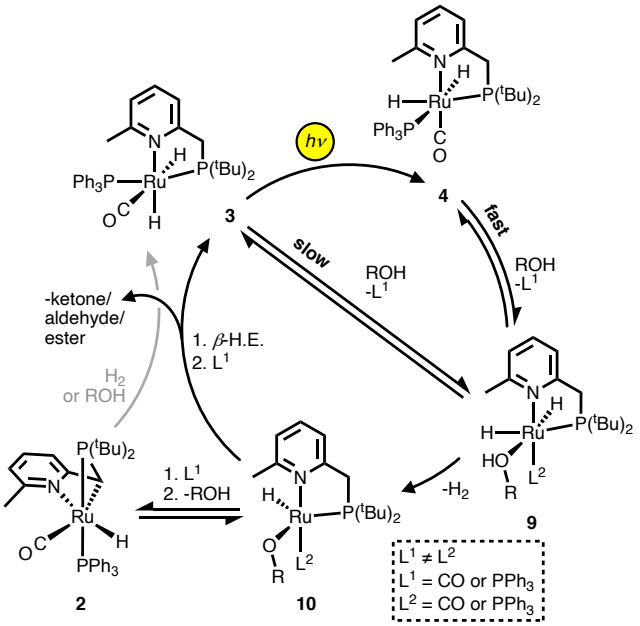

Figure 3. Proposed mechanism for photocatalysis for 2-propanol dehydrogenation. The off-path formation of **2** reforms catalyst **3** by means represented in Scheme 2 (grey).

33% when irradiated, with the hydrogen observed simply the result of the known photoelimination of H_2 from **6**.[26] This is not surprising as catalytic dehydrogenation from **6** requires high temperatures (110 °C).[24] Likewise, (Cl)(CO)(PPh_3)$_3$Ru(H) (**7**) and **1** were not catalysts.

Mechanism of photodehydrogenation. The two accepted conventional paths for acceptorless alcohol dehydrogenation are the inner sphere and outer sphere mechanisms and these have been discussed at length.[13] We recently provided a rationale for a favored inner sphere path,[6] consistent with other literature,[27] and lately it has been recognized that MLC steps need not be invoked.[7] In addition the experimental results described herein, these factors influenced our mechanistic scheme (Figure 3). We recognize that the outer sphere path is also possible, but it is not discussed further.

Except for MeOH, post-irradiated solutions contain **3** and **4** as the major species indicating their overall stability in the catalytic system (Figure S48); the carbonylated byproduct **8** is a minor component (tentative structure shown in Scheme 5, Figure S49-51). We propose that the first step is the reversible photo-induced isomerization of **3** to **4**. The salient component of the mechanism is the enhanced lability of PPh_3 and/or CO in **4** because the of *trans*-effect of the hydride ligand and/or steric crowding from the *cis*-diphosphine motif. The lability enhancement allows for alcohol coordination and subsequent liberation of H_2 from proposed intermediate **9**. Loss of H_2 from **9** forms the proposed coordinatively unsaturated species **10**, which is predisposed to undergo beta-hydride elimination and ligand recoordination reforming **3**; thus, the dehydrogenation is an inner sphere mechanism and no MLC steps are necessary.

We strongly suspect that the role of light in photocatalysis is only to generate **4**, and not some other process. This supposition comes from our observation that the wavelength requirements for photocatalysis are the same as those required for isomerization (Fig. S46-47). It is tempting to consider a photo elimination of H_2 from **3** or **4**, but the isomerization of **4** back to **3** is unaffected when the entire experiment is conducted under static vacuum.

When **3** was irradiated in C_6D_6 in the presence of d_8-isopropanol, deuteration occurred on the ligand (Figures S44–S45). This would seem to indicate an MLC step in the photocatalysis. However, to explain this observation, we propose that **9** or **10** may react to form **2** (or species like it), which undergoes MLC activation of alcohol in an off-path step. Hence, the MLC chemistry observed here is not likely important for turnover, as depicted in Figure 3.

Finally, we found that sub-stoichiometric H_2 formed when light was excluded in reactions between **3** and 2-propanol, indicating thermal pathways are also possible when the net reaction is favored. In fact, carrying out the photolysis at elevated temperature improves the yields of H_2 from isopropanol (450% at 40 °C compared to 300% at 23 °C). All of these steps are consistent with the mechanism in Figure 3.[6]

Extension to other systems. The catalytic conversions are low compared to photocatalytic alcohol dehydrogenation with Wilkinson's catalyst and other photocatalytic systems,[23] but the conditions we used (r.t., neat alcohol, $\lambda > 345$ nm) are very mild. A notable example of mild photochemical alcohol dehydrogenation uses a platinum(II) diphosphite complex at r.t. and with visible light $\lambda = 410$ nm, but requires a biphasic H_2O and CH_2Cl_2 conditions and a phase transfer reagent.[29] Conventional acceptorless alcohol dehydrogenation uses high temperatures[10,13] or photosensitizers.[28] Hence, achieving unsensitized photocatalysis H_2 production (i.e. single component systems)[29–33] at low temperatures is desirable and one possible means is to take advantage of photoswitchable *cis*-dihydrides and we wondered if this could be extended to other systems.

We considered that Ru-MACHO, which is a known effective alcohol dehydrogenation catalysts at low temperatures,[34,35] might have photo-enhanced r.t. catalysis. Testing this hypothesis indicates that it does not. Specifically, Ru-MACHO (Ph substituted) exhibited TON = 6 (4 h), with or without light, for 2-propanol dehydrogenation in 4 h. This is in contrast to the work with **3**, which is very slow at r.t. in the dark (TON ≈0.3, 4 h, Table 1 Entry 4) compared to when irradiated to generate its more labile isomer **4** (TON = 3, 4 h, Table 1 Entry 5), effectively demonstrating the photoswitchable nature of the system.

We also tested Milstein's Ru-PNN *trans*-dihydride **3Py** and obtained TON = 1-3 with or without light, but **3Py** is known to spontaneously lose H_2 when standing in solution at r.t.,[7] and we found that even the chlorido precursor to **3Py** (i.e. **1Py**) produces hydrogen when irradiated in anhydrous benzene, so the comparison is rather inconclusive.[36] We also note that irradiation of Ru-MACHO and **3Py** with broad band light resulted in solutions containing a multitude of hydride resonances in the ^{1}H NMR spectrum and speciation by ^{31}P{^{1}H} NMR was complicated. Therefore, careful studies is necessary to infer the action of light on these systems which is outside the scope of this current study. Rather, our current studies on **3** and **4** provide a working hypothesis for future combined coordination and photochemical investigations, namely that photoisomerizations of TMH is a new photoswitch that can be used for acceptorless alcohol dehydrogenation.

CONCLUSION

Our work with **2**, having an atypical mode of MLC, provides new intermediates to consider when invoking MLC on pyridine-derived ligands. Nevertheless, our mechanistic investigation of the catalytic acceptorless alcohol dehydrogenation does not require MLC steps, consistent with a growing body of literature that has de-emphasized the importance of

aromatization/dearomatization in catalytic cycles. The atypical MLC H_2 activation resulted in the formation of a *cis*-dihydride motif in **3**, which in turn exhibited reversible light-induced isomerization, something that is potentially less likely on analogous *trans*-dihydride catalysts. The photogenerated labile compound **4** was competent to engage in catalytic r.t. alcohol dehydrogenation. Albeit, the conversions are low. Certain decomposition pathways for **4** were identified and are possible sources for the poor TON. The photo-enhanced catalysis was not observed in related Ru complexes, so we suspect that designing systems with reversible photoisomerizations (or other photochemical processes) is vital to using TMH as photoswitchable catalysts and, to our knowledge, this is the first example of photoswitchable catalysis with dihydride isomerization as the photoswitch.

ASSOCIATED CONTENT

Supporting Information. The Supporting Information is available free of charge.

AUTHOR INFORMATION

Corresponding Author

David C. Lacy Email: DCLacy@ Buffalo.edu

Notes

The authors declare no competing financial interest.

ACKNOWLEDGMENT

This work was completed using the resources of the UB Chemistry Instrument Center (CIC). Financial support was provided by the University at Buffalo (UB) and NSF CAREER award 1847933.

REFERENCES

(1) Perutz, R. N.; Procacci, B. Photochemistry of transition metal hydrides. *Chem. Rev.* **2016**, *116*, 8506-8544.

(2) Selected examples of M–H photolysis in catalysis: (a) Hoffman, N. W.; Brown, T. L. Thermal and photochemical substitution reactions of the tricarbonyl(cyclopentadienyl)hydrido compounds of tungsten and molybdenum. *Inorg. Chem.* **1978**, *17*, 613-617. (b) Yu, M. M.; Jing, H. Z.; Liu, X.; Fu, X. F. Visible-light-promoted generation of hydrogen from the hydrolysis of silanes catalyzed by rhodium(III) porphyrins. *Organometallics* **2015**, *34*, 5754-5758.

(3) Example of light-induced $M(H)_2$ reductive elimination in catalysis: Schild, D. J.; Peters, J. C. Light enhanced Fe-mediated nitrogen fixation: mechanistic insights regarding H_2 elimination, HER, and NH_3 generation. *ACS Catal.* **2019**, *9*, 4286-4295.

(4) Examples of photoinduced H_2 release from MH and acid: (a) Heyduk, A. F.; Nocera, D. G. Hydrogen produced from hydrohalic acid solutions by a two-electron mixed-valence photocatalyst. *Science* **2001**, *293*, 1639-1641. (b) Pitman, C. L.; Miller, A. J. M. Molecular photoelectrocatalysts for visible light-driven hydrogen evolution from neutral water. *ACS Catal*. **2014**, *4,* 2727-2733.

(5) Freixa, Z. Photoswitchable catalysis using organometallic complexes. *Catal. Sci. Technol.* **2020**, *10*, 3122-3139.

(6) Fanara, P. M.; MacMillan, S. N.; Lacy, D. C. Planar-locked Ru-PNN catalysts in 1-phenylethanol dehydrogenation. *Organometallics* **2020**, *39*, 3628-3644.

(7) Gusev, D. Revised mechanisms of the catalytic alcohol dehydrogenation and ester reduction with the Milstein PNN complex of ruthenium. *Organometallics* **2020**, *39*, 258-270.

(8) He, T.; Buttner, J. C.; Reynolds, E. F.; Pham, J.; Malek, J. C.; Keith, J. M.; Chianese, A. R. Dehydroalkylative activation of CNN- and PNN-pincer ruthenium catalysts for ester hydrogenation. *J. Am. Chem. Soc.* **2019**, *141*, 17404-17413.

(9) Dawe, L. N.; Karimzadeh-Younjali, M.; Dai, Z.; Khaskin, E.; Gusev, D. G. The Milstein bipyridyl PNN pincer complex of ruthenium becomes a Noyori-type catalyst under reducing conditions. *J. Am. Chem. Soc.* **2020**, *142*, 19510-19522.

(10) Sordakis, K.; Tang, C.; Vogt, L. K.; Junge, H.; Dyson, P. J.; Beller, M.; Laurenczy, G. Homogeneous catalysis for sustainable hydrogen storage in formic acid and alcohols. *Chem. Rev.* **2018**, *118*, 372-433.

(11) Gunanathan, C.; Milstein, D. Metal–ligand cooperation by aromatization–dearomatization: a new paradigm in bond activation and "green" catalysis. *Acc. Chem. Res.* **2011**, *44*, 588-602.

(12) Crabtree, R. H. Homogeneous transition metal catalysis of acceptorless dehydrogenative alcohol oxidation: applications in hydrogen storage and to heterocycle synthesis. *Chem. Rev*. **2017**, *117*, 9228-9246.

(13) (a) Trincado, M.; Banerjee, D.; Grützmacher, H. Molecular catalysts for hydrogen production from alcohols. *Energy Environ. Sci.* **2014**, *7*, 2464–2503. (b) Trincado, M.; Bösken J.; Grützmacher, H. Homogeneously catalyzed acceptorless dehydrogenation of alcohols: a progress report. *Coord. Chem. Rev.* **2021**, *443*, 213967.

(14) Buhaibeh, R.; Filippov, O. A.; Bruneau-Voisine, A.; Willot, J. Duhayon, C.; Valyaev, D. A.; Lugan, N.; Canac, Y.; Sortais, J.-B. Phosphine-NHC manganese hydrogenation catalyst exhibiting a non-classical metal-ligand cooperative H_2 activation mode. *Angew. Chem. Int. Ed.* **2019**, *58*, 6727-6731.

(15) Chakraborty, S.; Gellrich, R.; Diskin-Posner, Y.; Leitus, G.; Avram, L; Milstein, D. Manganese-catalyzed N-formylation of amines by methanol liberating H_2: a catalytic and mechanistic study. *Angew. Chem. Int. Ed.* **2017**, *56*, 4229-4233.

(16) Devillard, M.; Ehlers, A.; Siegler, M. A.; van der Vlugt, J. I. Selective carbanion–pyridine coordination of a reactive P,N ligand to Rh^{I}. *Chem. Eur. J.* **2019**, *25*, 3875-3883.

(17) Werner, H.; Werner, R. J. Basic metals. *Organomet. Chem.* **1981**, *209*, C60-C64.

(18) Zhang, J.; Leitus, G.; Ben-David, Y.; Milstein, D. Facile conversion of alcohols into esters and dihydrogen catalyzed by new ruthenium complexes. *J. Am. Chem. Soc.* **2005**, *127*, 10840-10841.

(19) At 110 °C in toluene with static vacuum free ligand, $(CO)\{PPh_3\}_3Ru^{II}(H)_2$, and **3** were observed in a nearly 1:1:1 ratio.

(20) Ben-Ari, E.; Leitus, G.; Shimon, L. J. W.; Milstein, D. Metal−ligand cooperation in C−H and H_2 activation by an electron-rich PNP Ir(I) system: facile ligand dearomatization−aromatization as key steps. *J. Am. Chem. Soc.* **2006**, *128*, 15390-15391.

(21) Meakin, P.; Muetterties, E. L.; Tebbe, F. N.; Jesson, J. P. Stereochemically nonrigid six-coordinate molecules. I. A detailed mechanistic analysis for the molecule $FeH_2[P(OC_2H_5)_3]_4$. *J. Am. Chem. Soc.* **1971**, *93*, 4701-4709.

(22) (a) Gusev, D. G.; Vymentis, A. B.; Bakhmutov, V. I. Is $RuH_4(PPh_3)_3$ in solution indeed a non-classical hydride? *Inorganica Chim. Acta* **1991**, *179*, 195-201. (b) Khalsa, G. R. K.; Kubas, G. J.; Unkefer, C. J.; van Der Sluys, L. S.; Kubat-Martin, K. A. Molecular hydrogen complexes of the transition metals. 7. Kinetics and thermodynamics of the interconversion between dihydride and dihydrogen forms of $W(CO)_3(PR_3)_2H_2$ where R = isopropyl and cyclopentyl. *J. Am. Chem. Soc.* **1990**, *112*, 3855-3860.

(23) (a) See Table 2 in: Esswein, A. J.; Nocera, D. G. Hydrogen production by molecular photocatalysis. *Chem. Rev.* **2007**, *107*, 4022–4047. (b) Morton, D.; Cole-Hamilton, D. J.; Utuk, I. D.; Paneque-Sosa, M.; Lopez-Poveda, M. Hydrogen production from ethanol catalyzed by group 8 metal complexes. *J. Chem. Soc. Dalton Trans.* **1989**, 489.

(24) (a) Lorusso, P.; Ahmad, S.; Brill, K.; Cole-Hamilton, D. J.; Sieffert, N.; Bühl, M. On the catalytic activity of $[RuH_2(PPh_3)_3(CO)]$

(PPh_3=triphenylphosphine) in ruthenium-catalysed generation of hydrogen from alcohols: a combined experimental and DFT study. *ChemCatChem* **2020**, *12*, 2995–3009. (b) Pandey, A. M.; Digrawal, N. K.; Mohanta, N.; Jamdade, A. B.; Chaudhari, M. B.; Bisht, G. S.; Gnanaprakasam, B. Catalytic acceptorless dehydrogenation of amino alcohols and 2-hydroxybenzyl alcohols for annulation reaction under neutral conditions. *J. Org. Chem.* **2021**, *86*, 8805-8828.

(25) See SI for figures and methods detailing product identification and quantification.

(26) Geoffroy, G. L.; Bradley, M. G. L. Photochemistry of transition metal hydride complexes. 2. Chlorohydro(carbonyl)tris(triphenylphosphine)ruthenium, dihydro(carbonyl)tris(triphenylphosphine)ruthenium, and chlorohydro(dicarbonyl)bis(triphenylphosphine)ruthenium. *Inorg. Chem.* **1977**, *16*, 744-748.

(27) Tseng, K.-N. T.; Kampf, J. W.; Szymczak, N. K. Mechanism of *N,N,N*-amide ruthenium(II) hydride mediated acceptorless alcohol dehydrogenation: inner-sphere β-H elimination versus outer-sphere bifunctional metal-ligand cooperativity. *ACS Catal.* **2015**, *5*, 5468-5485.

(28) Fuse, H.; Mitsunuma, H.; Kanai, M. Catalytic acceptorless dehydrogenation of aliphatic alcohols. *J. Am. Chem. Soc.* **2020**, *142*, 4493-4499.

(29) Zhong, J.-J.; To, W.-P.; Liu, Y.; Lu, W.; Che, C.-M. Efficient acceptorless photo-dehydrogenation of alcohols and *N*-heterocycles with binuclear platinum(II) diphosphite complexes. *Chem. Sci.* **2019**, *10*, 4883-4889.

(30) Brereton, K. R.; Bonn, A. G.; Miller, A. J. M. Molecular photoelectrocatalysts for light-driven hydrogen production. *ACS Energy Lett.* **2018**, *3*, 1128-1136.

(31) Wang, W.; Rauchfuss, T. B.; Bertini, L.; Zampella, G. Unsensitized photochemical hydrogen production catalyzed by diiron hydrides. *J. Am. Chem. Soc*. **2012**, *134*, 4525-4528.

(32) Whittemore, T. J.; Xue, C.; Huang, J.; Gallucci, J.C.; Turro, C. Single-chromophore single-molecule photocatalyst for the production of dihydrogen using low-energy light. *Nat. Chem.* **2020**, *12*, 180-185.

(33) Huckaba, A. J.; Shirley, H.; Lamb, R. W.; Guertin, S.; Autry, S.; Cheema, H.; Talukdar, K.; Jones, T.; Jurss, J. W.; Dass, A.; Hammer, N. I.; Schmehl, R. H.; Webster, C. E.; Delcamp, J. H. A mononuclear tungsten photocatalyst for H_2 production. *ACS Catal.* **2018**, *8*, 4838-4847.

(34) Nielsen M.; Alberico, E.; Baumann, W.; Drexler, H.-J.; Junge, H.; Gladiali, S.; Beller, M.; Low-temperature aqueous-phase methanol dehydrogenation to hydrogen and carbon dioxide. *Nature* **2013**, *495*, 85-89.

(35) (a) Oldenhuis, N. J.; Dong, V. M.; Guan, Z. Catalytic acceptorless dehydrogenations: Ru-MACHO catalyzed construction of amides and imines. *Tetrahedron* **2014**, *70*, 4213-4218. (b) Bertoli, M.; Choualeb, A.; Lough, A. J.; Moore, B.; Spasyuk, D.; Gusev, D. G. Osmium and ruthenium catalysts for dehydrogenation of alcohols. *Organometallics* **2011**, *30*, 3479-3482.

(36) Fanara, P. M. *A Study of Aromatization/Dearomatization Metal-Ligand Cooperativity with Ruthenium(II)-based PNN and PN Complexes*, Chapter 5. Ph.D. Dissertation, University at Buffalo, State University of New York, Buffalo, NY, **2021**.

Supplementary Materials for

A Photoswitchable Ru *cis*-Dihydride Catalyst Accessed through Atypical Metal-Ligand Cooperative H_2 Activation: Photo-Enhanced Acceptorless Alcohol Dehydrogenation

Paul M. Fanara, Vipulan Vigneswaran, Parami S. Gunasekera, Samantha N. MacMillan, and David C. Lacy*

Correspondence to: dclacy@Buffalo.edu

Contents **Page**

METHODS AND MATERIALS

• ***General Methods.*** Chemicals were obtained from commercial vendors unless otherwise noted. All manipulations of oxygen sensitive compounds were performed under an argon atmosphere with standard Schlenk techniques or under nitrogen in a VAC Atmosphere Genesis Glovebox. Complex **1** was prepared according to literature.[1] Ru-MACHO (Ph, chloride complex) was converted into the dihydride following literature methods.[2] **3Py** was prepared following literature methods.[3] Anhydrous organic solvents were sparged with argon and purified using a Pure Process Technology solvent purification system and were stored over 3 Å molecular sieves before use. Molecular sieves were activated at 200 °C under vacuum (< 100 mTorr) for 3-4 days prior to use. Deuterated solvents were degassed via three freeze-pump-thaw cycles and stored over sieves in a glovebox. Solvents for syntheses of and manipulations involving **2** were further dried by passing over a plug of dry basic alumina on a medium fritted glass funnel in a glovebox and used immediately. Basic alumina was dried at 200 °C under vacuum (< 100 mTorr) for 2-3 days prior to use. NMR spectra were collected on a Varian Mercury-300 MHz, Inova-400 MHz, or an Inova-500 MHz spectrometer. FTIR-ATR spectra were collected inside of a VAC Atmospheres Genesis glovebox using a Bruker Alpha IR spectrometer with the "ATR Platinum" insert adapter (diamond crystal). Headspace analysis was obtained using a PerkinElmer Clarus 580 GC. High resolution mass spectrometry of **3** was conducted in MeOH using an FTICR Bruker 12 T mass spectrometer. Headspace GC-MS analysis for MeOH dehydrogenation product identification was performed on a Thermo Scientific Q-Exactive Gas Chromatographic Orbitrap Mass Spectrometer (QE-GCMSMS) equipped with a TG-5SILMS, 30m x 0.25 mm chromatographic column from Thermo Fisher Scientific. LC-MS analysis of reaction mixtures was performed on a Thermo Fisher Q-Exactive Liquid Chromatograph Orbitrap. Tandem Mass Spectrometer (QE-LCMSMS). T_1 measurements were recorded on a Inova-400 MHz instrument using the inversion recovery method according to literature.[4] The reported T_1 (min) are the lowest T_1 observed between 298-183 K in THF-d_8 (**3**) or C_7D_8 (**4**).

• ***Crystallographic Methods.*** Low-temperature X-ray diffraction data for Rlacy87 (**2**) (CCDC 2091357) and Rlacy86 (**3**) (CCDC 2091358) were collected on a Rigaku XtaLAB Synergy diffractometer coupled to a Rigaku Hypix detector with either Mo Kα radiation (λ = 0.71073 Å) or Cu Kα radiation (λ = 1.54184 Å), from a PhotonJet micro-focus X-ray source at 100 K and 104 K, respectively. The diffraction images were processed and scaled using the CrysAlisPro software.[5] The structures were solved through intrinsic phasing using SHELXT[6] and refined against F^2 on all data by full-matrix least squares with SHELXL[7] following established refinement strategies.[8] All non-hydrogen atoms were refined anisotropically. All hydrogen atoms bound to carbon were included in the model at geometrically calculated positions and refined using a riding model. Hydrogen atoms bound to ruthenium were located in the difference Fourier synthesis and subsequently refined freely. The isotropic displacement parameters of all hydrogen atoms were fixed to 1.2 times the Ueq value of the atoms they are linked to (1.5 times for methyl groups). Details of the data quality and a summary of the residual values of the refinements are listed in Table S1.

• ***General Photochemistry Methods***. All photolysis experiments were carried out in sealed vessels, which were positioned 2" away from the aperture of a 100 W xenon-arc lamp (Newport INC.; APEX2). Various filters were employed with the xenon arc lamp: no filter (i.e., broadband), UV band pass filter (50% Abs Cutoff = 382 nm; $\%T_{avg} \geq 70\%$ = 300 – 375 nm; $\%T_{avg} \leq 1\%$ = 400 –

635 nm; $\%T_{avg} \leq 10\% = 280 – 290$ nm), a 345 nm cutoff filter ($\lambda \geq 345$ nm), a 420 nm cutoff filter ($\lambda \geq 420$ nm), and a 512 nm cutoff filter ($\lambda \geq 512$ nm). Temperature control was achieved by immersing the Schlenk tubes in water contained in a water-cooling jacket set to the desired temperature.

• ***Photocatalysis***. In a N_2 filled glovebox, 200 μL of a stock solution of complex **3** (0.04 M) in dry benzene was added to a 50 mL Schlenk tube along with a stir bar. The specified alcohol was dried over basic alumina (1-phenylethanol and isopropanol) or 3 Å molecular sieves for at least 2 days (methanol and ethanol) before 2.0 mL was added to the tube. The final concentration of catalysts was 0.004 M. The Schlenk tube was then sealed with a rubber septum, taken out of the glovebox, and irradiated at 23 °C. Each alcohol was performed in triplicate, except when H_2 yields were below 100%. The overnight experiments for each alcohol were sampled after 4 h and again after 12 h. Note, **3** has poor solubility in neat alcohols. Irradiations of **3** in neat alcohols resulted in homogeneous solutions during the course of irradiation (except for MeOH), and the yields of H_2 for each alcohol were comparable (sometimes slightly higher) to those that used benzene stock solutions of **3**.

• ***H_2 Quantification from Photocatalysis.*** H_2 quantification was achieved by removing 3 mL of headspace with a gas-tight syringe and analyzed using gas chromatography. The area of the H_2 peak was compared to a calibration curve to determine the percent H_2 in the headspace.

• ***Determination of organic products from the photolysis of 3 in methanol, ethanol, and 1-phenylethanol***. In a N_2-filled glovebox, a stock solution of **3** in C_6D_6 (0.0062 M) was prepared. Approximately 0.500 mL (0.00310 mmol, 1 equiv.) was transferred by glass syringe to an NMR tube equipped with J-Young valve. The alcohol (0.155 mmol, 50 equiv. for methanol and ethanol; 0.0931 mmol, 30 equiv. for 1-phenylethanol) was subsequently added by glass syringe. An initial ^{1}H NMR spectra was collected, and the tube was subsequently irradiated with a 100 W Xe arc lamp through a 345 nm cut off filter. ^{1}H NMR spectra were collected 2, 4.5 and 23 hours after initial photolysis for methanol and ethanol; for 1-phenylethanol photolysis was stopped after 7 hours and spectra was collected at this time. After 23 hours, compound **4** was still present in the sample containing ethanol whereas in the sample containing methanol the only identifiable product was the carbonylated product **8**. In the ethanol experiment, ethyl acetate resonances were present after photolysis and were observed to grow in over time. The presence of ethyl acetate was confirmed by spiking this sample with 1 μL of dry ethyl acetate (Fig. S37). For 1-phenylethanol, peaks characteristic of acetophenone were observed and confirmed by spiking this sample with 1 μL of dry acetophenone (Fig. S38).

• ***Determination of organic products from the photolysis of 3 in 2-propanol (large scale).*** 3 mL of a 0.005 M 2-propanol solution of **3** was irradiated for 19 h (broadband). The apparatus was attached to a bubbler to vent H_2. To quantify acetone, the post-irradiated mixture was measured into a graduated cylinder and treated with standard (hexamethyldisiloxane) and an aliquot was dissolved in $CDCl_3$ and analyzed by ^{1}H NMR spectroscopy. The yield of acetone was 700% relative to **3**.

• ***Determination of organic products from the photolysis of 3 in 2-propanol (small scale).*** An NMR tube equipped with a J-Young valve was charged with 0.400 mL of a solution of **3** in C_6D_6

(0.012 M) in a N2-filled glovebox. Dry 2-propanol (0.097 mmol, 20 equiv.) was added via glass syringe to the tube. Initial spectra were collected before photolysis and then subsequently collected at 4, 6 and 12 hours after irradiation. After 12 hours, the single characteristic peak of acetone was observed to grow in and was confirmed by spiking this sample with 1 μL of acetone (Fig. S39).

• ***Additional determination of organic products from the photolysis of 3 in neat CD_3OD.*** In a N_2-filled glovebox, compound **3** (2.0 mg, 0.0031 mmol) was suspended in 0.500 mL of CD_3OD in a tared vial (Note: **3** is only partially soluble in methanol). This suspension was transferred to a J-Young NMR tube and ^1H and ^2H NMR spectra were obtained. The initial ^1H NMR spectrum shows the presence of HD and H_2. After irradiation for a period of an hour, the hydridic resonances of **3** and **4** were not observed. Subsequent irradiation for 5 hours revealed a signal characteristic of carbonylated species **8** as determined by ^1H NMR (Fig. S40).

• ***Mass spectrometric analysis of products from the photolysis of 3 in methanol.*** In a N_2-filled glovebox, a 20 mL headspace GC vial was charged with 1.000 mL of methanol and 50 μL of a benzene solution of **3** (0.04 M). A stir bar was placed in the vial and was subsequently irradiated with a 100 W Xe arc lamp with a 345 nm cutoff filter for a period of 4 hours. Headspace GC-MS analysis using selective ion-monitoring showed the presence of formaldehyde (Fig. S41). Positive mode LC-MS analysis of the reaction mixture revealed the presence of signals consistent with $[\{LutP\}Ru(H)(CO)]^+$ and $[\{LutP\}Ru(H)(CO)_2]^+$ (Fig. S42).

• ***Photolysis of 3 with paraformaldehyde.*** To test the effects of formaldehyde in irradiations of **3** we performed the following experiment. In a N_2-filled glovebox, paraformaldehyde (1.7 mg, 0.057 mmol, 12 equiv.) was added to a solution of **3** (3.0 mg, 0.046 mmol, 1 equiv.) in 0.400 mL of C_6D_6 in a vial (Note: paraformaldehyde is not soluble in C_6D_6). The suspension was transferred to a J-Young NMR tube. Initial ^1H NMR spectrum, prior to photolysis, revealed the presence of H_2 indicating formaldehyde dehydrogenation. The tube was irradiated for 4 hours and a ^1H NMR spectrum was collected. The only hydridic signals observed were from carbonylated species **8**, the same product obtained when **3** was irradiated under CO in C_6D_6. Additionally, other organic products, including methanol and some aldehydic species were observed (Fig. S43). Collectively, this indicates that **3** also dehydrogenates formaldehyde.

Synthesis of Compounds

• **Synthesis of (CO)(H)(PPh_3)(κ^3-*N,C,P*-LutP`)ruthenium(II) (2)**

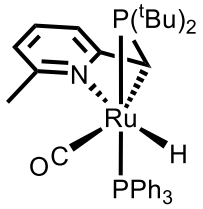

2

<u>*K[N(SiMe$_3$)$_2$] Method.*</u> In a N_2-filled glovebox, a 20 mL scintillation vial with a stir bar was charged with freshly dried THF (4 mL) and **1** (50.0 mg, 0.0736 mmol). This mixture was stirred until homogeneous. The solution was subsequently cooled to -35 °C in a cold-well before

$K[N(SiMe_3)_2]$ (14.6 mg, 0.0736 mmol) was added. Upon addition of $K[N(SiMe_3)_2]$, the solution became an amber color. The solution was stirred for 5 minutes at -35 °C. The amber solution was then removed from the cold-well and the solvent was removed *in vacuo*. The remaining residue was treated with dry diethyl ether (5 mL). The resulting amber suspension was filtered and the solids were washed with diethyl ether until the filtrate was colorless. Solvent was then removed from the filtrate *in vacuo* to yield an amber-brown solid (43.0 mg, 91%). Amber crystals suitable for diffraction were grown from diethyl ether at -35 °C.

KOtBu Method. In a N_2-filled glovebox, a 20 mL scintillation vial with a stir bar was charged with freshly dried benzene (2 mL) and **1** (20.0 mg, 0.0294 mmol). This mixture was stirred until homogeneous. Subsequently, KO^{t}Bu (3.6 mg, 0.032 mmol) was added to the stirring pale-yellow solution at room temperature. Upon addition of KO^{t}Bu at room temperature, the solution became an amber color. The solution was stirred for a further hour at room temperature during which a white solid (KCl) formed. After an hour had passed the amber mixture was filtered and solvent was removed *in vacuo* leaving an amber-brown solid behind. To this residue dry diethyl ether (5 mL) was added, and the resulting amber suspension was filtered. The remaining solid residue was washed with diethyl ether until the filtrate was colorless. Solvent was then removed from the filtrate *in vacuo* to yield an amber-brown solid (18.0 mg, 95%).

NOTE: Compound **2** is extremely water sensitive as well as thermally unstable and must be stored at -35 °C or used immediately after isolation. Thus, HRMS analyses were unsuccessful.

Spectroscopic Data for **2**: ^{1}H NMR (300 MHz, C_6D_6): δ 7.74 (m, 6H, P(*o*-(C_6H_5)$_3$)), 7.00 (m, 9H, P(*m*,*p*-(C_6H_5)$_3$)), 6.59 (t, *J* = 8 Hz, 1H, py), 5.83 (vt, *J* = 9 Hz, 2H, py), 1.78 (d, *J* = 3 Hz, 1H, C*H*P), 1.70 (s, 3H, CH_3), 1.40 (d, *J* = 14 Hz, 9H, P(C(CH_3)$_3$)$_a$), 1.14 (d, *J* = 14 Hz, 9H, P(C(CH_3)$_3$)$_b$), -14.16 (dd, *J* = 23, 19 Hz, 1H, Ru*H*). ^{1}H NMR (300 MHz, C_7D_8): δ 7.83 – 7.65 (m, 6H, P(*o*-(C_6H_5)$_3$)), 7.15 – 6.97 (m, 9H, P(*m*,*p*-(C_6H_5)$_3$)), 6.67 (t, *J* = 8 Hz, 1H, py), 5.92 (d, *J* = 8 Hz, 1H, py), 5.86 (d, *J* = 8 Hz, 1H, py), 1.79 (d, *J* = 3 Hz, 1H, C*H*P), 1.74 (s, 3H, CH_3), 1.44 (d, *J* = 13 Hz, 9H, P(C(CH_3)$_3$)$_a$), 1.19 (d, *J* = 13 Hz, 9H, P(C(CH_3)$_3$)$_b$), -14.21 (dd, *J* = 23, 19 Hz, 1H, Ru*H*). ^{31}P{^{1}H} NMR (121 MHz, C_6D_6): δ 118.0 (d, *J* = 234 Hz, *P*(*t*Bu)$_2$), 54.7 (d, *J* = 233 Hz, *P*(Ph)$_3$). ^{31}P NMR (121 MHz, C_7D_8): δ 118.3 (dd, *J* = 235, 5 Hz, *P*(*t*Bu)$_2$), 54.87 (dd, *J* = 235, 7 Hz, *P*Ph$_3$). ^{13}C{^{1}H} NMR (75 MHz, C_6D_6): δ 211.52 (*C*O), 168.5 (d, *J* = 2.8 Hz, py), 157.72 (py), 139.02 (d, *J* = 34.3 Hz, P(*C*$_6$H$_5$)$_3$), 134.18 (py), 134.07 (d, *J* = 12.3 Hz, P(*o*-(*C*$_6$H$_5$)$_3$)), 128.83 (P(*C*$_6$H$_5$)$_3$), 127.94 (P(*C*$_6$H$_5$)$_3$), 117.00 (py), 113.50 (d, *J* = 3.4 Hz, py), 36.14 (dd, *J* = 13.2, 8.8 Hz, P(*C*(CH$_3$)$_3$)$_a$), 35.09 (d, *J* = 25.6 Hz, P(*C*(CH$_3$)$_3$)$_b$), 31.65 (d, *J* = 6.1 Hz, P(C(*C*H$_3$)$_3$)$_a$), 30.95 (d, *J* = 4.1 Hz, P(C(*C*H$_3$)$_3$)$_b$), 22.25 (*C*H$_3$), 12.41 (dd, *J* = 6.8, 4.5 Hz, *C*HP). FTIR-ATR: 1880 cm^{-1} (ν_{CO}).

• **Synthesis of (CO)-*cis*-(H)$_2$-*trans*-(PPh$_3$) (*κ*^{2}-*N*,*P*-LutP)ruthenium(II) (3)**

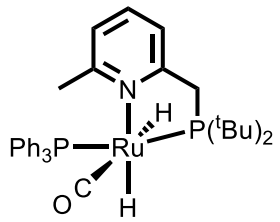

3

Dihydrogen Method. In a N_2-filled glovebox, an oven-dried Schlenk flask equipped with a stir bar was loaded with **1** (80.0 mg, 0.118 mmol). Freshly dried THF (10 mL) was added, and the mixture was stirred until the solid was fully dissolved to yield a pale-yellow solution. To the Schlenk flask, a solid addition arm loaded with $K[N(SiMe_3)_2]$ (23.5 mg, 0.118 mmol) was equipped. The flask was sealed and brought out of the glovebox and attached to a Schlenk line. The solution was subjected to three freeze-pump-thaw cycles and then brought under an atmosphere of dihydrogen (1 atm) at room temperature and stirred for 10 minutes. $K[N(SiMe_3)_2]$ was then dispensed into the flask in one portion. Color changes were noted over a period of 10 minutes from pale-yellow to dark-yellow and finally to amber. The amber solution was allowed to stir for another hour under dihydrogen. Subsequently, solvent was removed *in vacuo* to yield an amber residue. The Schlenk flask was brought back into the glovebox and the residue was dissolved in dry benzene and filtered into a tared scintillation vial. The solution was placed in a freezer at -35 °C for a period of 20 minutes and then lyophilized over a period of 2 hours to yield a pale-yellow, fluffy solid that was identified as the title compound (66 mg, 87%). Pale-yellow crystals were grown from layering a solution of **3** under hexane at -35 °C.

NOTE: Compound **2** can also be prepared independently and subjected to direct addition of H_2. However, owing to the high-moisture sensitivity of **2**, it is advised to access **2** *in situ* to avoid decomposition products that are difficult to separate from the final product, **3**.

Isopropanol Method. A J-Young NMR tube was charged with of a solution of **2** (8.0 mg, 0.012 mmol) in freshly dried C_6D_6 (0.75 mL). Degassed, freshly dried 2-propanol (3.1 μL, 0.041 mmol) was added to this solution via glass syringe. An NMR of the resulting solution 15 min after addition of 2-propanol revealed a mixture of **3**, excess 2-propanol, and acetone in a 1:2.3:1 ratio.

Spectroscopic Data for **3**: ^{1}H NMR (300 MHz, C_6D_6): δ 7.93 – 7.75 (m, 6H, P(*o*-(C_6H_5)$_3$)), 7.13 – 6.91 (m, 9H, P(*m*,*p*-(C_6H_5)$_3$)), 6.78 (t, J = 8 Hz, 1H, py), 6.58 (d, J = 8 Hz, 1H, py), 6.29 (d, J = 8 Hz, 1H, py), 3.51 (dd, J = 16, 6 Hz, 1H, CH_2P), 3.23 (ddd, J = 16, 9, 4 Hz, 1H, CH_2P), 2.51 (s, 3H, CH_3), 1.39 (d, J = 13 Hz, 9H, P(C(CH_3)$_3$)$_a$), 1.11 (d, J = 12 Hz, 9H, P(C(CH_3)$_3$)$_b$), -5.69 (dddd, J = 38, 22, 6, 4 Hz, 1H, Ru*H*), -15.59 (ddd, J = 31, 17, 6 Hz, 1H, Ru*H*). ^{31}P{^{1}H} NMR (121 MHz, C_6D_6): δ 108.7 (d, J = 251 Hz, *P*(*t*Bu)$_2$), 59.4 (d, J = 253 Hz, *P*Ph$_3$). ^{13}C{^{1}H} NMR (101 MHz, C_6D_6): δ 210.47 (*C*O), 163.71 (dd, J = 5.0, 1.9 Hz, py), 162.97 (py), 141.98 (d, J = 37.6 Hz, P((*C*$_6$H$_5$)$_3$)), 134.54 (py), 134.11 (d, J = 11.5 Hz, P(*o*-(*C*$_6$H$_5$)$_3$)), 128.59 – 128.37 (m, P(*C*$_6$H$_5$)$_3$)), 127.74 (P(*C*$_6$H$_5$)$_3$)), 121.47 (py), 119.32 (d, J = 7.3 Hz, py), 41.50 (d, J = 16.0 Hz, *C*H$_2$P), 36.59 (t, J = 2.9 Hz, P(*C*(CH$_3$)$_3$)$_a$), 33.58 (d, J = 19.0 Hz, P(*C*(CH$_3$)$_3$)$_b$), 31.89 (d, J = 5.9 Hz, *C*H$_3$), 31.68 (d, J = 4.9 Hz, P(C(*C*H$_3$)$_3$)$_a$), 29.35 (d, J = 5.9 Hz, P(C(*C*H$_3$)$_3$)$_b$). FTIR-ATR: 1901 cm^{-1} (ν_{CO}). HRMS (FT-ICR-MS): [($C_{15}H_{26}NP$)(PPh$_3$)(CO)(H)$_2$Ru]$^+$ ([M-H]$^+$); m/z$_{(found)}$ = 644.176504; m/z$_{(calcd.)}$ = 644.177959. $T_{1(min@400\ Hz)}$: 315 ms (-5.69 ppm, 223 K, C_7D_8) and 421 ms (-15.60 ppm, 213 K, C_7D_8).

• Characterization of (CO)-*cis*-(H)$_2$-*cis*-(PPh$_3$)(κ^2-*N*,*P*-LutP)ruthenium(II) (4)

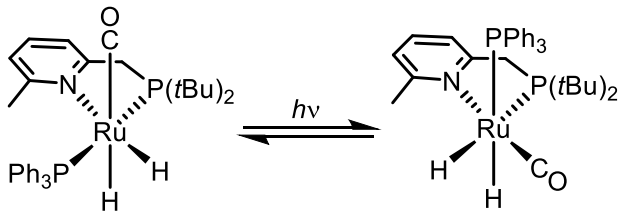

3 **4**

*Synthesis from **2**.* A J-Young NMR tube was charged with a solution of **2** (10 mg, 0.016 mmol) in dry C_6D_6 (~0.5 mL) in a N_2-filled glovebox. This tube was subjected to three freeze-pump-thaw cycles, after which the headspace was charged with dihydrogen (1 atm, r.t) to give a yellow-orange solution. After 15 min a ^{1}H NMR spectrum was taken to confirm complete conversion to **3**. Once the conversion was complete by NMR, the tube was irradiated with a 100 W xenon-arc lamp with no filter (i.e., broadband irradiation) in a 23 °C water bath for 1 h. A ^{1}H NMR spectrum taken after irradiation was ceased (~5-10 min) indicates an ~80:20 ratio of **4**:**3**. Complex **4** converts cleanly back to **3** over the course of 12 h.

*Synthesis from **3**.* A J-young tube was charged with a solution of **3** (9.5 mg, 0.016 mmol) in dry C_6D_6 (~0.5 mL) in a N_2-filled glovebox. This solution was irradiated with a 100 W xenon-arc lamp with no filter in a 23 °C water bath for 1 h. A ^{1}H NMR spectrum taken after irradiation was ceased (~5-10 min) indicates an ~80:20 ratio of **4**:**3**.

Note: Photolysis of **3** in THF-d_8 resulted in degradation products.

Spectroscopic Data for **4**: ^{1}H NMR (500 MHz, C_6D_6): δ 7.77 – 7.64 (m, 6H, P(*o*-(C_6H_5)$_3$)), 7.12 – 6.98 (m, 9H, P(*m*,*p*-(C_6H_5)$_3$)), 6.59 (t, J = 8 Hz, 1H, py), 6.38 (d, J = 8 Hz, 1H, py), 6.16 (d, J = 8 Hz, 1H, py), 3.06 (dd, J = 16, 8 Hz, 1H, CH_2P), 2.76 (dd, J = 17, 5 Hz, 1H, CH_2P), 2.56 (s, 3H, CH_3), 1.30 (d, J = 12 Hz, 9H, P(C(CH_3)$_3$)$_a$), 1.11 (d, J = 13 Hz, 9H, P(C(CH_3)$_3$)$_b$), -5.14 (dd, J = 101, 25 Hz, 1H, Ru*H*), -6.10 (dd, J = 92, 17 Hz, 1H, Ru*H*). ^{31}P{^{1}H} NMR (202 MHz, C_6D_6): δ 77.92 (d, J = 11 Hz, *P*(*t*Bu)$_2$), 42.69 (d, J = 11 Hz, *P*Ph$_3$). FTIR-ATR: 1886 cm^{-1} (ν_{CO}). $T_{1(min@400\ Hz)}$: 349 ms (-5.14 ppm, 243 K, C_7D_8) and 391 ms (-6.03 ppm, 243 K, C_7D_8).

• Characterization of 2c (tentative structure shown)

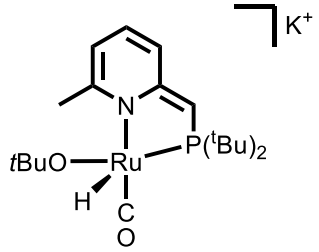

2c

*Reaction of **2** with excess KOtBu (**2c**).* When more than one equivalent of KO^{t}Bu was used in the synthesis of **2** from **1**, free PPh$_3$ and an anionic {LutP}Ru(O^{t}Bu) complex (**2c**) was formed in addition to **2** (Figs. S9(top)–S10(top)). The reaction of **2** with one equiv. of KO^{t}Bu and one equiv. of 18-crown-6 gave complete conversion to **2c** and other unidentified byproducts (Figs. S9 (bottom)–S10 (bottom)). Attempts to isolate **2c** have so far been unsuccessful.

Spectroscopic data for **2c**: ^{1}H NMR (500 MHz, THF-d_8) δ 6.28 (t, J = 8 Hz, 1H, py), 5.90 (d, J = 9 Hz, 1H, py), 5.21 (d, J = 6 Hz, 1H, py), 3.10 (s, 1H, C*H*P), 2.19 (s, 3H, CH_3), 1.37 (d, J = 12 Hz, 9H, P(C(CH_3)$_3$)$_a$), 1.32 (s, 9H, O(C(CH_3)$_3$)), 1.15 (d, J = 13 Hz, 9H, P(C(CH_3)$_3$)$_b$), -19.14 (d, J = 36 Hz, 1H, Ru*H*). ^{31}P NMR (202 MHz, THF-d_8) δ 120.74 (d, J = 24 Hz, *P*(*t*Bu)$_2$).

• Reactions involving deuterium (D_2 and 2-propanol-d_8)

*Reaction of **2** with D_2.* A solution of **2** (10 mg, 0.016 mmol) in dry C_6D_6 (~0.5 mL) was added to a J-young tube in a N_2-filled glovebox. This tube was subjected to three freeze-pump-thaw cycles, after which the headspace was charged with D_2 (1 atm, r.t). A ^{1}H NMR spectrum was taken. The tube was then brought back into the glovebox, transferred to a 20 mL scintillation vial, and the solvent was removed *in vacuo*. The residue was dissolved C_6H_6 (~0.5 mL) and C_6D_6 (~5 µL) and transferred to a new J-Young tube before a ^{2}H NMR spectrum was taken.

After 1 h under ambient light (Figs. S17–S18), the ^{1}H and ^{2}H NMR spectra indicate deuterium incorporation at both the ruthenium center and the methylene arm of the ligand. Two hydride/deuteride isotopomers are observed in a 1:1 ratio with minor shoulders with are suspected to be the diastereomers of these major complexes. In the absence of light these minor peaks are not observed, indicating that light is involved in the isomerization process (Figs. S19–S20).

Note: H_2 and HD were observed in the ^{1}H NMR spectrum when **2** was treated with D_2 indicating exchange with free dihydrogen in the presence of light (Figs. S17–S18). In the absence of light only trace amounts of H_2 and HD were detected by NMR (Figs. S19–S20).

*Reaction of **3** with D_2.* A solution of **3** (10 mg, 0.016 mmol) in dry C_6D_6 (~0.5 mL) was added to a J-Young tube in a N_2-filled glovebox. This tube was subjected to three freeze-pump-thaw cycles, after which the headspace was charged with D_2 (1 atm, r.t). A ^{1}H NMR spectrum was taken. The tube was then brought back into the glovebox, transferred to a 20 mL scintillation vial, and the solvent was removed *in vacuo*. The residue was dissolved C_6H_6 (~0.5 mL) and C_6D_6 (~5 µL) and transferred to a new J-Young tube before a ^{2}H NMR spectrum was taken.

With ~1 h of broadband irradiation with a 100 W xenon-arc lamp (Figs. S31–S32) or ~4 days in the dark (Fig. S33), ^{1}H and ^{2}H NMR spectra indicate nearly complete incorporation of deuterium into both hydride resonances. Importantly, no incorporation in the ligand was observed.

Note: H_2 and HD were observed in the ^{1}H NMR spectrum when **3** was treated with D_2 indicating exchange with free dihydrogen when irradiated (Figs. S31–S32). In the absence of light only trace amounts of H_2 and HD were detected by NMR (Fig. S33).

*Reaction of **3** with 2-propanol-d_8.* A solution of **3** (9.25 mg, 0.0143 mmol), 2-propanol-d_8 (2.2 µL, 0.029 mmol) in dry C_6D_6 (~0.5 mL) J-young tube N_2-filled glovebox. This tube was irradiated with a 100 W xenon-arc lamp with no filter in a 23 °C water bath for ~1.5 h. A ^{1}H NMR spectrum (Fig. S44) was taken. The tube was then brought back into the glovebox, transferred to a 20 mL scintillation vial, and the solvent was removed *in vacuo*. The residue was dissolved C_6H_6 (~0.5 mL) and C_6D_6 (~5 µL) and transferred to a new J-Young tube before a ^{2}H NMR spectrum was taken (Fig. S45).

With ~1.5 h of irradiation, ^{1}H and ^{2}H NMR spectra clearly show incorporation of deuterium into the ligand methylene arm (Figs S44–S45).

• **Wavelength required for H_2 production from 2-propanol and 3.** A solution of **3** (10 mg, 0.016 mmol) in 2-propanol (2.0 mL) was added to a 50 mL Schlenk tube in an N_2-filled glovebox. This tube was sealed with an unpunctured septa and secured with electrical tape before bringing out of the glovebox. The tube was irradiated with a 100 W xenon-arc lamp for 1 h at 23 °C using a 520 nm cutoff filter before the headspace was sampled and analyzed for H_2 by gas chromatography. This was repeated using 420 nm and 345 nm cutoff filters. The 512 nm and 420 nm filters yielded nominal H_2 while the 345 nm cutoff filter yielded significantly more H_2 (Fig. S46).

• **Wavelength required for photoisomerization of 3 to 4.** To determine the wavelength of light required to isomerize **3** to **4**, a solution of 10 mg **3** (10 mg, 0.016 mmol) in dry C_6D_6 (0.5 mL) was added to a J-Young NMR tube in an N_2-filled glovebox. This tube was sealed, brought out of the glovebox, and photolyzed for 1 min at 23 °C using a filter before a ^1H NMR spectrum was taken to determine the ratio of **4** to **3**. A 515 nm cutoff filter, a 420 nm cutoff filter, a 345 nm cutoff filter, and a UV band pass filter were used. Very little conversion to **4** was observed for the 515 nm cutoff filter (~2%), 420 nm cutoff filter (~7 %), and UV band pass filter (~5%). The 345 nm cutoff filter yielded significant conversion to **4** (~24%) (Fig. S47).

• **Other byproducts from irradiation of 3.**

Summary of byproducts observed. In some cases, when less than pristine samples of **3** were irradiated under H_2 for long periods of time, $[(PPh_3)_3Ru(H)_4]$ (Fig. S36), $[(CO)(PPh_3)_3Ru(H)_2]$ (**6**) (Fig. S36), and carbonylated byproduct **8** were observed (Figs. S49-S51)

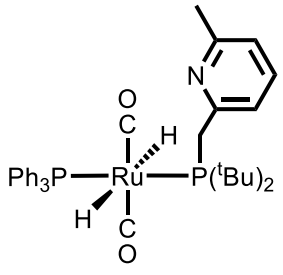

8

*Carbonylated product (**8**): irradiation of **3** under CO.* An NMR sample of **3** (6.7 mg, 0.010 mmol) in C_6D_6 (0.450 mL) was prepared in a nitrogen filled glovebox and quantitatively transferred to a J-Young tube. The tube was removed from the glovebox and then connected to a Schlenk line and subjected to three freeze-pump-thaw cycles. After the tube had returned to room temperature, CO (10% in $Ar_{(g)}$, 1 atm) was introduced to the sample for a period of two minutes. The tube was inverted and shaken and subsequently irradiated with broadband light for one hour. The sample was then quickly analyzed by ^1H and ^{31}P $\{^1H\}$ NMR spectroscopy with no further isolation or purification (Figs. S49-S51). The major product (**8**) contains ^1H and $^{31}P\{^1H\}$ NMR resonances which suggest a carbonylated product in which the pyridine ring of LutP has dissociated and substituted with a CO ligand. When **8** was prepared for an overnight ^{13}C NMR experiment, other products (from a multitude of ^{13}C signals) and free H_2 were observed in a subsequent ^1H NMR experiment suggesting that **8** is not indefinitely stable under an atmosphere of CO and precluded its isolation for definitive characterization. Complex **8** is also observed when **3** is irradiated under

N_2, and is a commonly observed byproduct in post-irradiated indicating that CO photolysis is another possible photochemical reaction of **3**.

Spectroscopic Data for **8**: ^{1}H NMR (300 MHz, C_6D_6): δ 7.85 – 7.71 (m, 6H, P(*o*-(C_6H_5)$_3$)), 7.41 (d, *J* = 8 Hz, 1H, py), 6.62 (d, *J* = 7 Hz, 1H, py), 3.44 (dd, *J* = 10, 2 Hz, 2H, CH_2P), 2.39 (s, 3H, CH_3), 1.45 (d, *J* = 13 Hz, 18H, P(C(CH_3)$_3$)$_2$), -7.30 (dd, *J* = 25, 21 Hz, 2H, Ru*H*). ^{31}P{^{1}H} NMR (202 MHz, C_6D_6): δ 96.90 (d, *J* = 212.0 Hz, *P*(*t*Bu)$_2$, 58.58 (d, *J* = 212.7 Hz, *P*Ph$_3$). FTIR-ATR: (Major stretches) 2009 cm^{-1}, 1962 cm^{-1}, 1891 cm^{-1}, 1872 cm^{-1}.

• Half-life determination of 4.

A J-Young tube was charged with a solution of **3** (9.5 mg, 0.016 mmol) and hexamethylbenzene (0.4 mg, 0.002 mmol) in dry C_6D_6 (0.5 mL) in a N_2-filled glovebox. This solution was used as is (N_2 atmosphere); subjected to three freeze-pump-thaw cycles (static vacuum); or subjected to three freeze-pump-thaw cycles followed by addition of H_2 before being irradiated with a 100 W xenon arc lamp (broad band, no filter) for a period of 1 h at 23 °C. The samples were monitored by ^{1}H NMR after irradiation to measure the disappearance of **4** and reappearance of **3** by comparing the integrations of the δ_{CH3} of **4** and **3**. All experiments were performed in triplicate and average $t_{1/2}$ is reported (Figs. S21–S24, S29–S30).

Eyring plot of 4 exchange with H_2.

A solution of 10 mg of **3** in ~0.5 mL C_6D_6 was added to a J-Young tube in a N_2 filled glovebox. This tube was sealed and irradiated with a 100 W xenon arc lamp with a 345 nm cutoff filter for 1 h. ^{1}H NMR spectra were taken from 25 °C to 45 °C in 2.5 °C increments. Line fitting analysis was performed on the -5.14 ppm and -6.10 ppm resonances of **4** sand the average width at half height (w_t) of each resonance was determined. The rate constant at each temperature (k_T) was calculated using the following equation:

$$k_t = \pi(w_t - w_0)$$

Where w_t is the width at half height of the resonance at a specific temperature and w_0 is the width at half height at 25 °C. An Eyring plot (*ln* [k_T/T] vs 1/T) was constructed from this data which furnished a straight line with an R^2 = 0.993 (Figs. S34–S35). This plot furnished a $\Delta H^‡$ value of 24.0 ± 1.2 kcal·mol^{-1} and $\Delta S^‡$ value of 22.9 ± 3.4 cal·K^{-1}·mol^{-1}. The $\Delta G^‡$ at 293K was calculated to from these values as 17.2 ± 0.17 kcal·mol^{-1}. This experiment was repeated in triplicate.

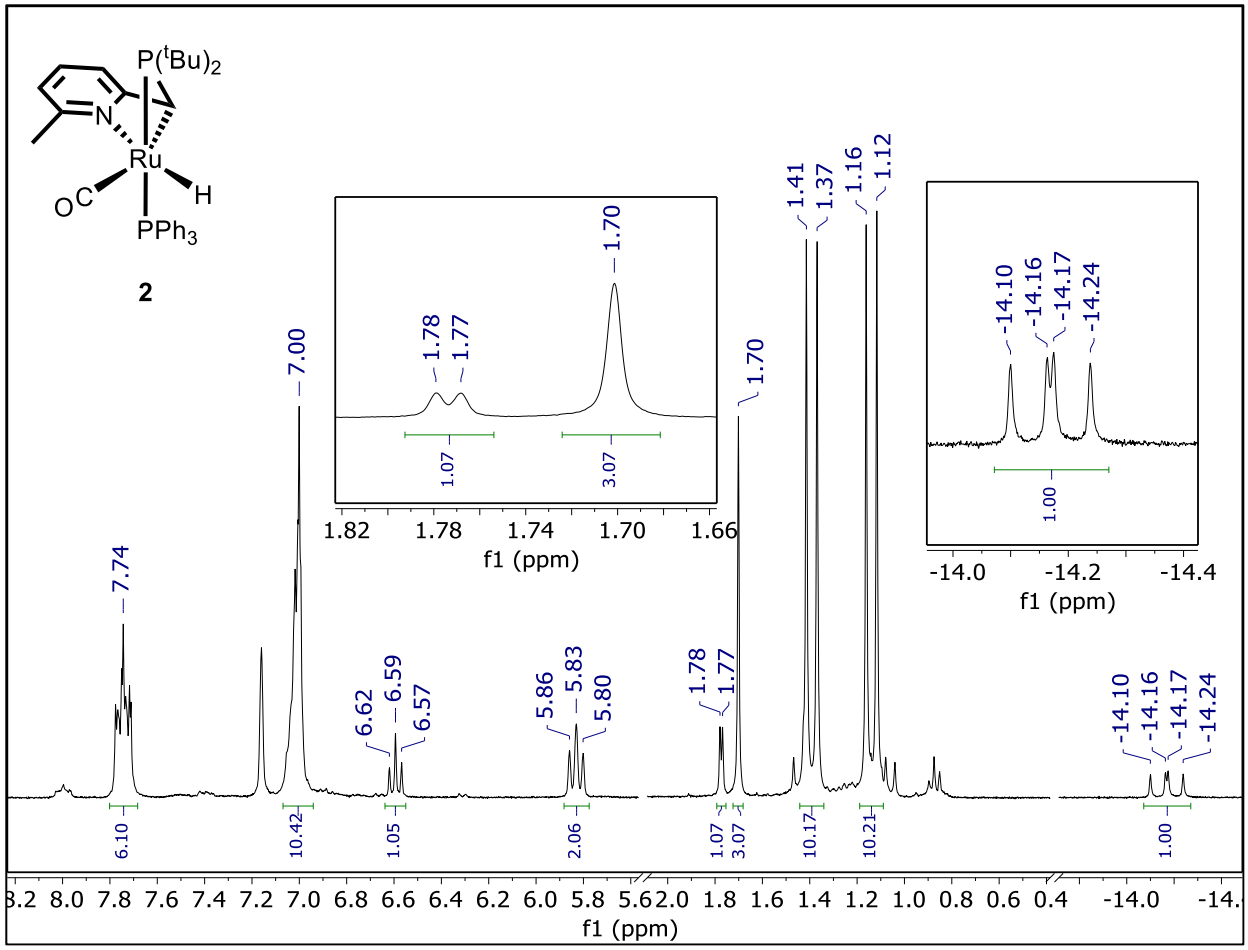

Figure S1. 300 MHz ^{1}H NMR spectrum of **2** in C_6D_6.

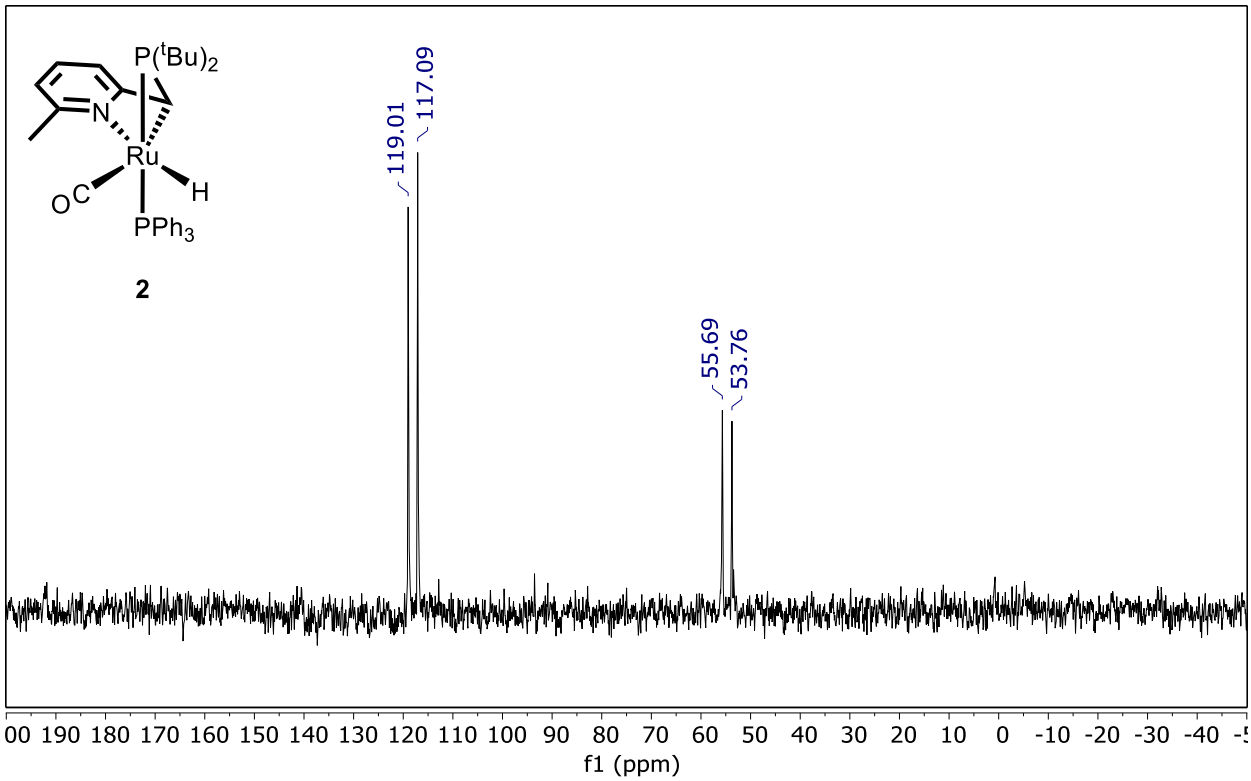

Figure S2. 121 MHz $^{31}P\{^{1}H\}$ NMR spectrum of **2** in C_6D_6.

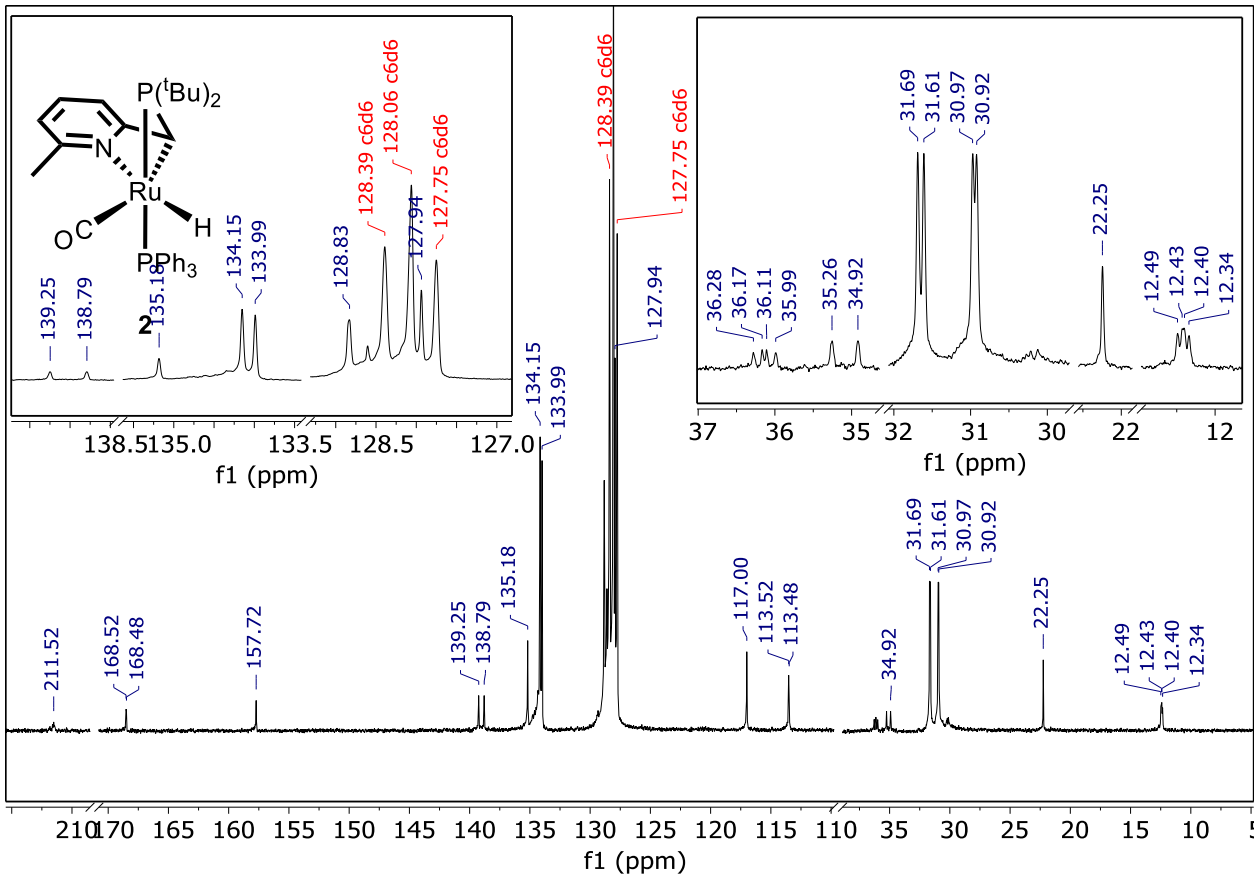

Figure S3. 75 MHz $^{13}C\{^{1}H\}$ NMR spectrum of **2** in C_6D_6.

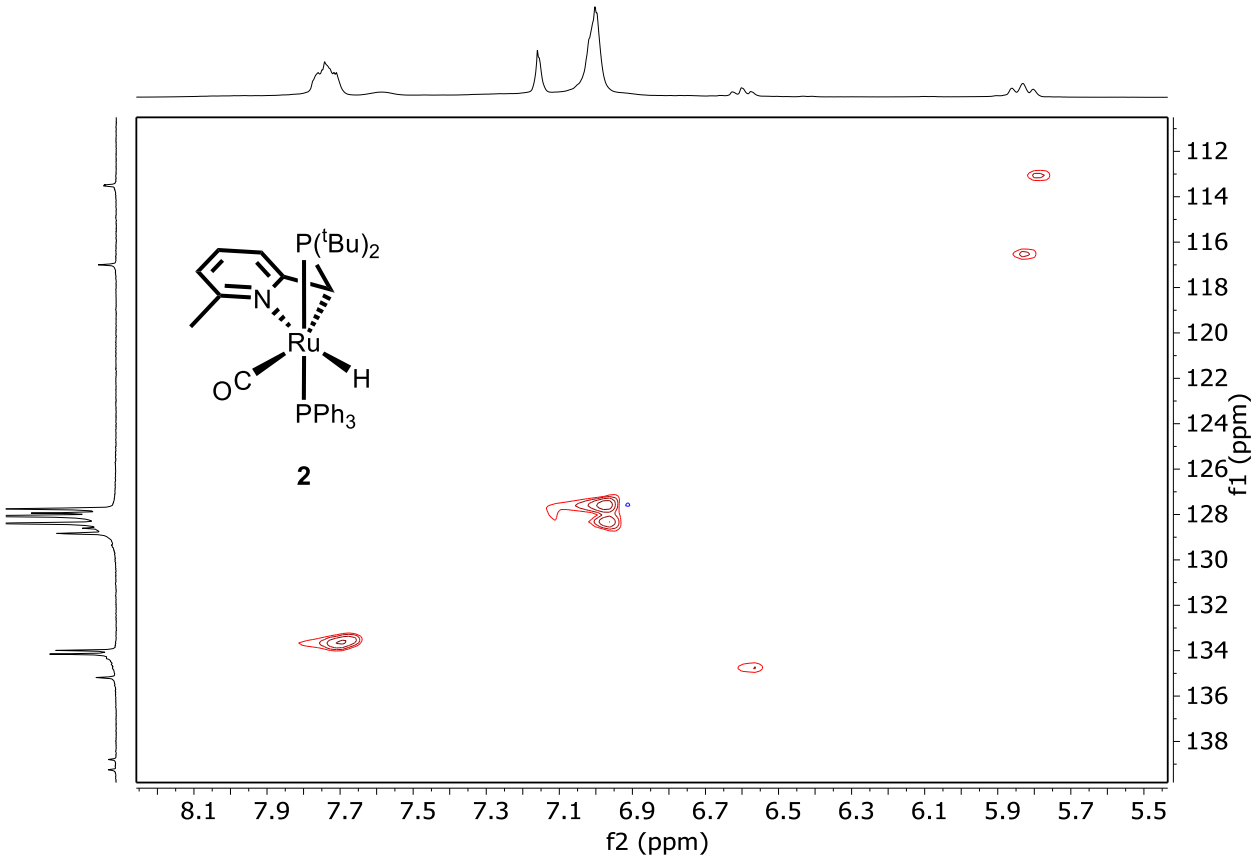

Figure S4. $^{1}H/^{13}C$ correlated HSQC spectrum of **2** in C_6D_6 zoomed in on the aromatic region.

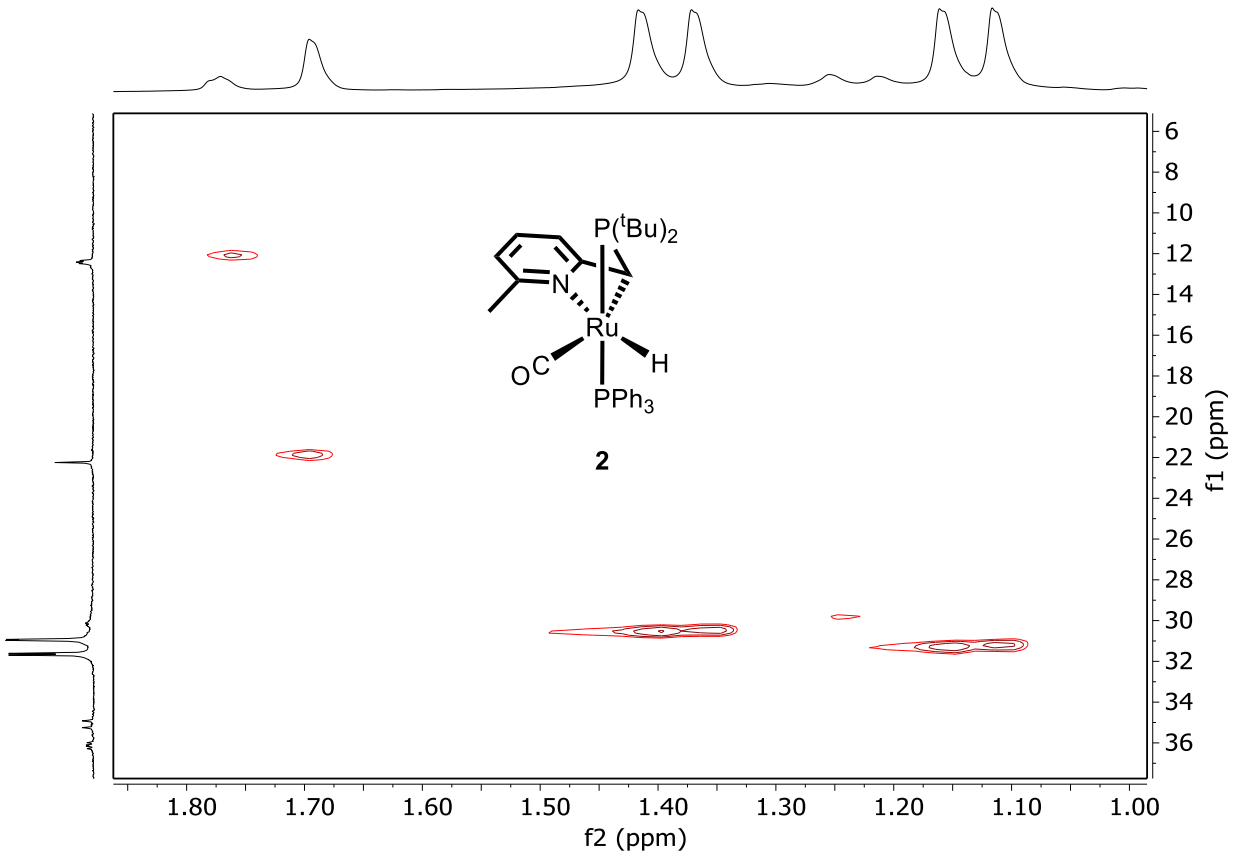

Figure S5. $^{1}H/^{13}C$ correlated HSQC spectrum of **2** in C_6D_6 zoomed in on the aliphatic region.

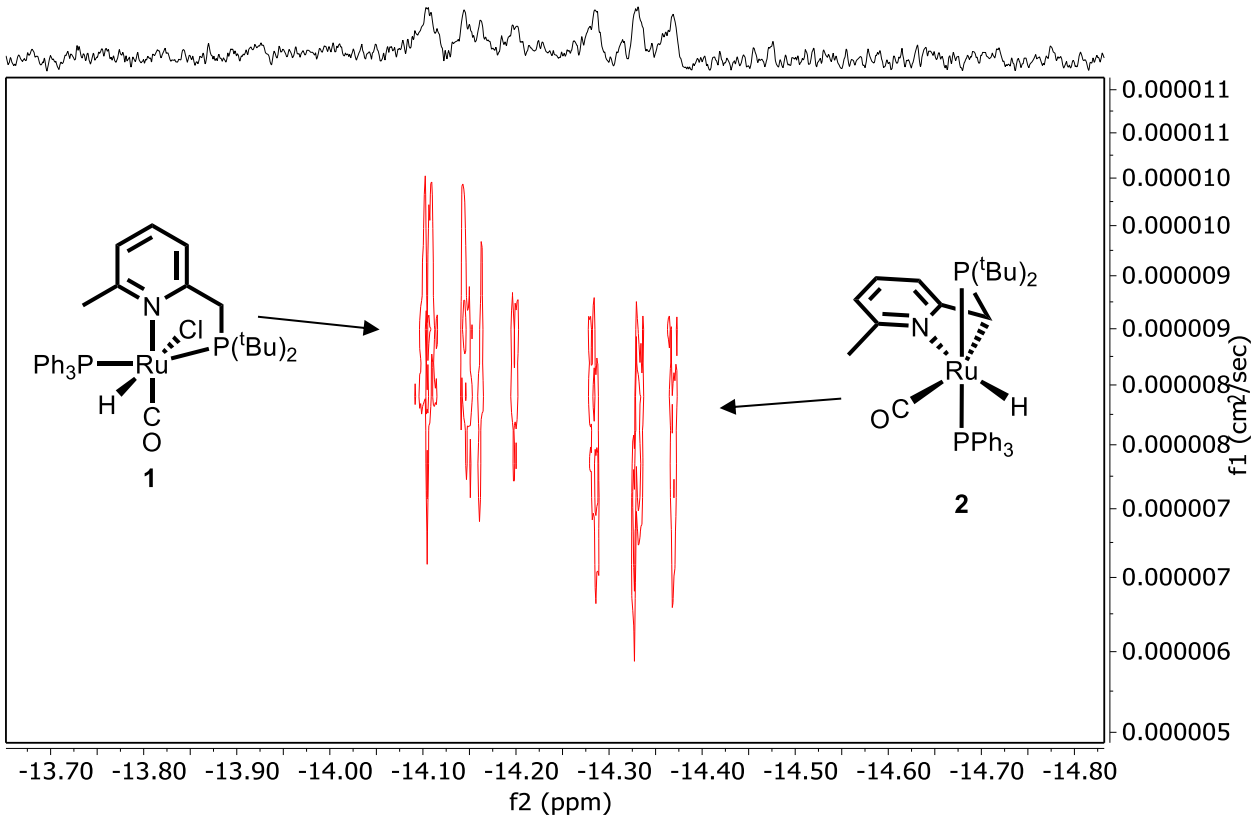

Figure S6. DOSY spectra of a 50:50 mixture of **1**:**2** in C_6D_6 zoomed in on the hydride region.

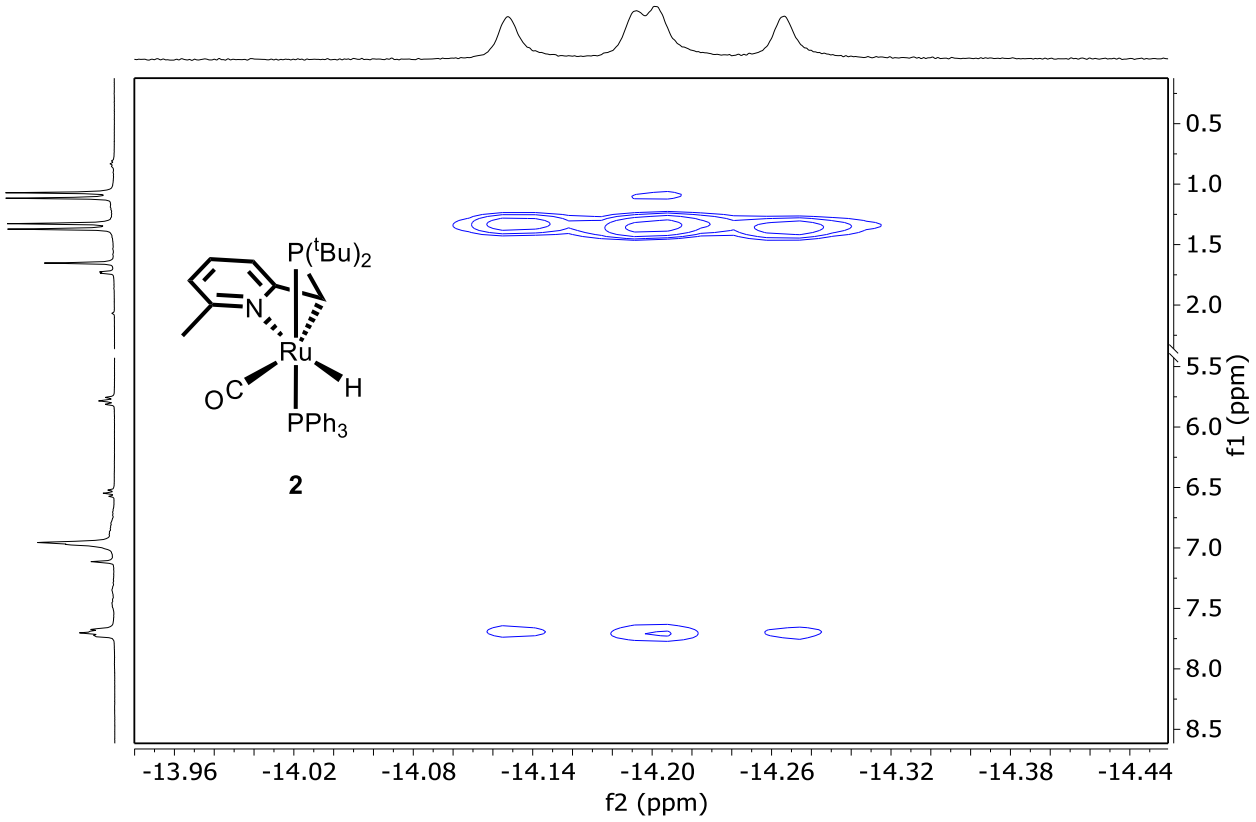

Figure S7. ^{1}H-^{1}H ROESY NMR spectrum of **2** in C_6D_6 zoomed in on the hydride region.

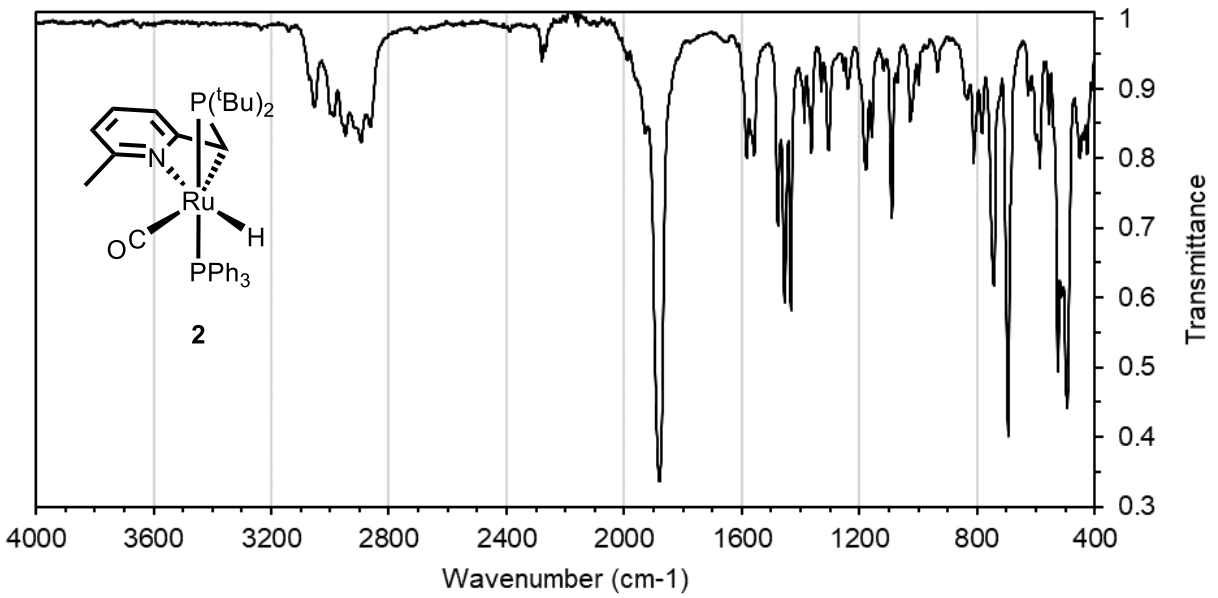

Figure S8. Drop-cast FTIR-ATR spectrum of **2**.

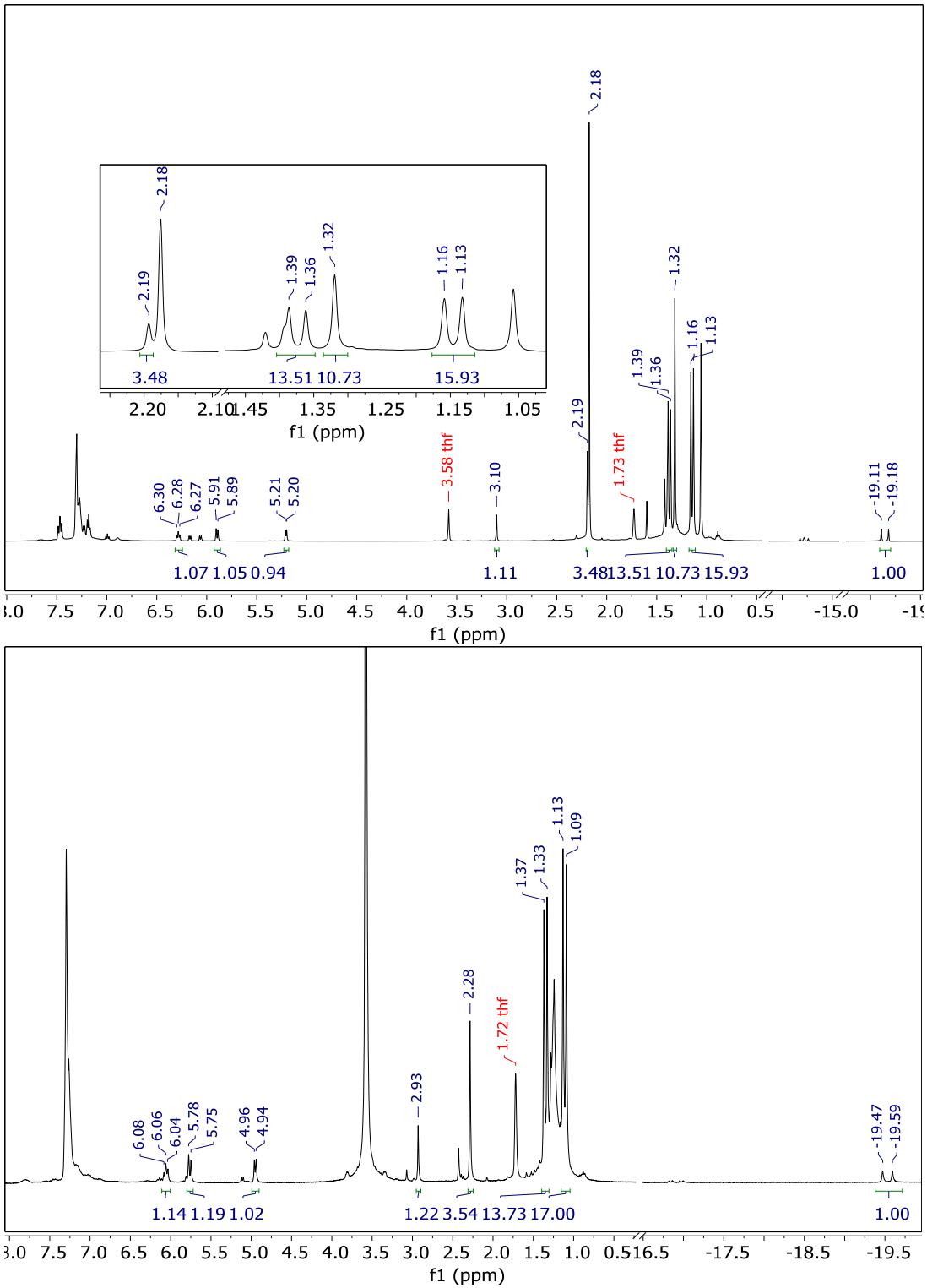

Figure S9. (top) *In-situ* 500 MHz ^{1}H NMR spectrum of the reaction of **1** with 2 equiv. of KO*t*Bu in THF-d_8 at 25°C. The integrated resonances are from **2c**. (bottom) *In-situ* 300 MHz ^{1}H NMR of the reaction of **2** with 1 equiv. of KO*t*Bu and 1 equiv. of 18-crown-6 in THF-d_8.

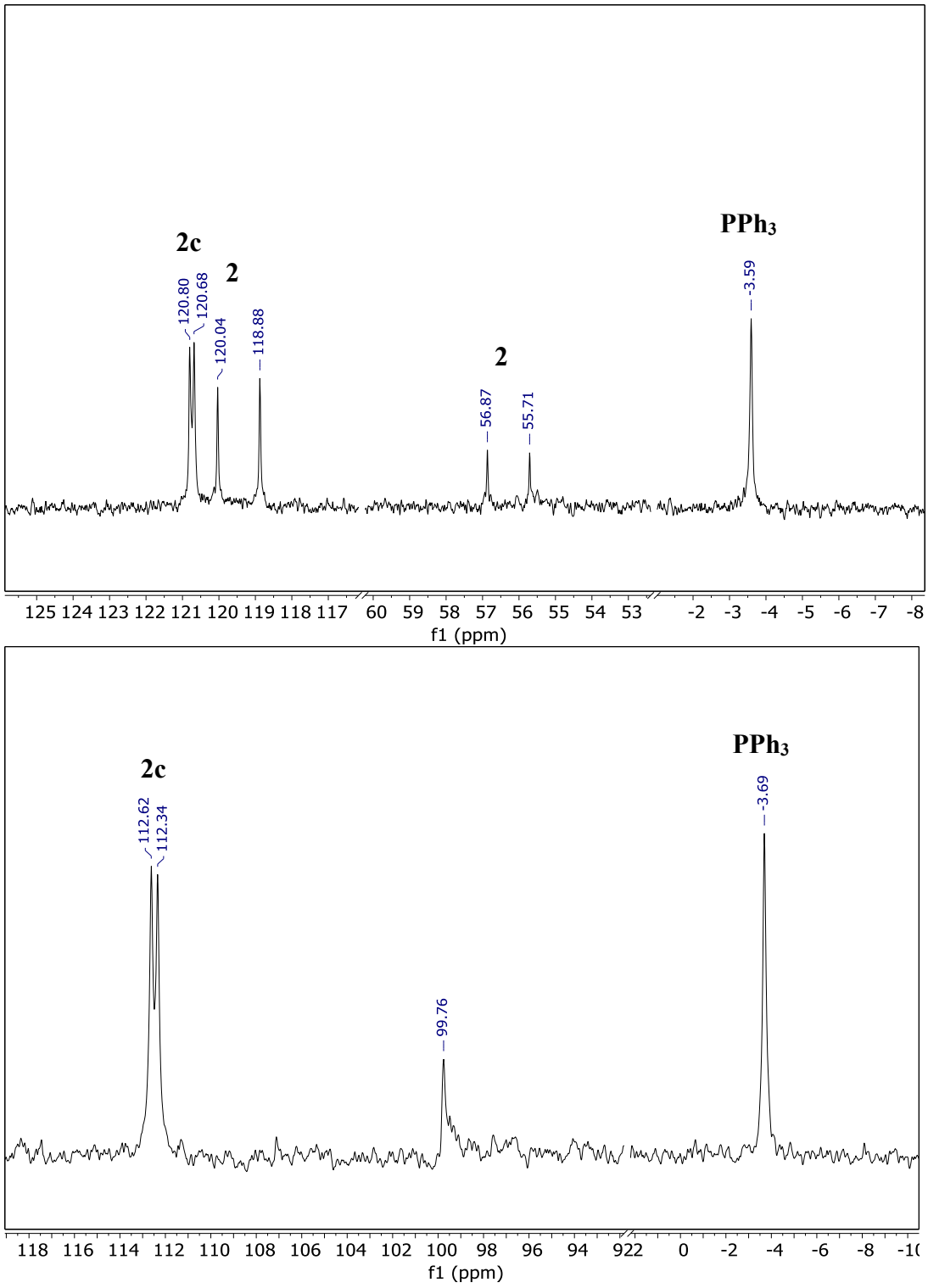

Figure S10. (top) *In-situ* 202 MHz $^{31}P\{^{1}H\}$ NMR spectrum of the reaction of **1** with 2 equiv. of KO*t*Bu in THF-d_8. (bottom) *In-situ* 121 MHz $^{31}P\{^{1}H\}$ NMR spectrum of a solution of **2** in THF-d_8 treated with 1 equiv. of KO*t*Bu and 1 equiv. of 18-crown-6. The resonance at 99 ppm is unidentified.

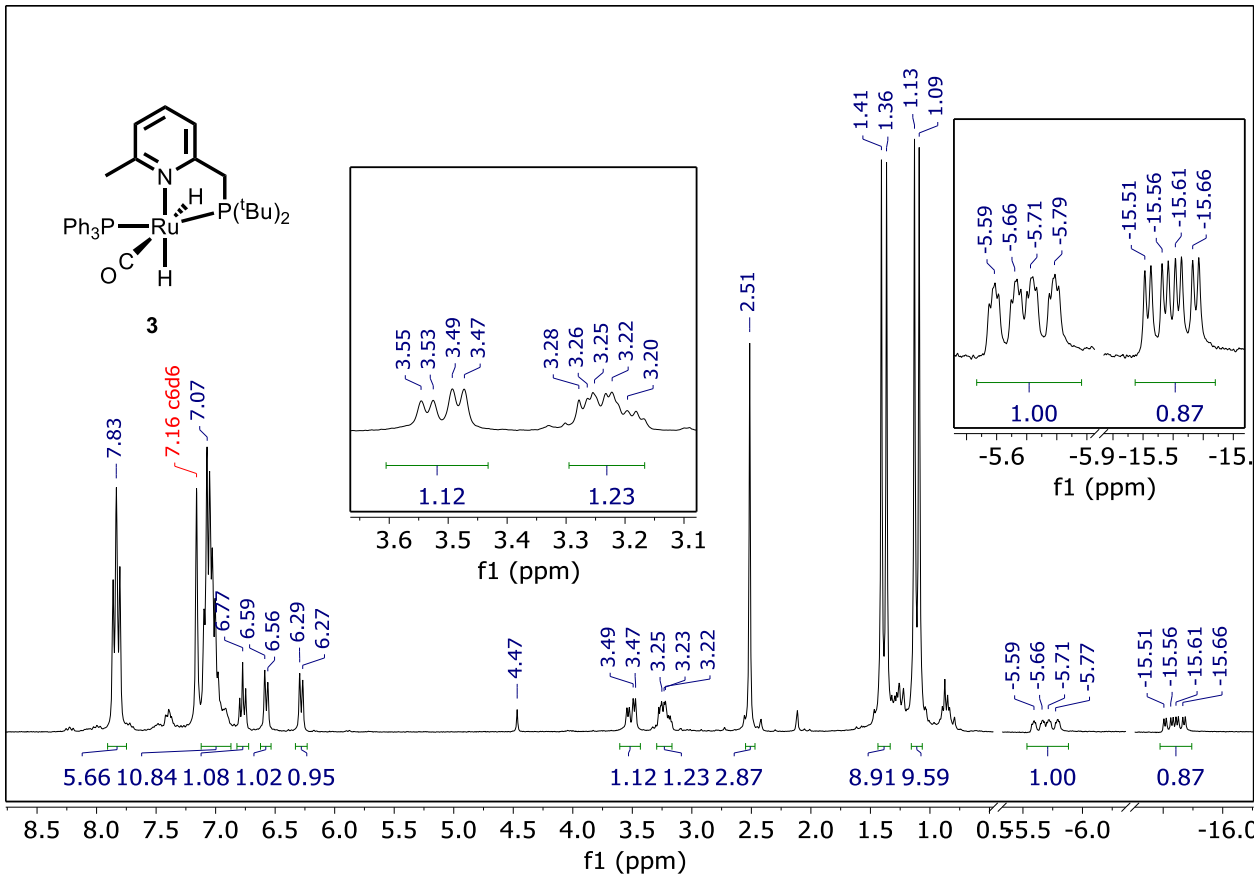

Figure S11. 300 MHz ^{1}H NMR spectrum of **3** in C_6D_6.

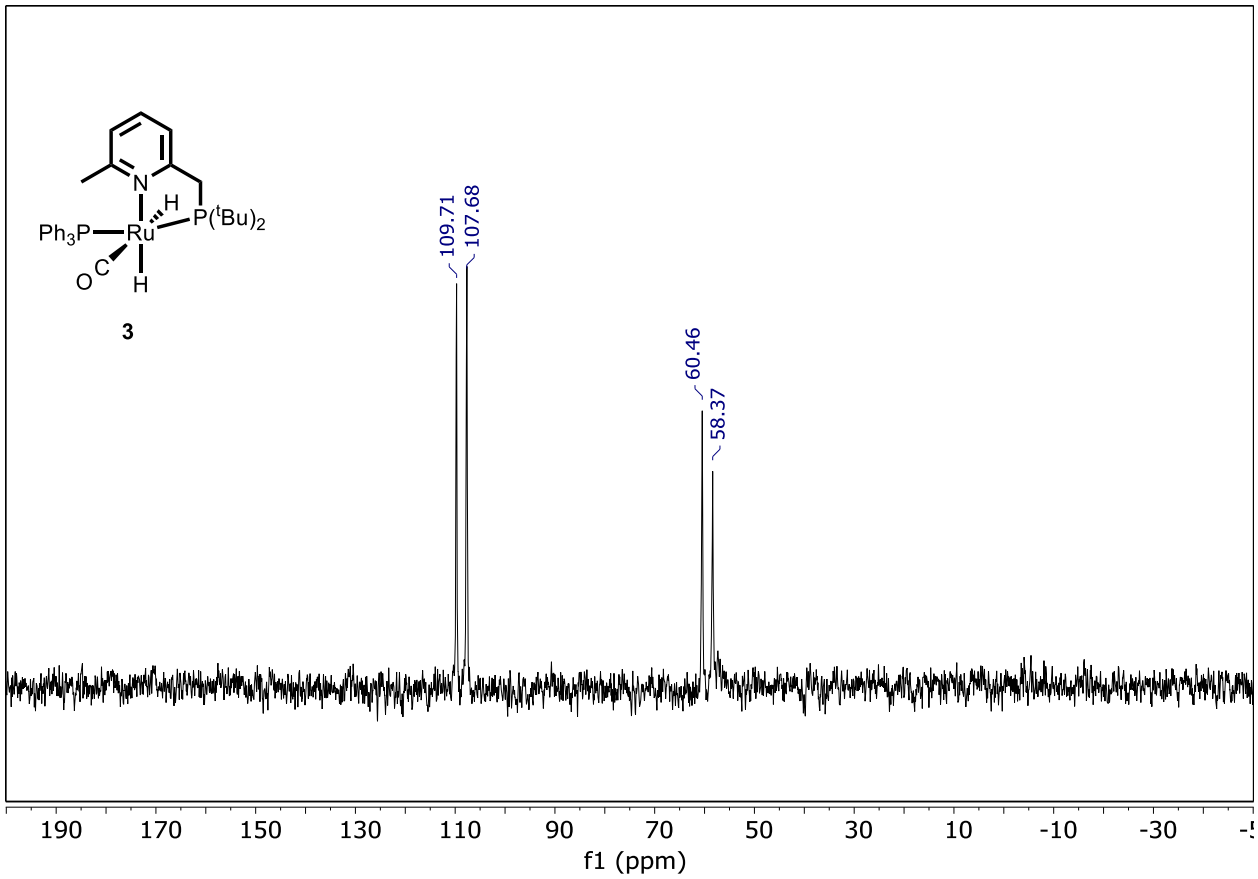

Figure S12. 121 MHz $^{31}P\{^{1}H\}$ NMR spectrum of **3** in C_6D_6.

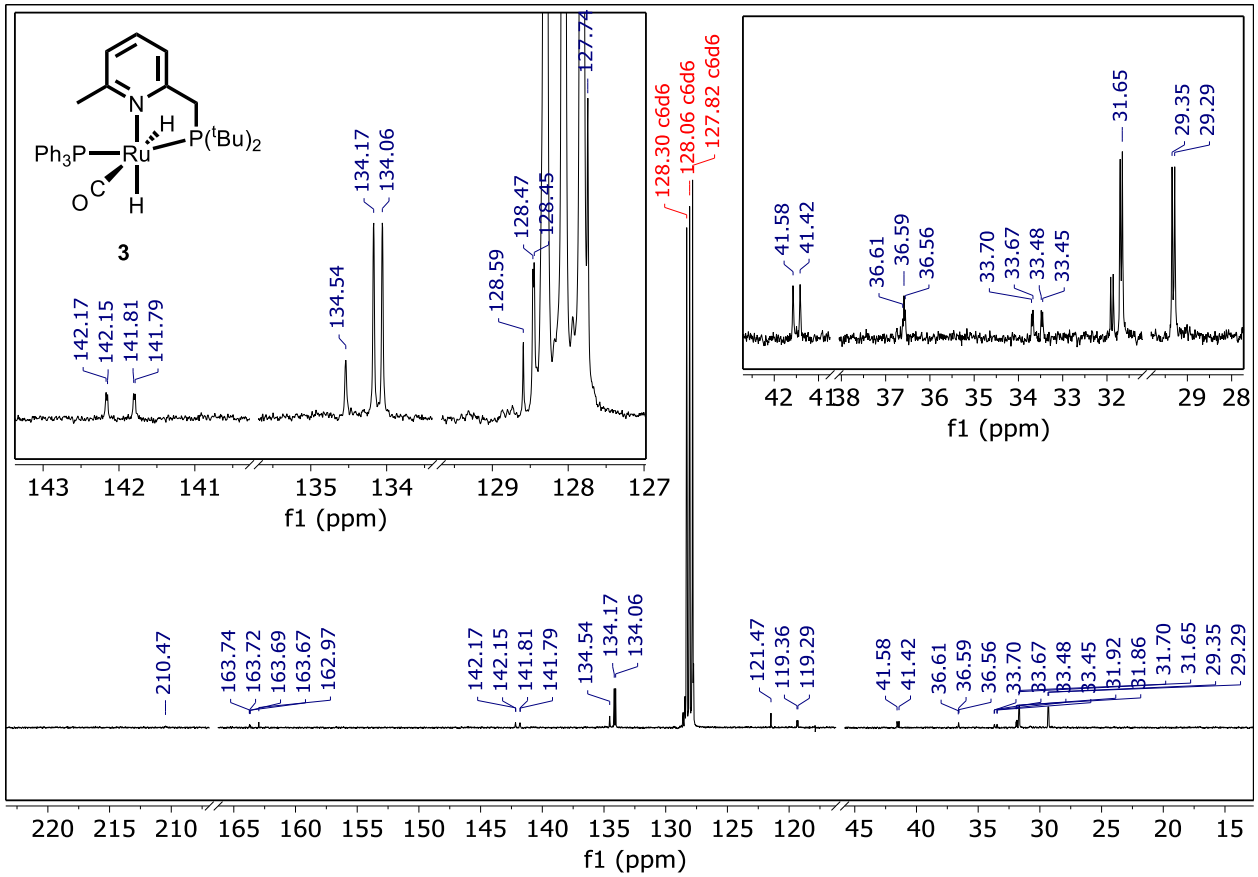

Figure S13. 101 MHz $^{13}C\{^{1}H\}$ NMR spectrum of **3** in C_6D_6.

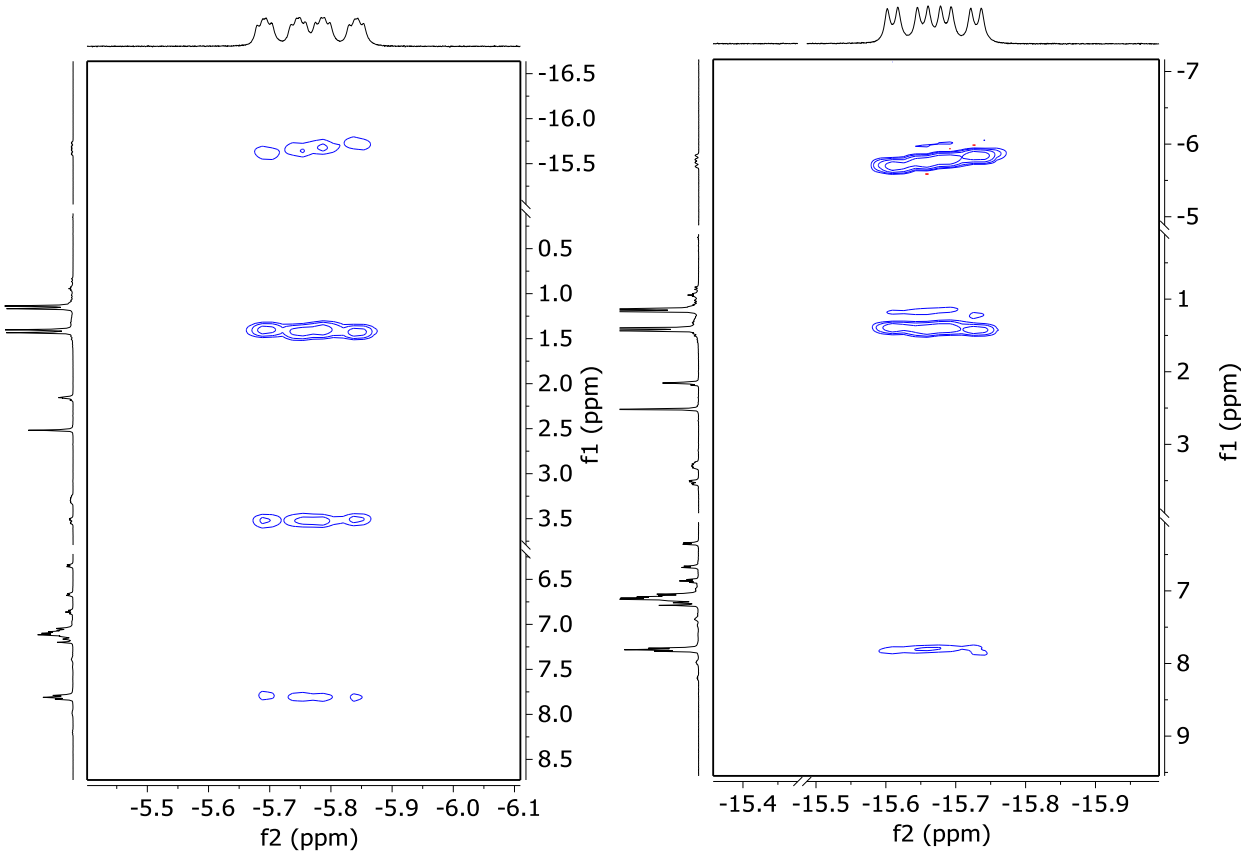

Figure S14. 400 MHz ^{1}H-^{1}H ROESY NMR spectrum of **3** in C_6D_6 zoomed in on the hydride region.

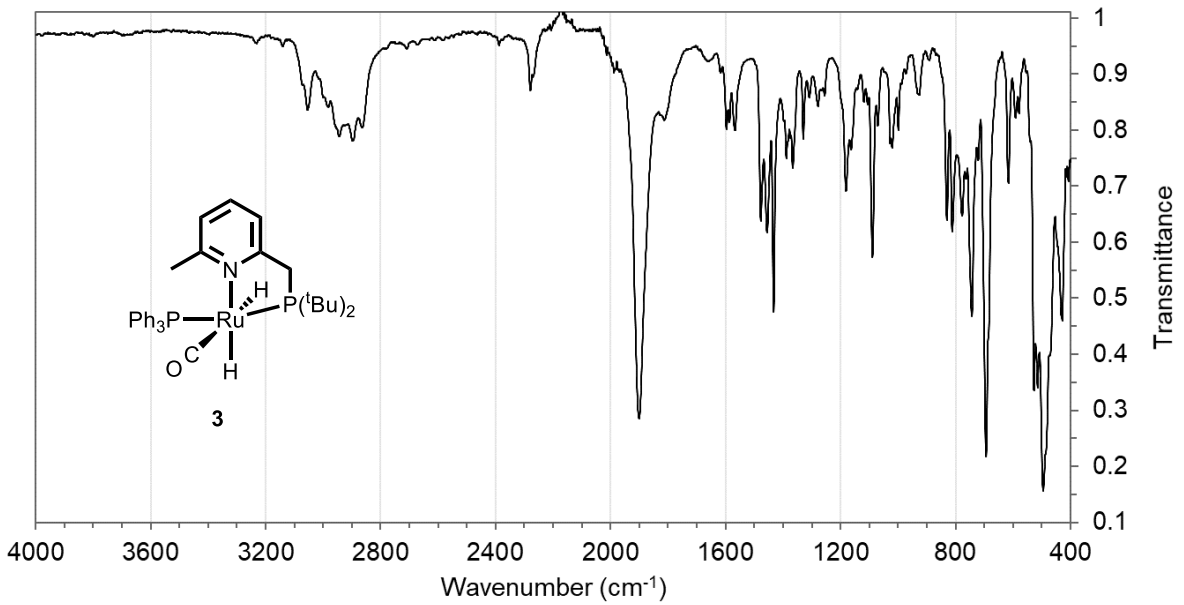

Figure S15. Drop-cast FTIR-ATR spectrum of **3**.

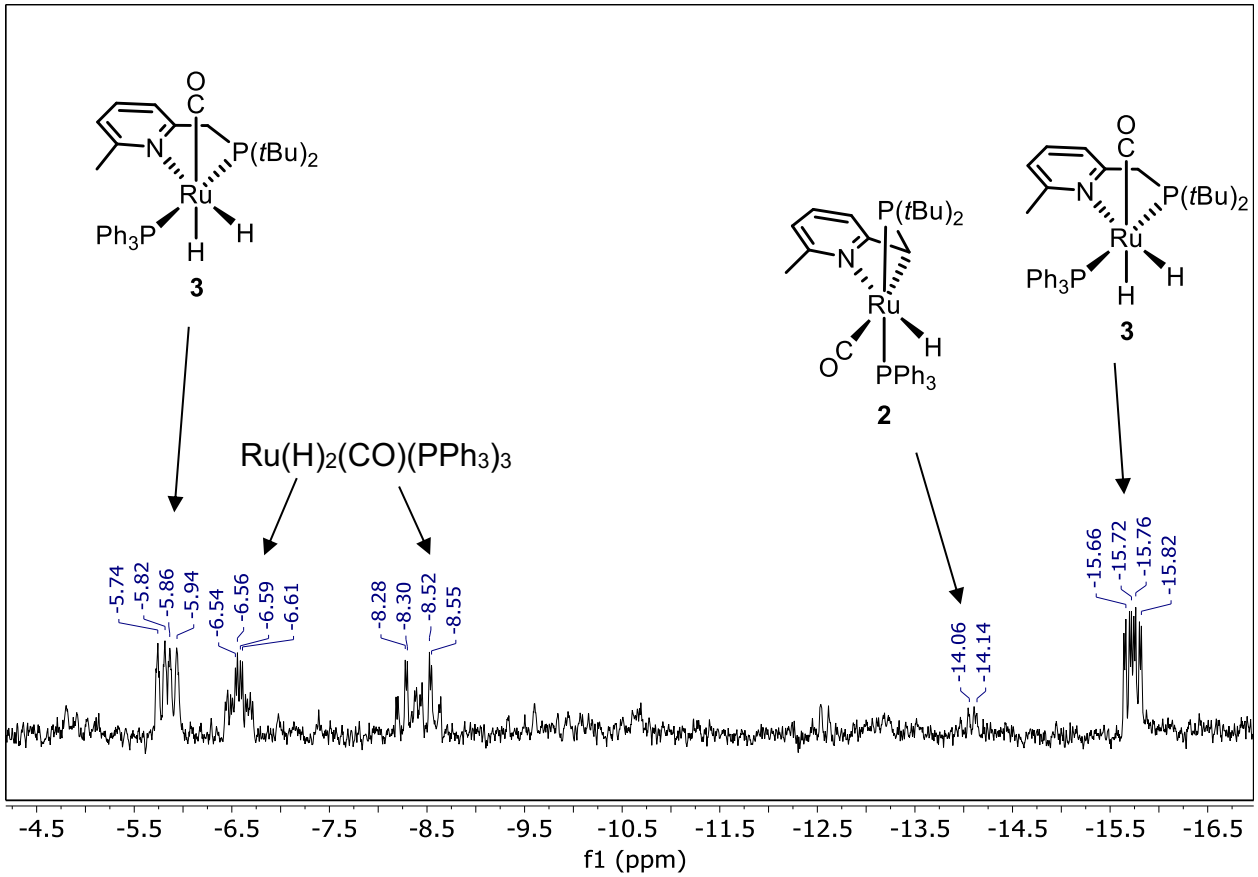

Figure S16. 300 MHz ^{1}H NMR spectrum of the hydride region of complex **3** in C_7D_8 after heating to 110 °C for 4 h. The resonances at -5.6 ppm and -15.6 ppm are from **3**. Trace amounts of complex **2** can be observed at -14.1 ppm. $Ru(H)_2(CO)(PPh_3)$ can also be observed at -6.5 ppm and -8.5 ppm.

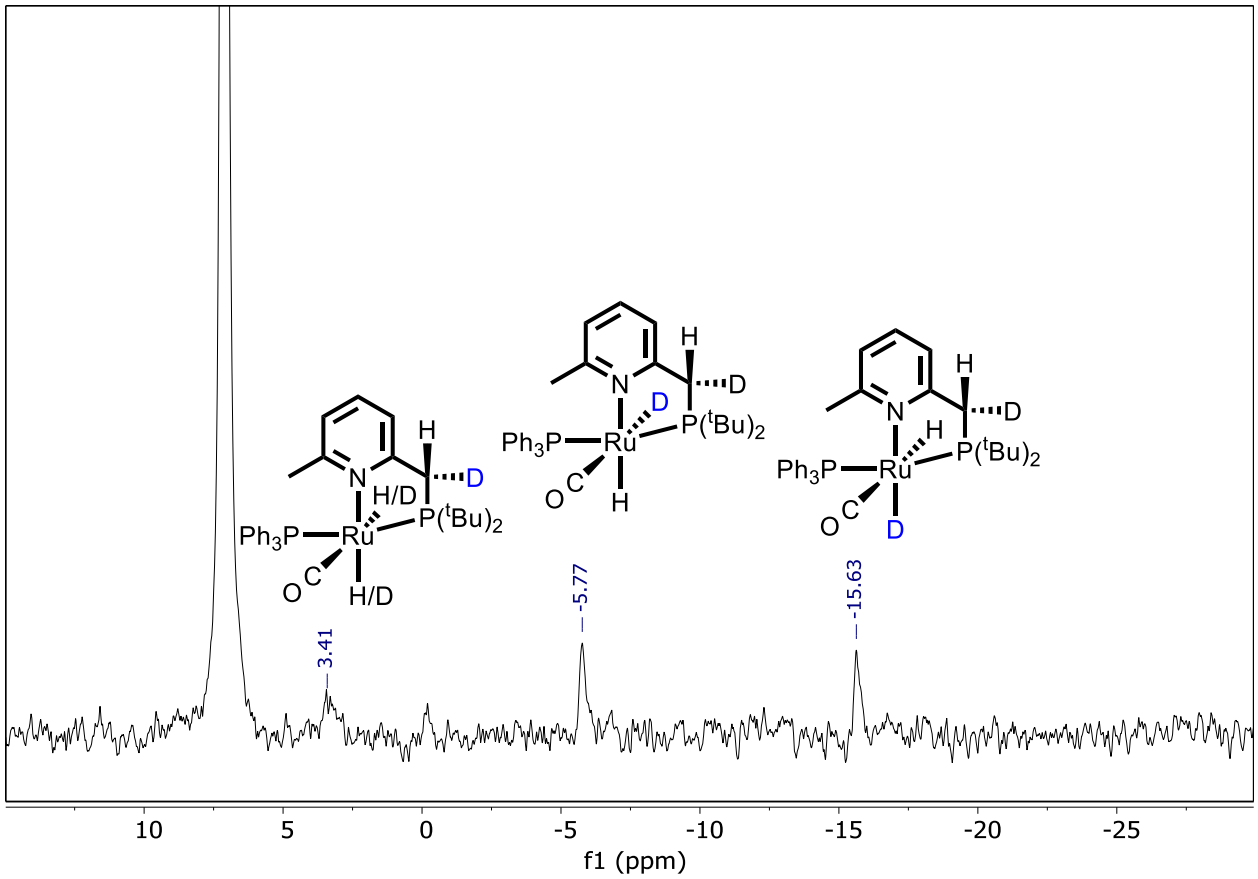

Figure S17. 500 MHz ^{2}H NMR spectrum of the reaction of **2** with D_2 in C_6H_6 after ~1.5 h under ambient light.

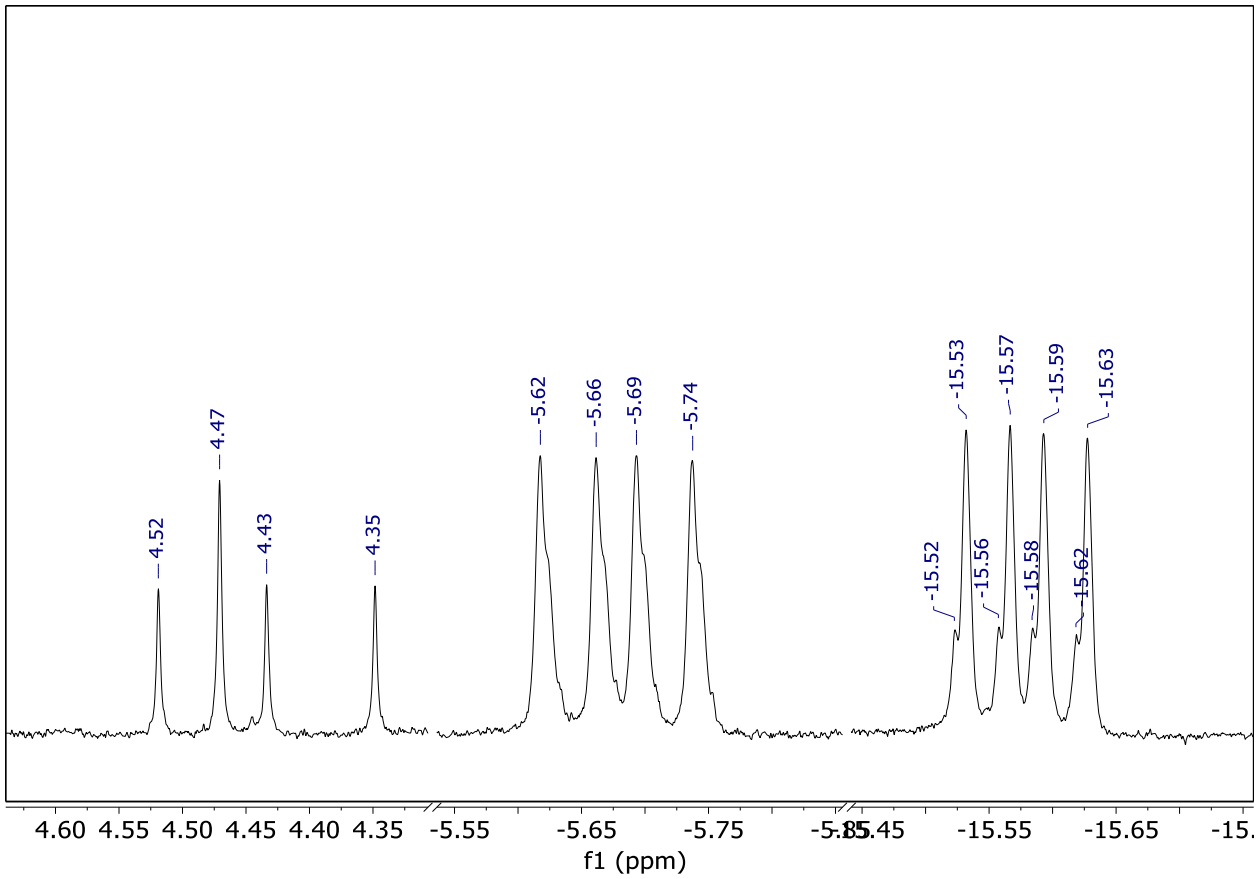

Figure S18. 500 MHz ^{1}H NMR spectrum of the reaction of **2** with D_2 in C_6D_6 after ~1 h under ambient light. Zoomed in on the H_2 (4.47 ppm) and HD (t, 4.43 ppm) resonances observed (left) and the hydride resonances (right).

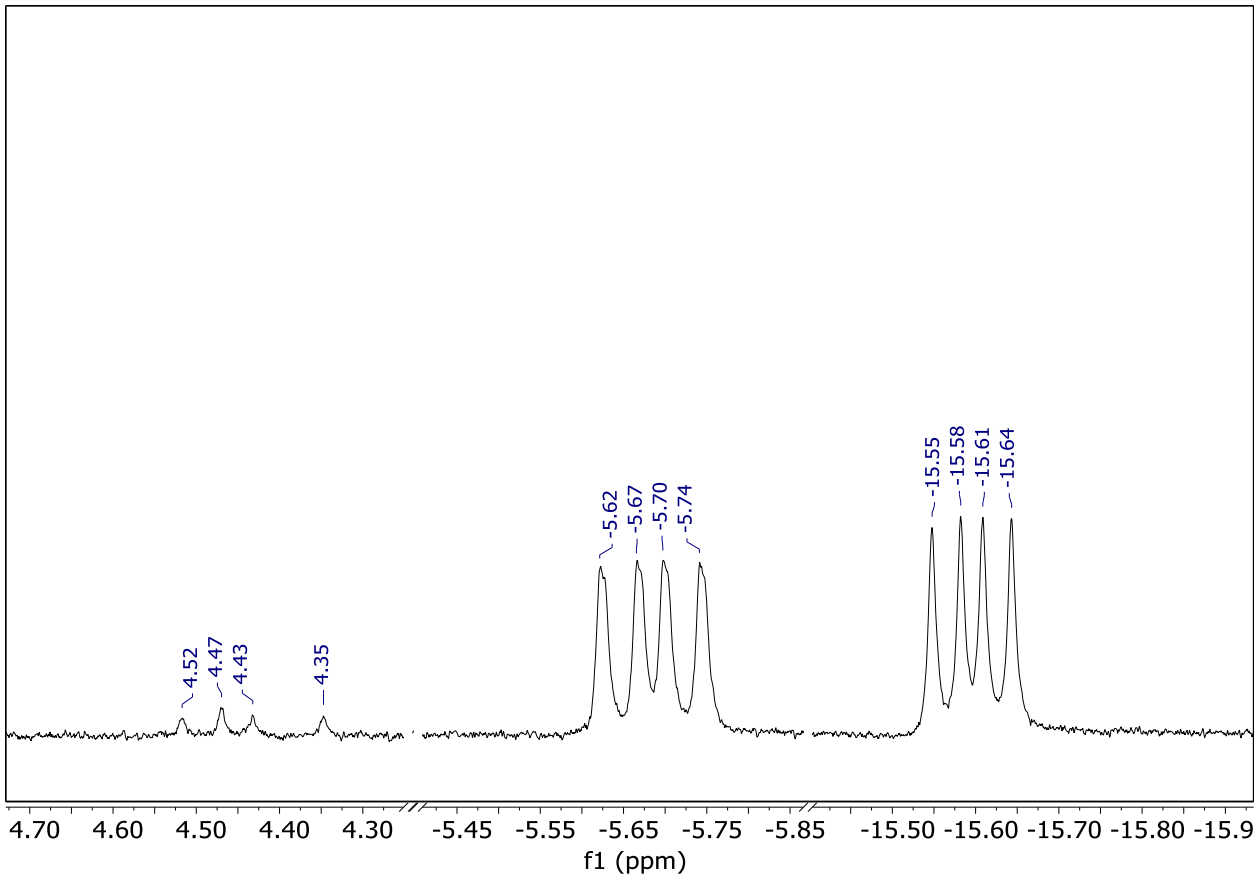

Figure S19. 500 MHz ^{1}H NMR spectrum of a solution of **2** treated with D_2 in C_6D_6 after 15 min in the dark. Zoomed in on the H_2 (4.47 ppm) and HD (t, 4.43 ppm) resonances observed (left) and the hydride resonances (right).

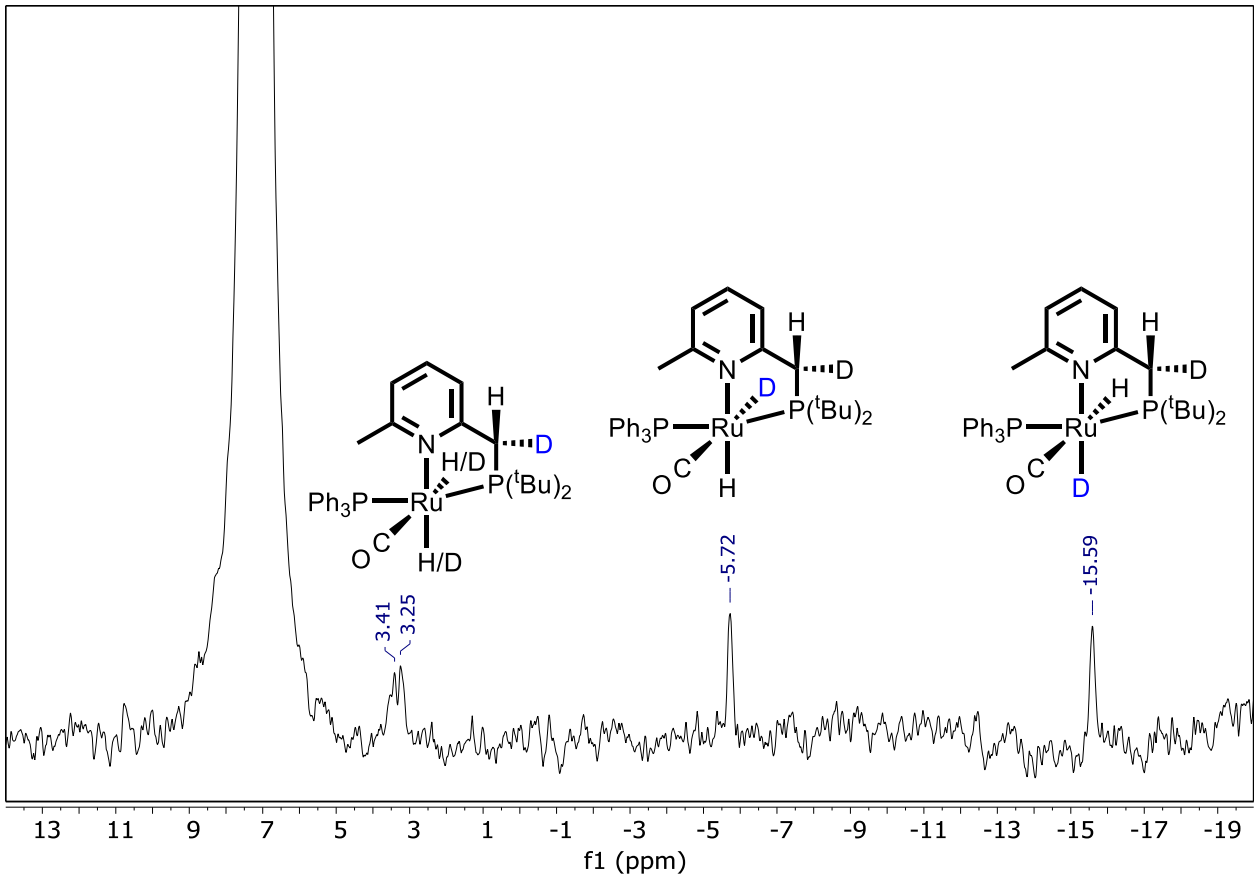

Figure S20. 500 MHz ^{2}H NMR spectrum of a solution of **2** treated with D_2 in C_6H_6 spiked with C_6D_6 after 30 min in the dark.

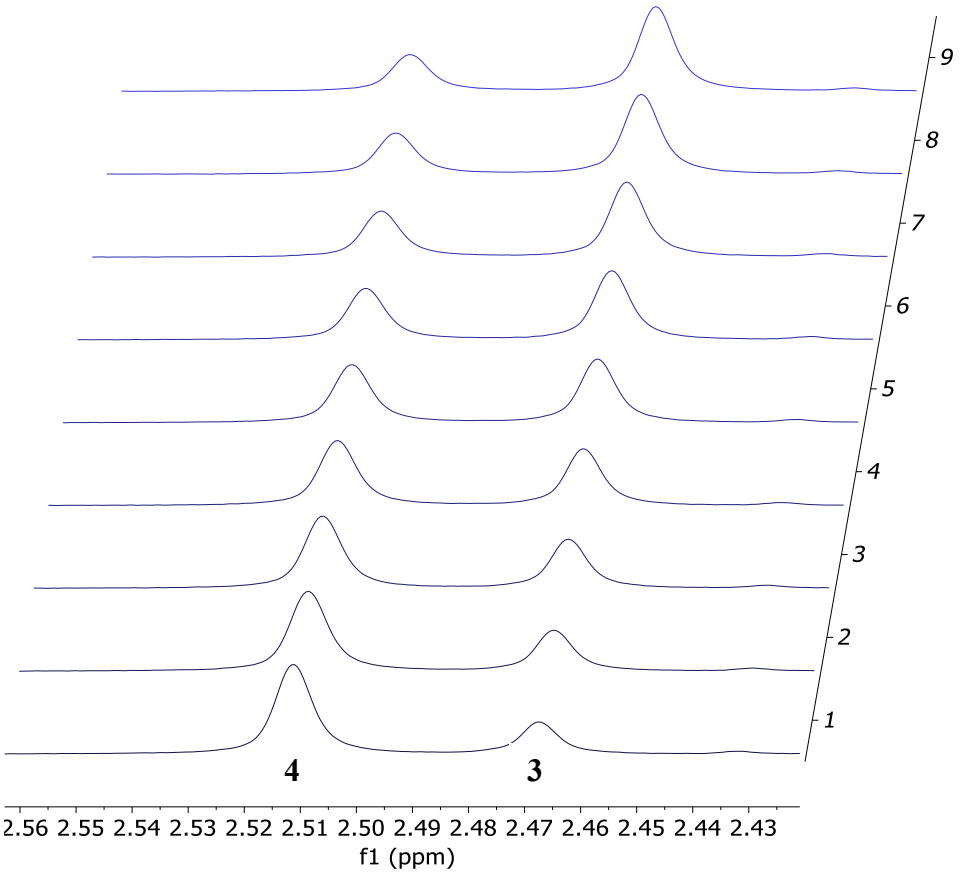

Figure S21. 300 MHz ^{1}H NMR spectra of the δ_{CH3} of **3** and **4** over the course of 2.5 h (bottom to top) after 1 h of broadband irradiation of a solution of **3** in C_6D_6 at 23 °C under N_2(g).

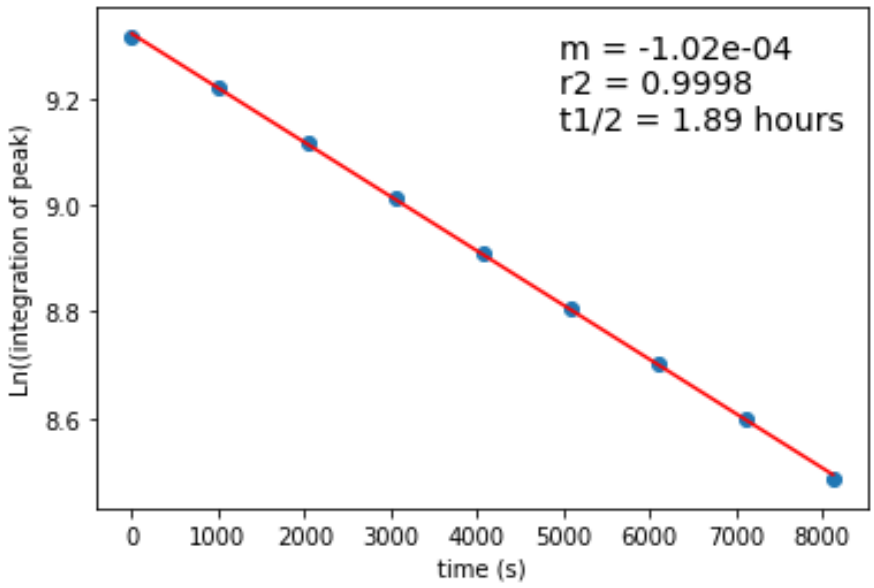

Figure S22. Plot of the ln of the peak area of the δ_{CH3} of **4** versus time (*s*) under N_2(g).

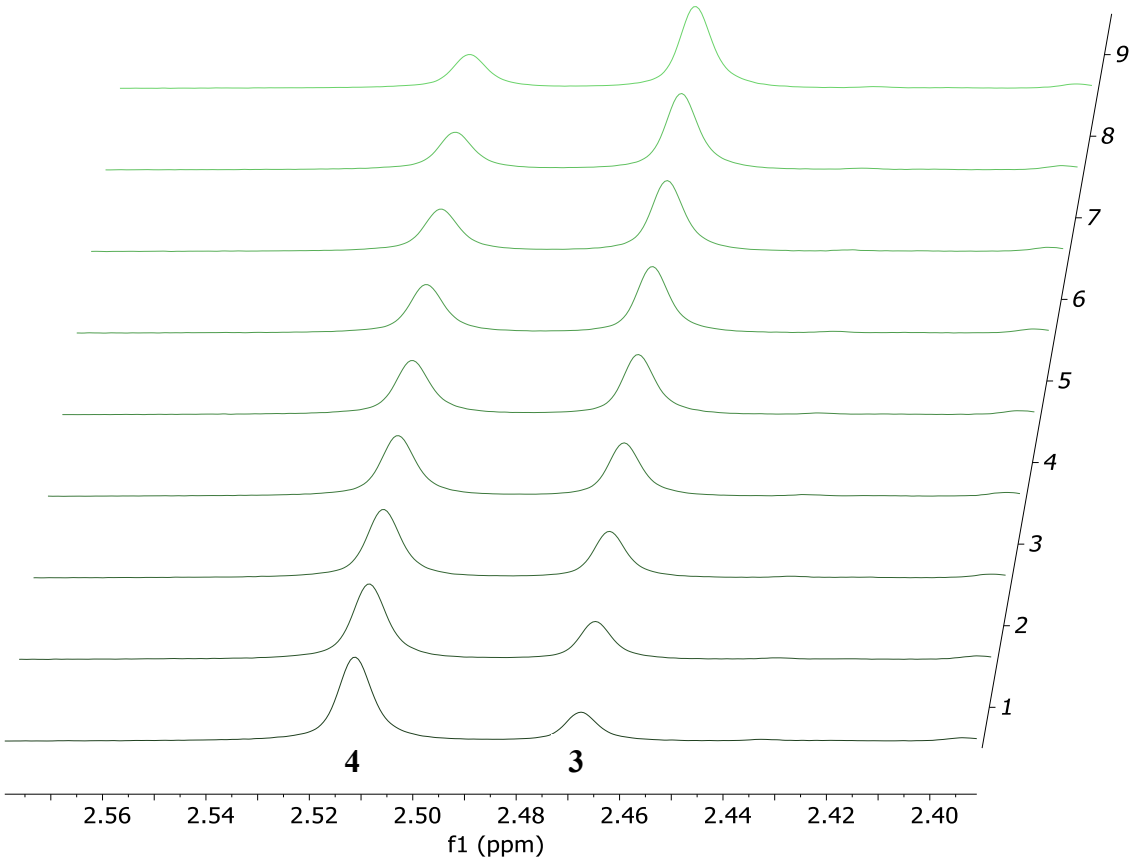

Figure S23. 300 MHz ^{1}H NMR spectra of the δ_{CH3} of **3** and **4** over the course of 2.5 h (bottom to top) after 1 h of broadband irradiation of a solution of **3** in C_6D_6 at 23 °C under static-vacuum.

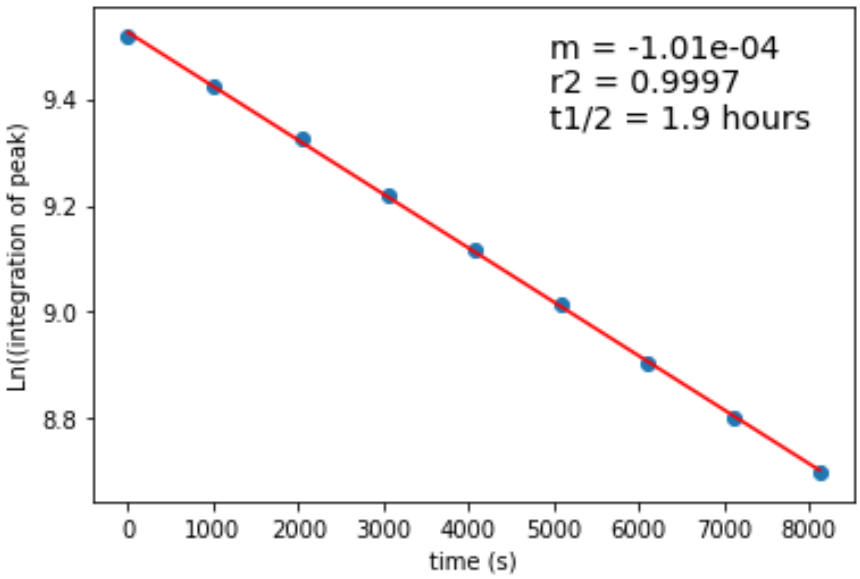

Figure S24. Plot of the ln of the peak area of the δ_{CH3} of **4** versus time (*s*) under static-vacuum.

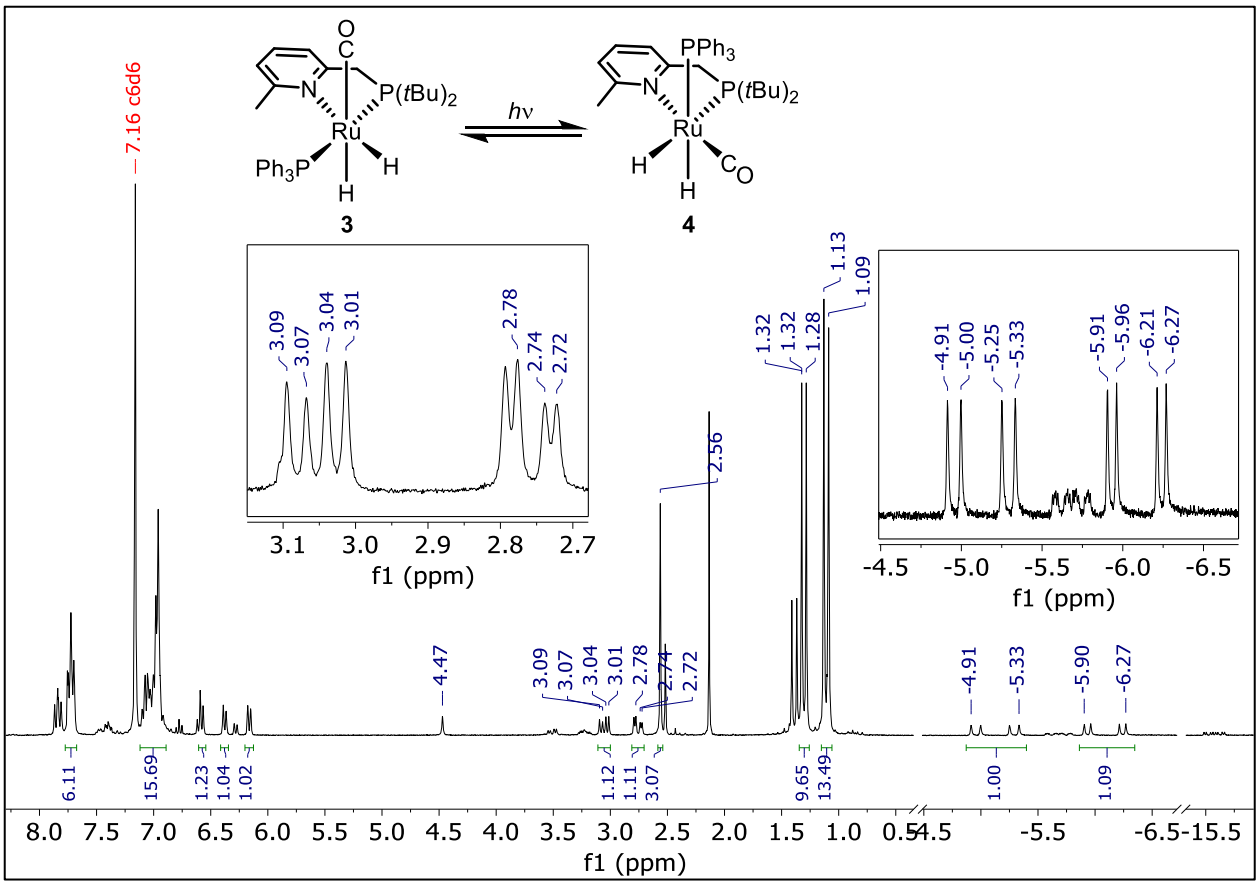

Figure S25. 500 MHz ^{1}H NMR spectrum of a solution of **3** in C_6D_6 under H_2 after 1 h of broadband irradiation at 23 °C. The integrated resonances are from complex **4**.

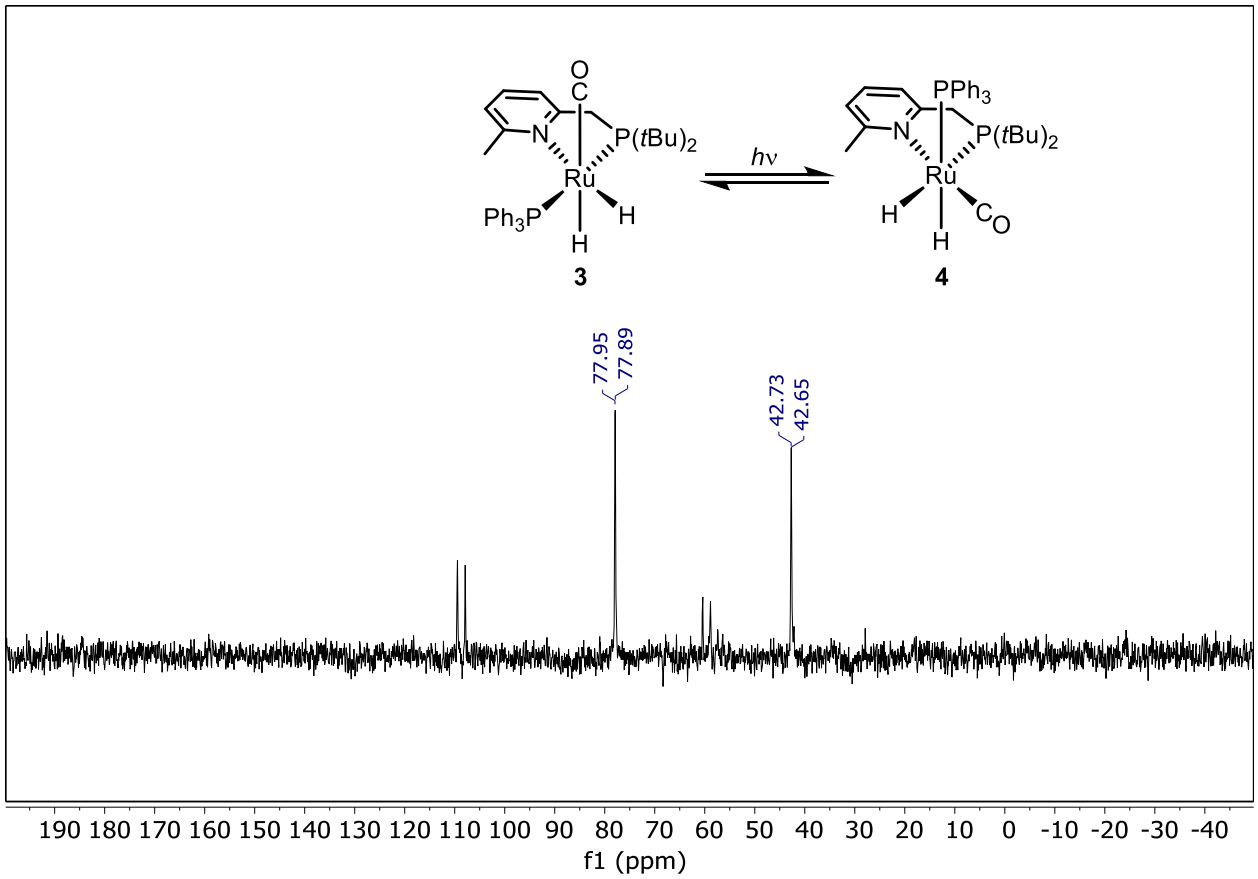

Figure S26. 121 MHz ^{31}P $\{^{1}H\}$ NMR of a solution of **3** in C_6D_6 under H_2 after 1 h of broadband irradiation at 23 °C. The labelled peaks are for compound **4**. The unlabeled resonances at ~109 ppm and ~60 ppm are from complex **3**.

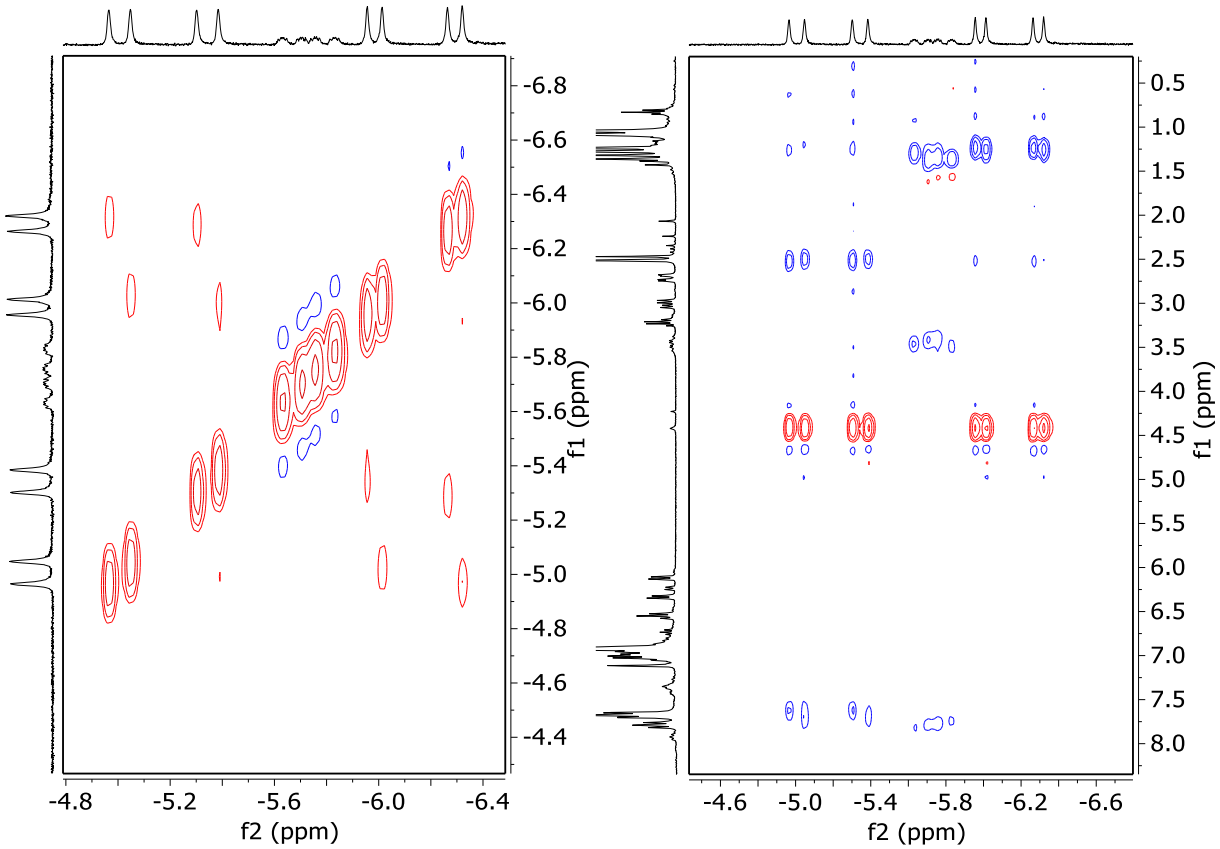

Figure S27. 300 MHz ^{1}H-^{1}H ROESY spectrum of a solution of **3** in C_6D_6 under H_2(g) after 1 h of broadband irradiation at 23 °C. (left) Zoomed in on the hydride-hydride exchange correlation, (right) other correlations seen with the hydride resonances. Blue represents through space coupling and red represents exchange coupling.

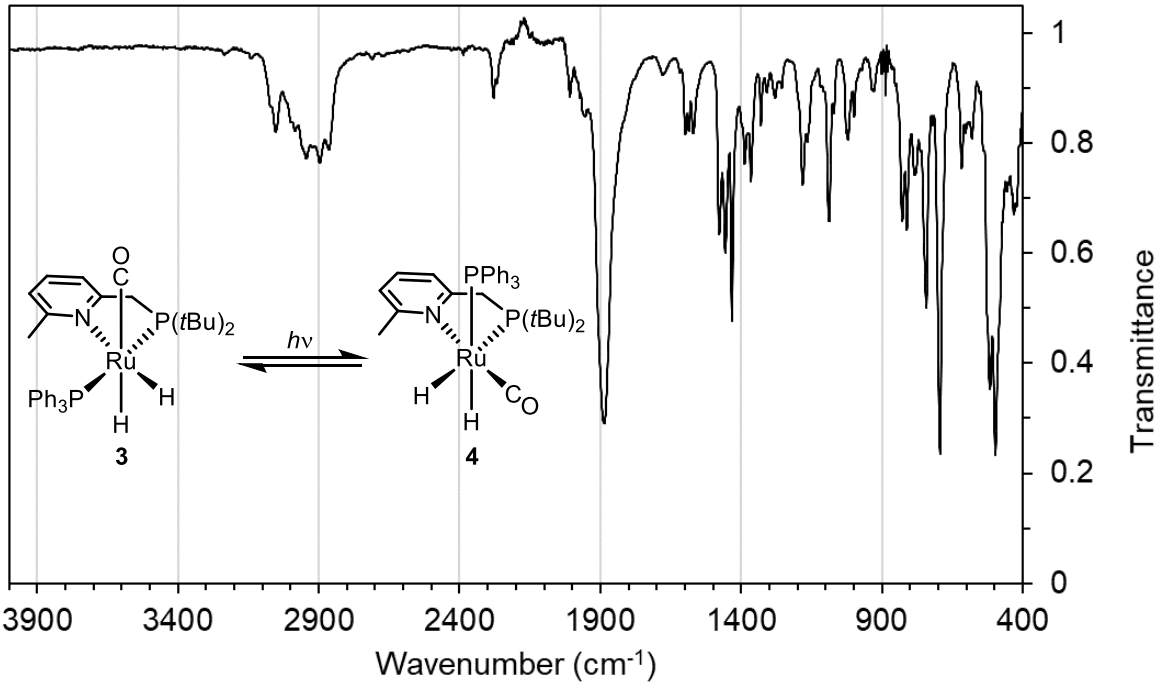

Figure S28. FTIR-ATR spectrum of a solution of **3** in C_6D_6 under H_2(g) after 1 h of broadband irradiation at 23 °C.

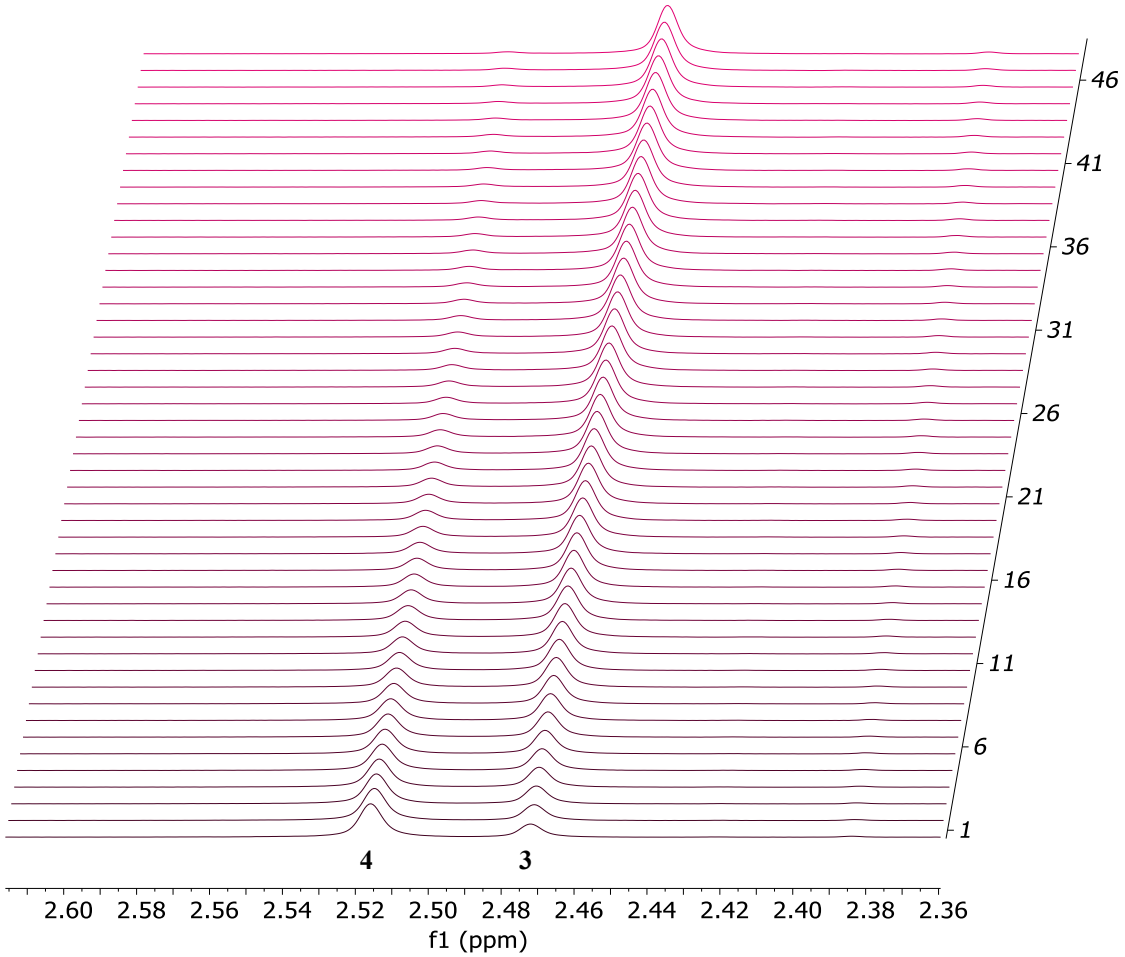

Figure S29. 300 MHz ^{1}H NMR spectra of the δ_{CH3} of **3** and **4** over the course of 2.5 h (bottom to top) after 1 h of broadband irradiation of a solution of **3** in C_6D_6 at 23 °C under H_2(g).

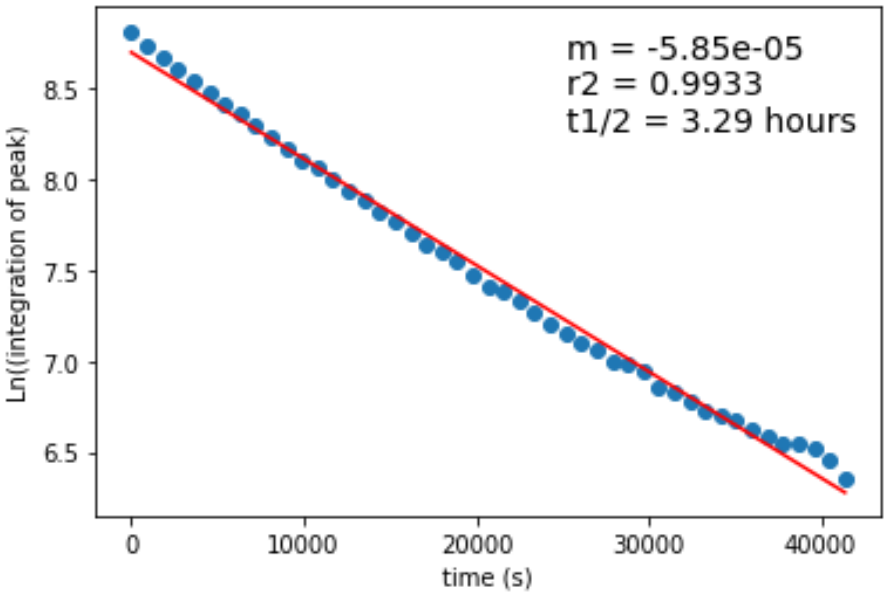

Figure S30. Plot of the ln of the peak area of the δ_{CH3} of **4** versus time (*s*) under H_2(g).

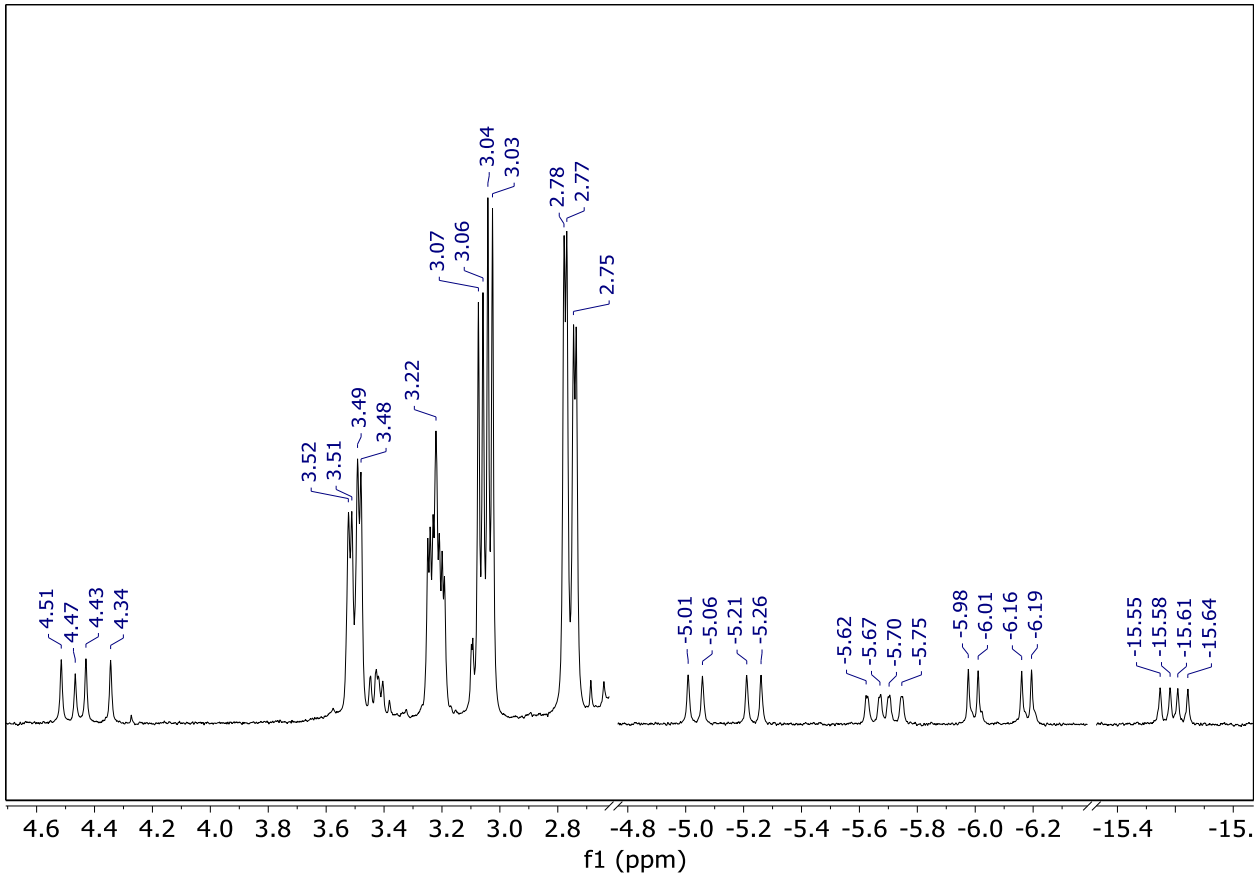

Figure S31. 500 MHz ^{1}H NMR spectrum of a solution of **3** in C_6D_6 under D_2 after irradiation with a 345 nm cutoff filter for 1 h at 23 °C. (left) The H_2 (4.47 ppm) and HD (t, 4.43 ppm) resonances observed. (middle) Zoomed in on the δ_{CH2} of **3** and **4**. (right) Zoomed in on the hydride region.

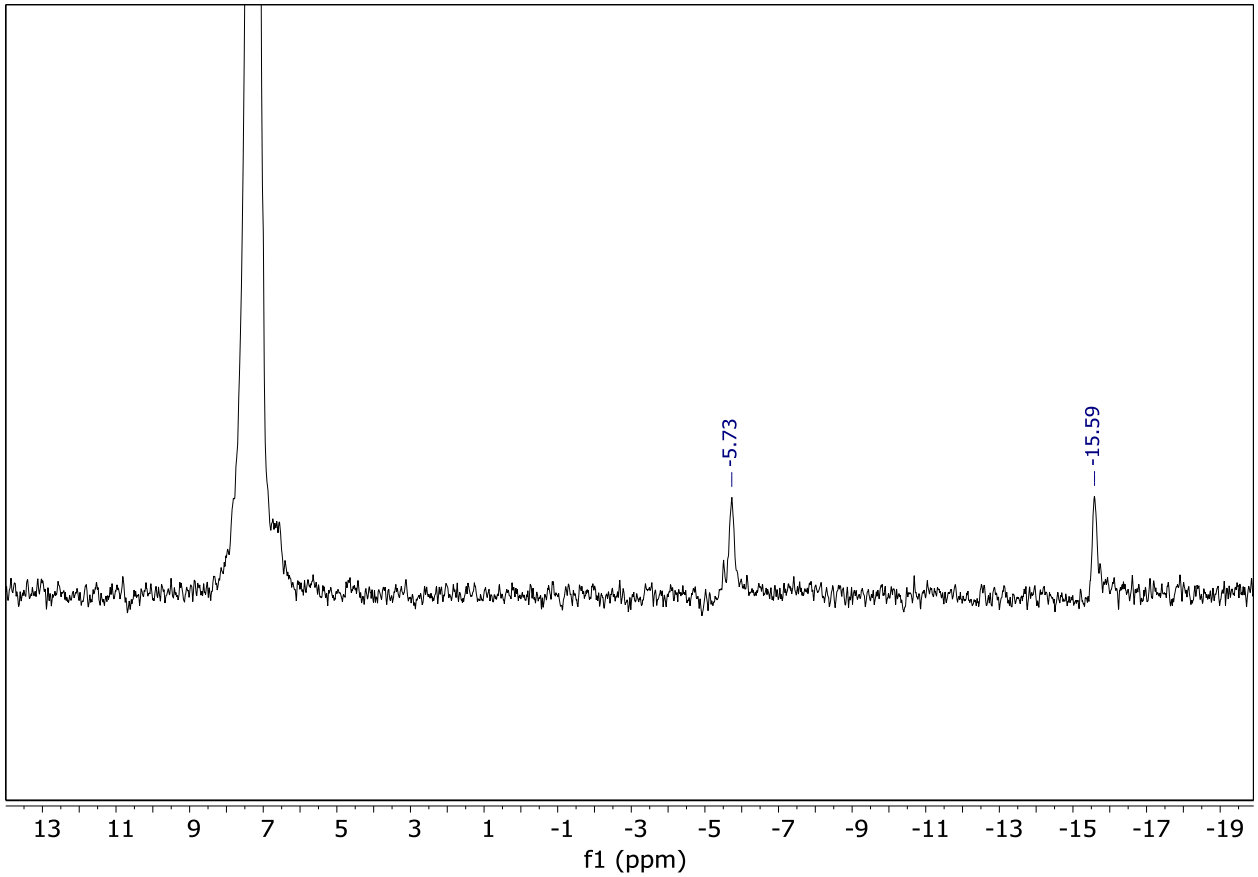

Figure S32. 500 MHz ^{2}H NMR spectrum of a solution of **3** in C_6H_6 spiked with C_6D_6 under D_2 after irradiation with a 345 nm cutoff filter for 1 h at 23 °C.

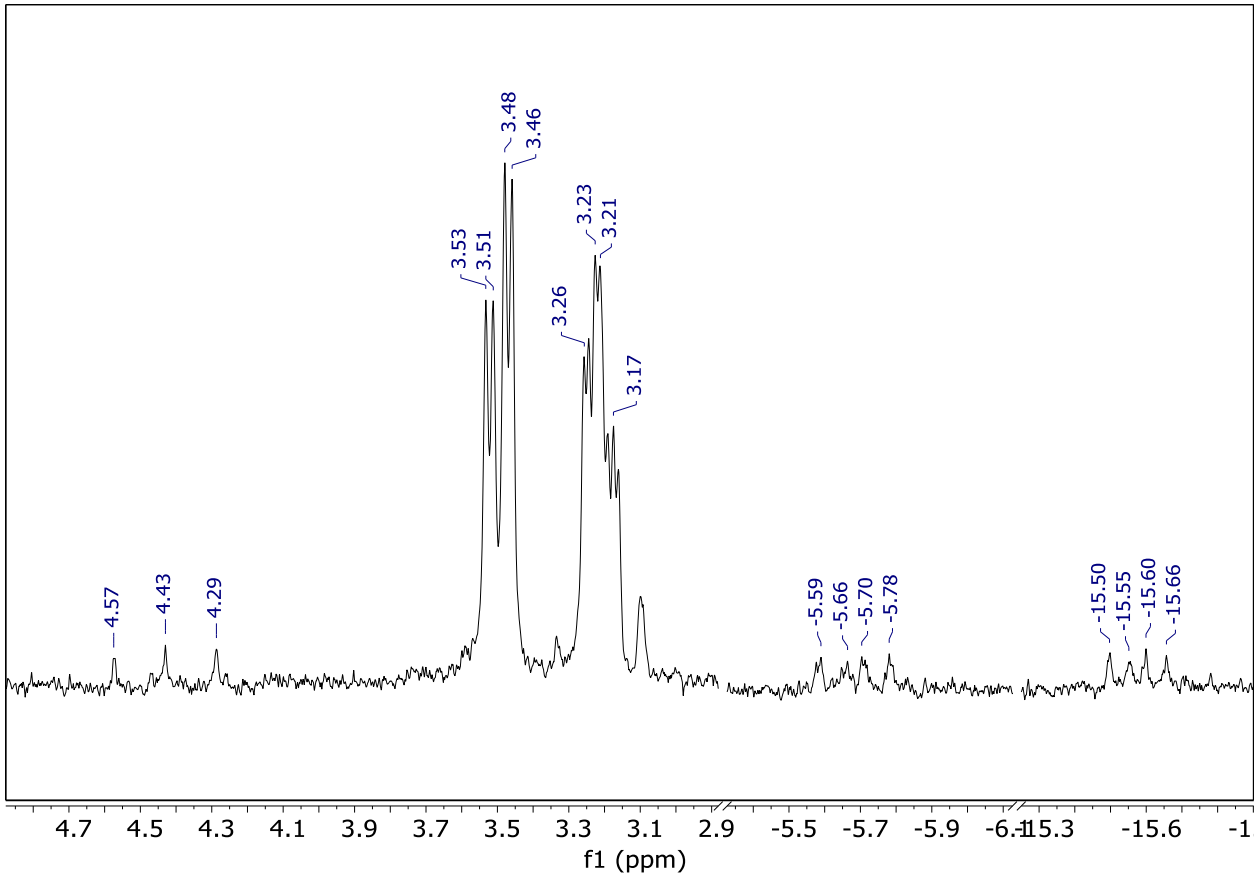

Figure S33. 300 MHz ^{1}H NMR spectrum of a solution of **3** in C_6D_6 under D_2 after 4 days in the dark. (left) The trace H_2 (4.47 ppm) and HD (t, 4.43 ppm) resonances observed. (middle) Zoomed in on the δ_{CH2} of 3. (right) Zoomed in on the hydride region.

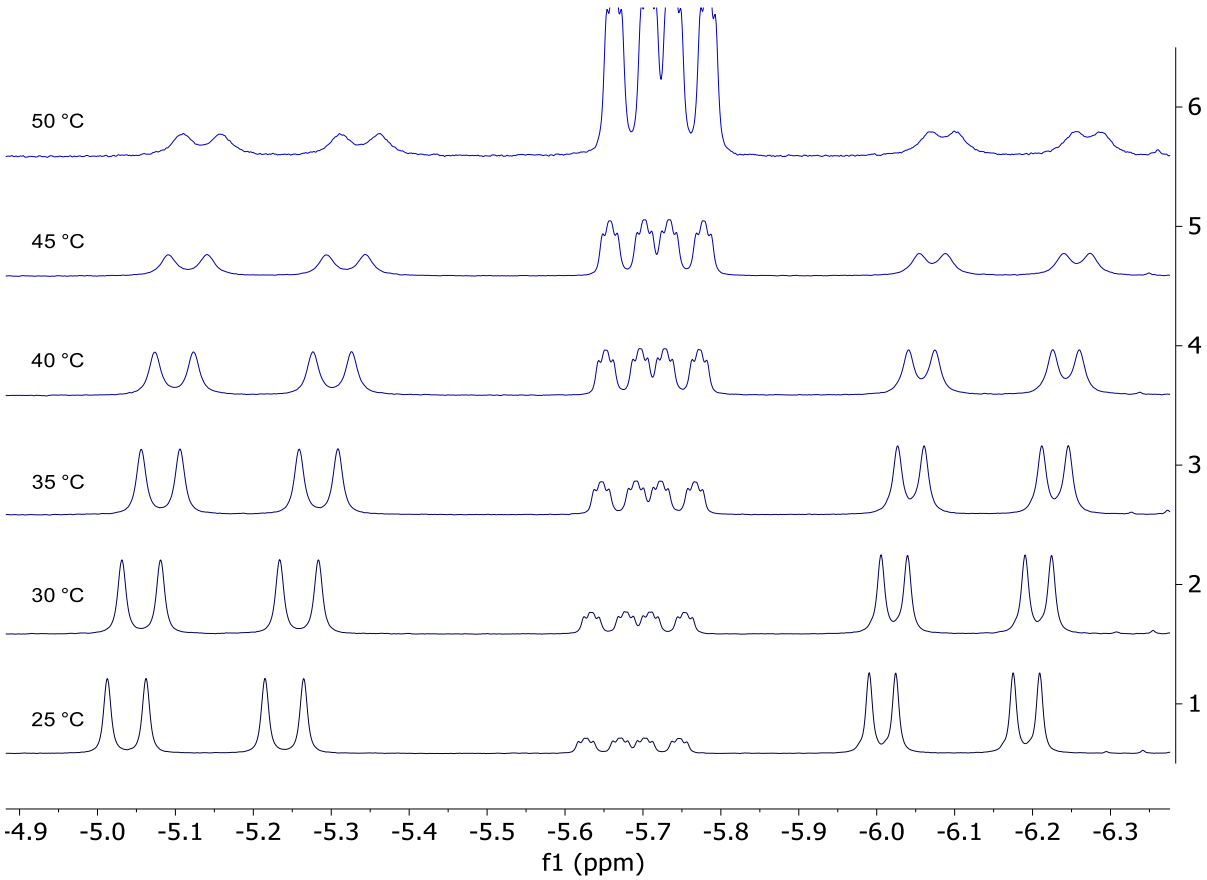

Figure S34. A VT 500 MHz ^{1}H NMR spectra of a solution of **4** in C_6D_6 under H_2(g) (1 atm) at 25–50 °C.

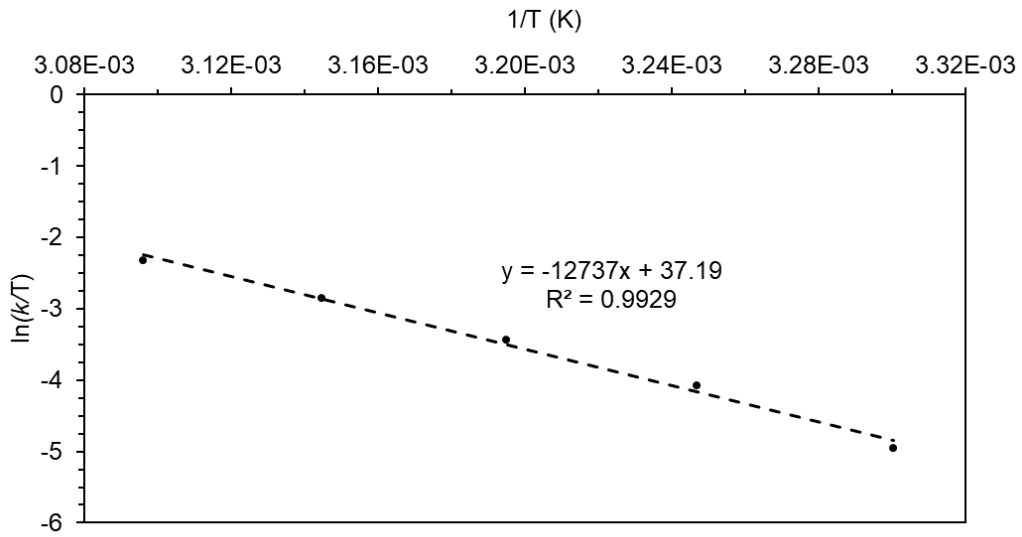

Figure S35. Representative Eyring plot of the rates of exchange obtained from line width analysis of the hydride resonances of **4** under H_2 (1 atm). The barrier ($\Delta G^{\ddagger}$ = 17.2 ± 0.17 kcal·mol^{-1}) was calculated from the slope ($\Delta H^{\ddagger}$ = 24.0 ± 1.2 kcal·mol^{-1}) and x-intercept ($\Delta S^{\ddagger}$ = 22.9 ± 3.4 cal·K^{-1}·mol^{-1}). VT studies were carried out between 25 °C – 50 °C.

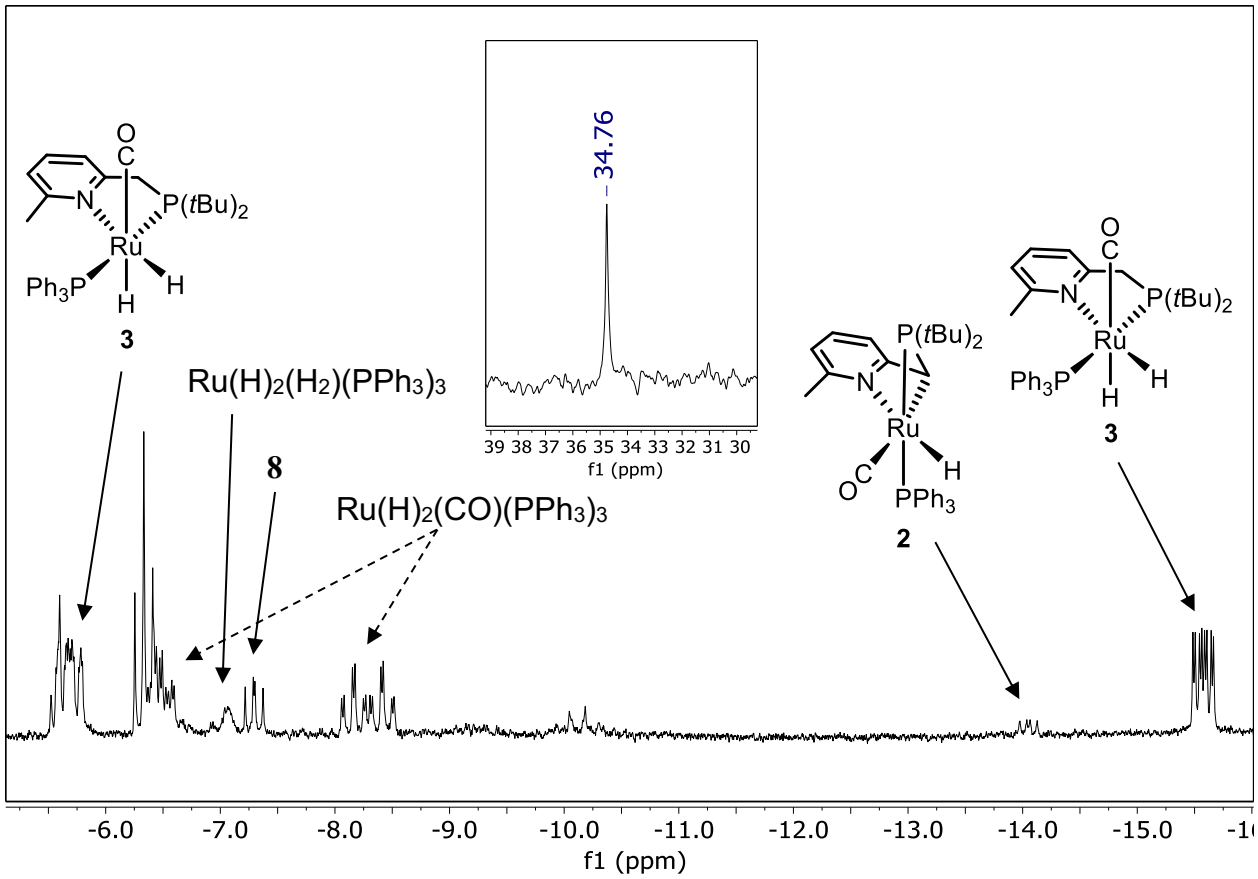

Figure S36. 300 MHz ^{1}H NMR of a solution of **3** and 10 equiv. PPh_3 in C_6D_6 after 2 h of broadband irradiation at 23 °C zoomed in on the hydride region. Unlabeled peaks are unknown products. (insert) 121 MHz $^{31}P\{^{1}H\}$ NMR of free ligand observed.

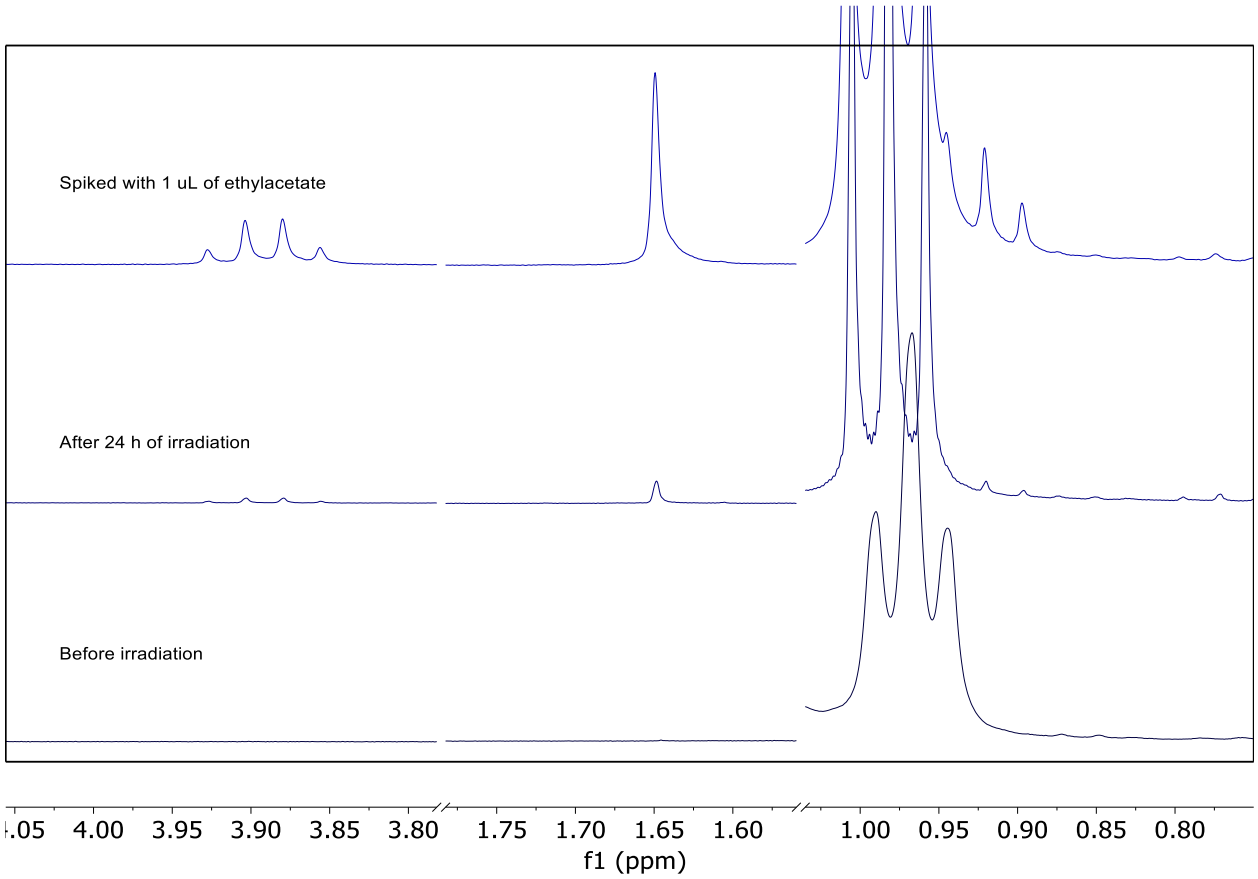

Figure S37. 300 MHz ^{1}H NMR spectra of a solution of 0.00310 mmol of **3** in C_6D_6 with 0.155 mmol of ethanol before irradiation (bottom), after 24 h of irradiation with a 345 nm cutoff filter (middle), and after spiking the sample with 1 µL of ethyl acetate.

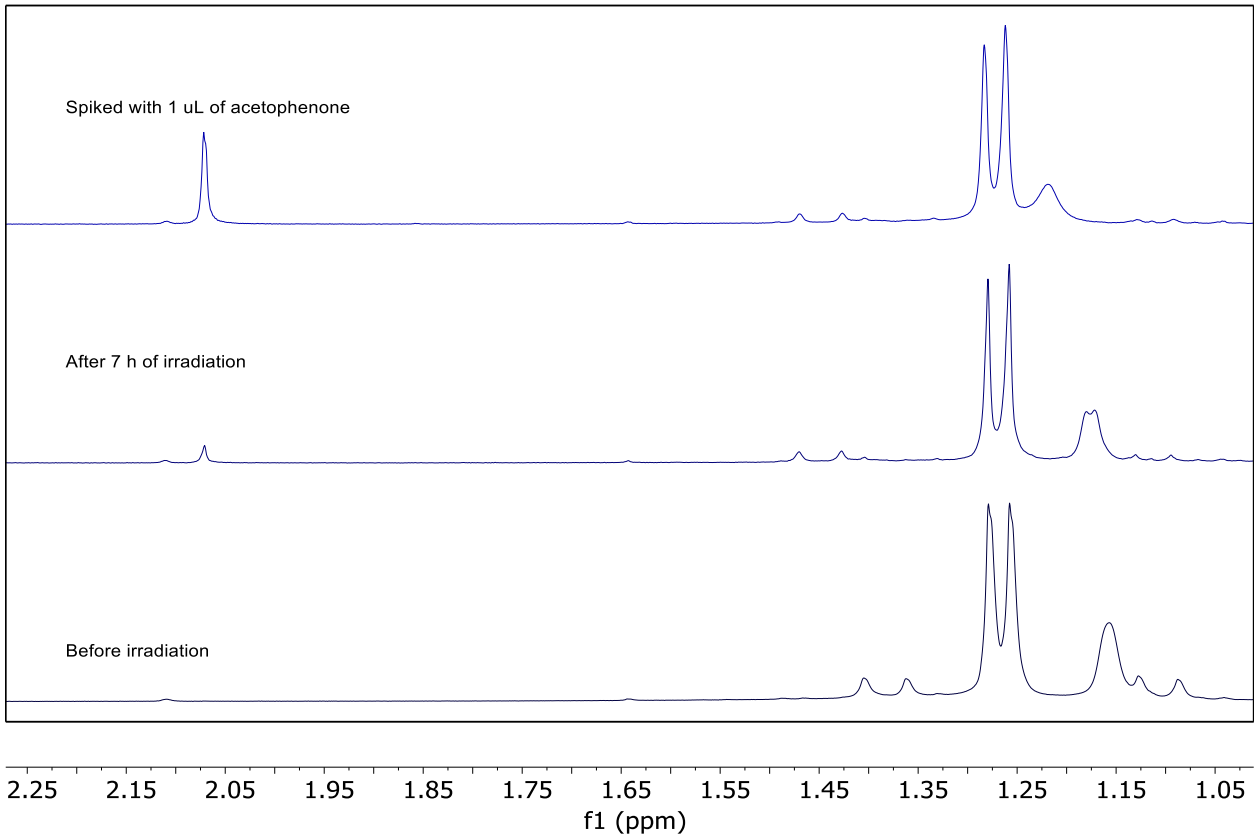

Figure S38. 300 MHz ^{1}H NMR spectra of a solution of 0.00310 mmol of **3** in C_6D_6 with 0.0931 mmol of 1-phenylethanol before irradiation (bottom), after 7 h of irradiation with a 345 nm cutoff filter (middle), and after spiking the sample with 1 µL of acetophenone.

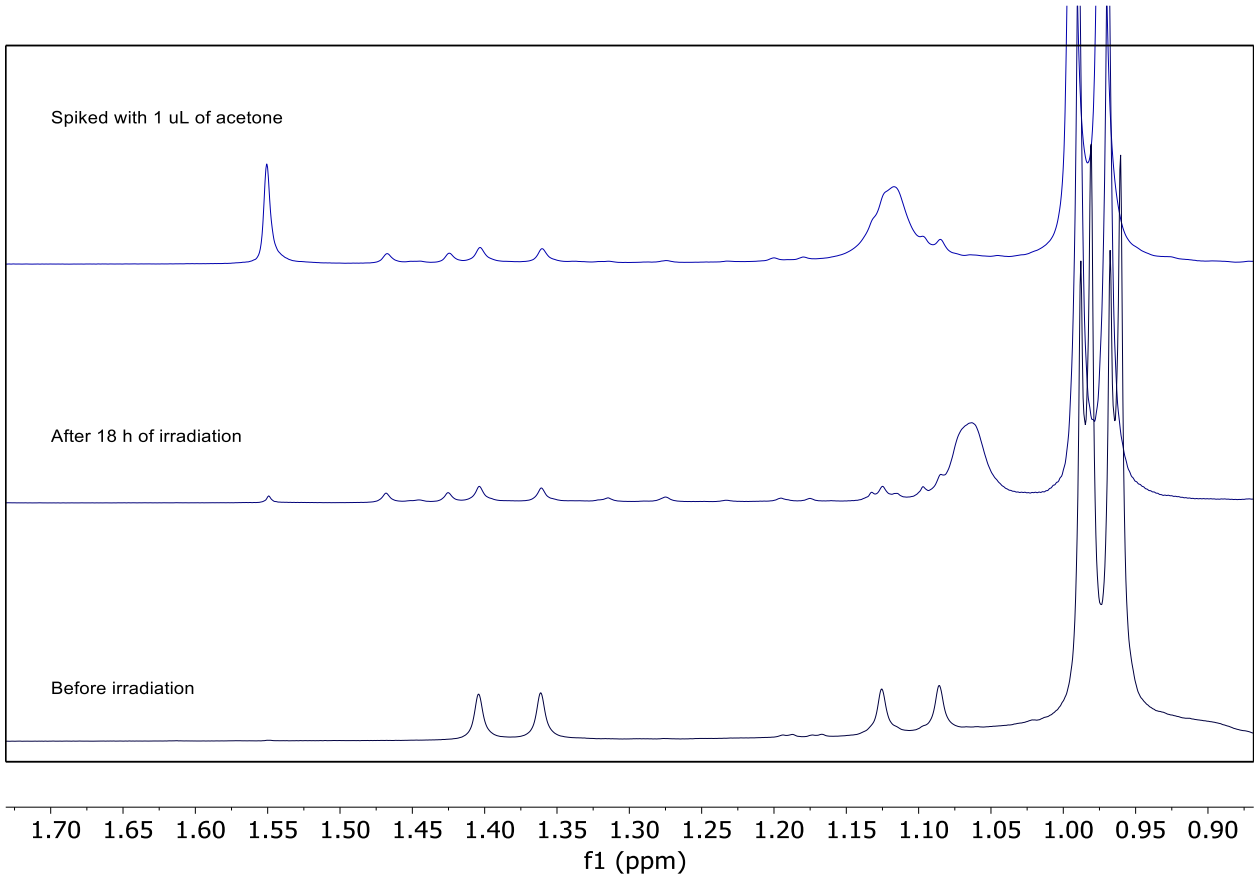

Figure S39. 300 MHz ^{1}H NMR spectra of a solution of 0.00480 mmol of **3** in C_6D_6 with 0.0970 mmol of 2-propanol before irradiation (bottom), after 18 h of irradiation with a 345 nm cutoff filter (middle), and after spiking the sample with 1 μL of acetone.

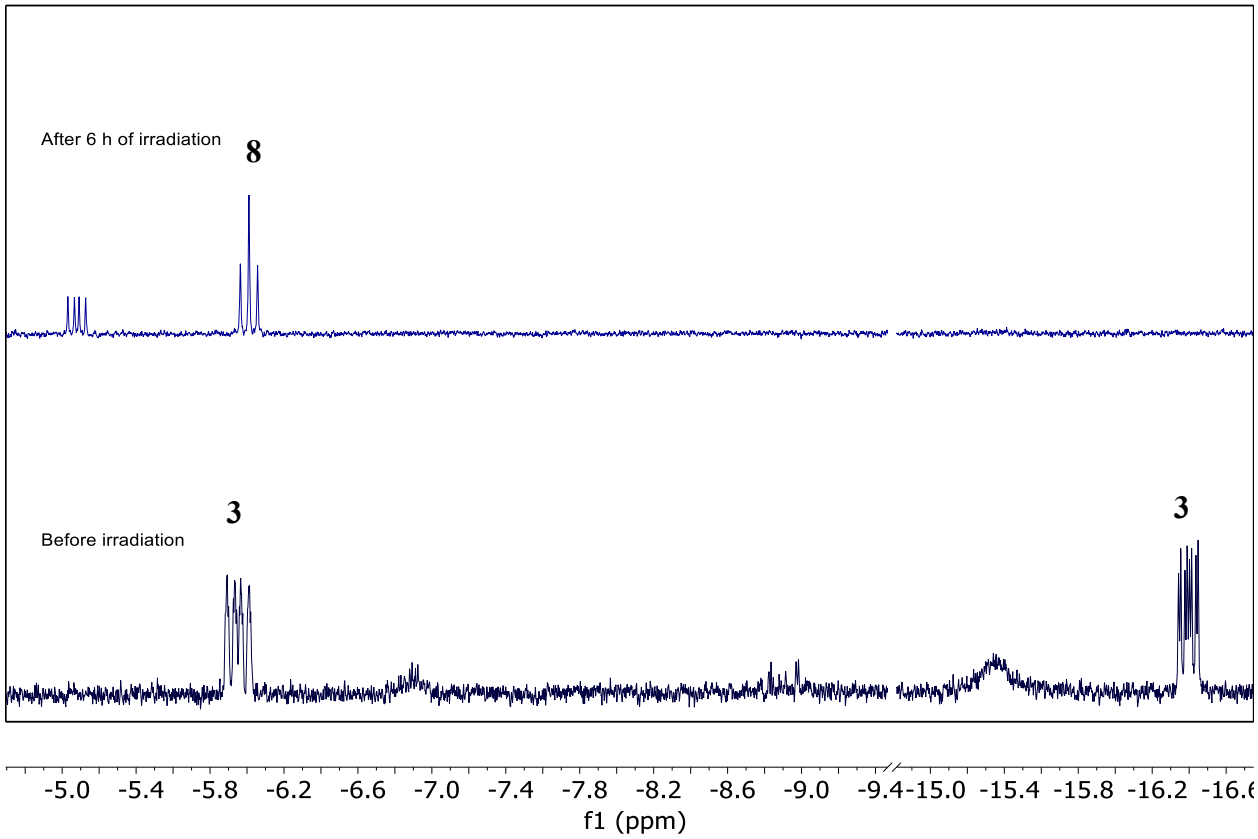

Figure S40. 500 MHz ^{1}H NMR spectra of the hydride region of a solution of 0.0030 mmol of **3** in CD_3OD before irradiation (bottom) and after 6 h of irradiation with a 345 nm cutoff filter (top).

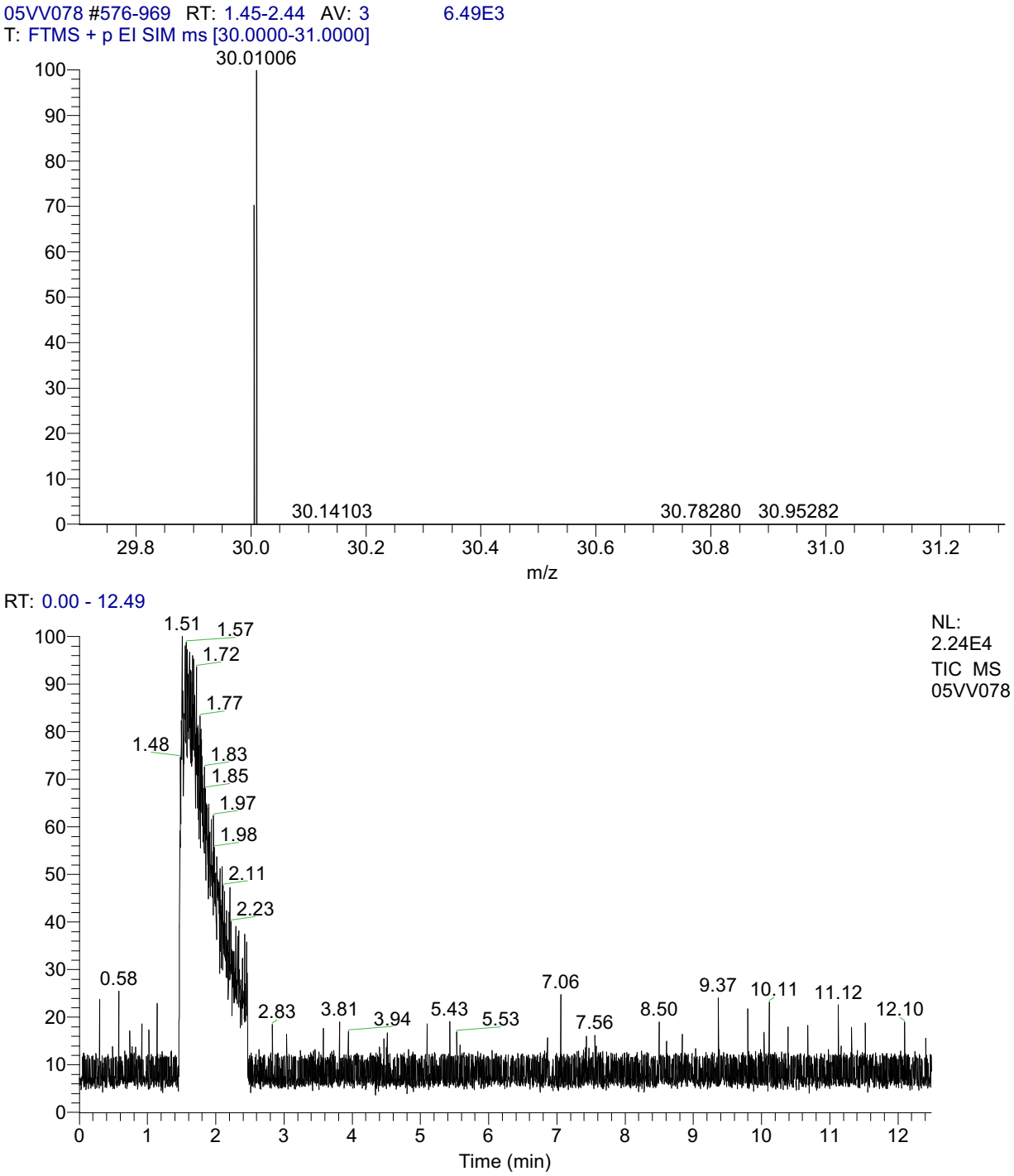

Figure S41. QE-GCMSMS headspace mass spectrum (above) and chromatogram (below) of an aliquot (10 µL) of a solution of **3** in methanol after 5 h of irradiation with a 345 nm cutoff filter at 23 °C. A broad peak at 1.50 minutes corresponded to a mass of 30.0101 amu which is in agreement to the formula CH_2O ($M_{calc'd}$ = 30.0106) with a 1.46 ppm error.

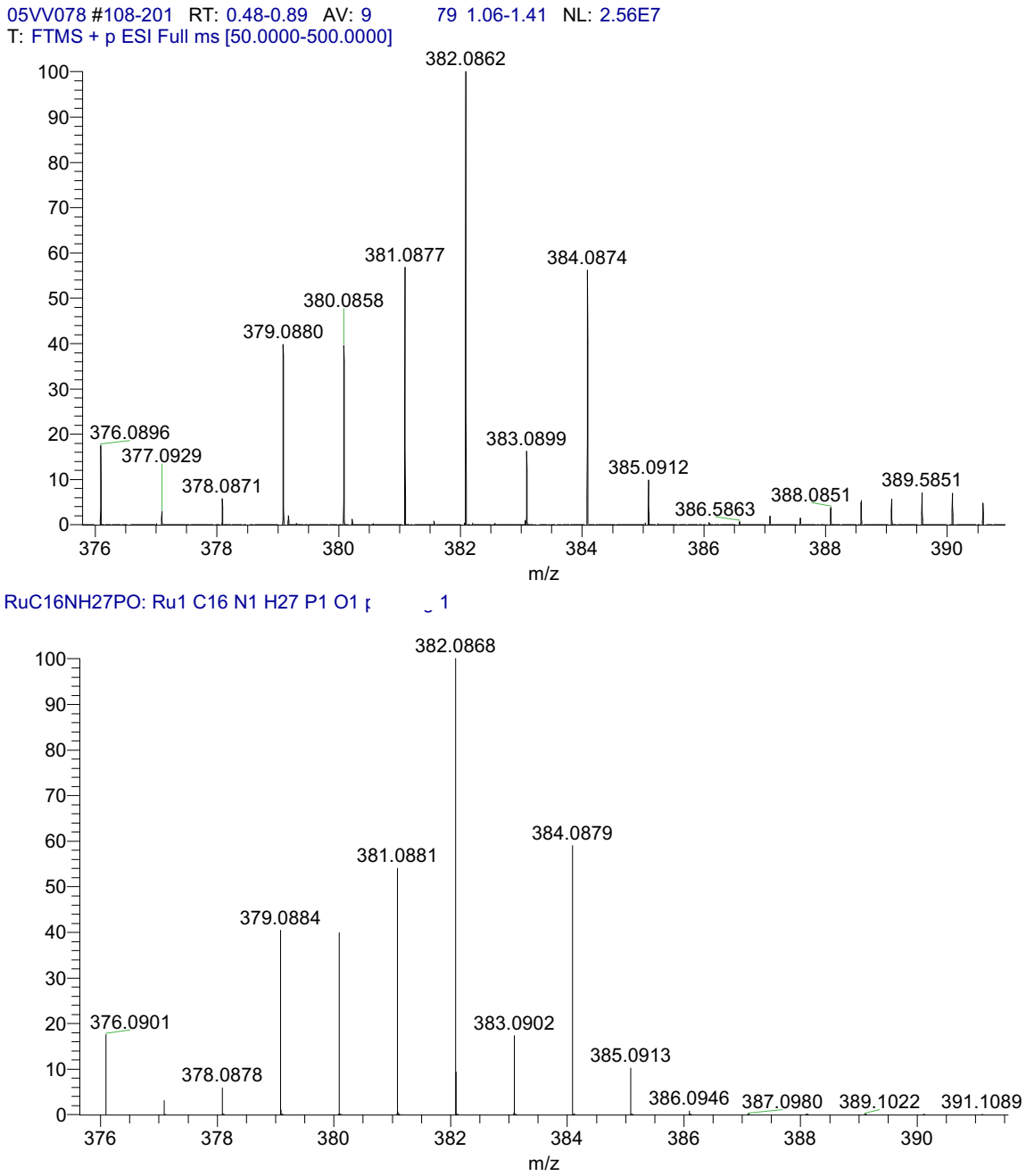

Figure S42. Direct injection (10 µL) of an aliquot of a solution of **3** in methanol after 5 h of irradiation with a 345 nm cutoff filter at 23 °C, exposed to ambient atmosphere, into a QE-LCMSMS (above) showed a peak consistent with the formula, $[Ru(H)(LutP)(CO)]^+$ ($[M+]_{calc'd}$ = 382.0868; $[M+]_{found}$ = 382.0862) and consistent with calculated isotopic distribution (below). A second peak consistent with carbonylation was observed ($[M+CO]_{calc'd}$ = 410.0817 ;$[M+CO]_{found}$ = 410.0811). In addition, peaks with masses consistent with oxidized LutP and triphenylphosphine were observed in the mass spectrum.

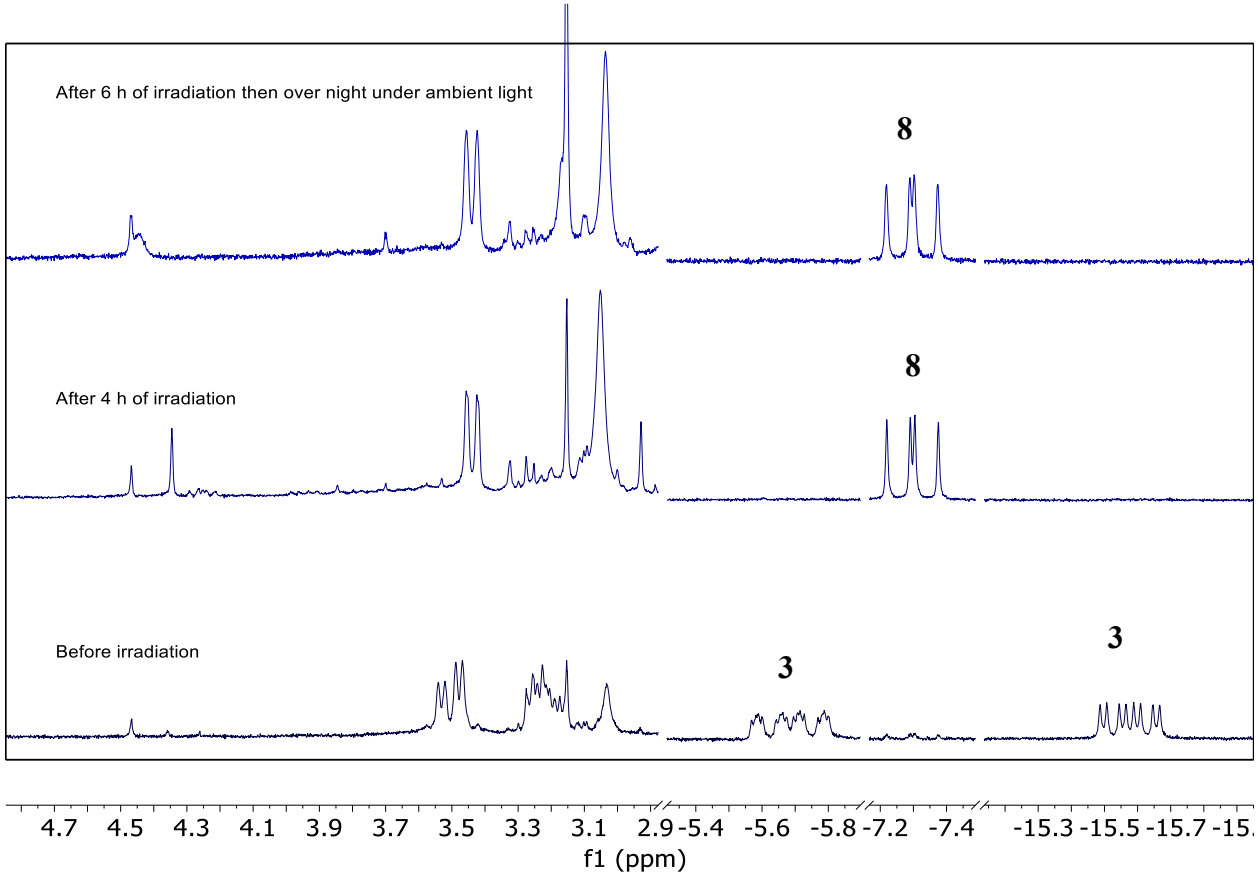

Figure S43. 300 MHz ^{1}H NMR spectra of a solution of 0.046 mmol of **3** in C_6D_6 and 0.057 mmol of paraformaldehyde before irradiation (bottom), after 4 h of irradiation with a 345 nm cutoff filter (middle), and after 6 h of irradiation with a 345 nm cutoff filter and left overnight in ambient light (top).

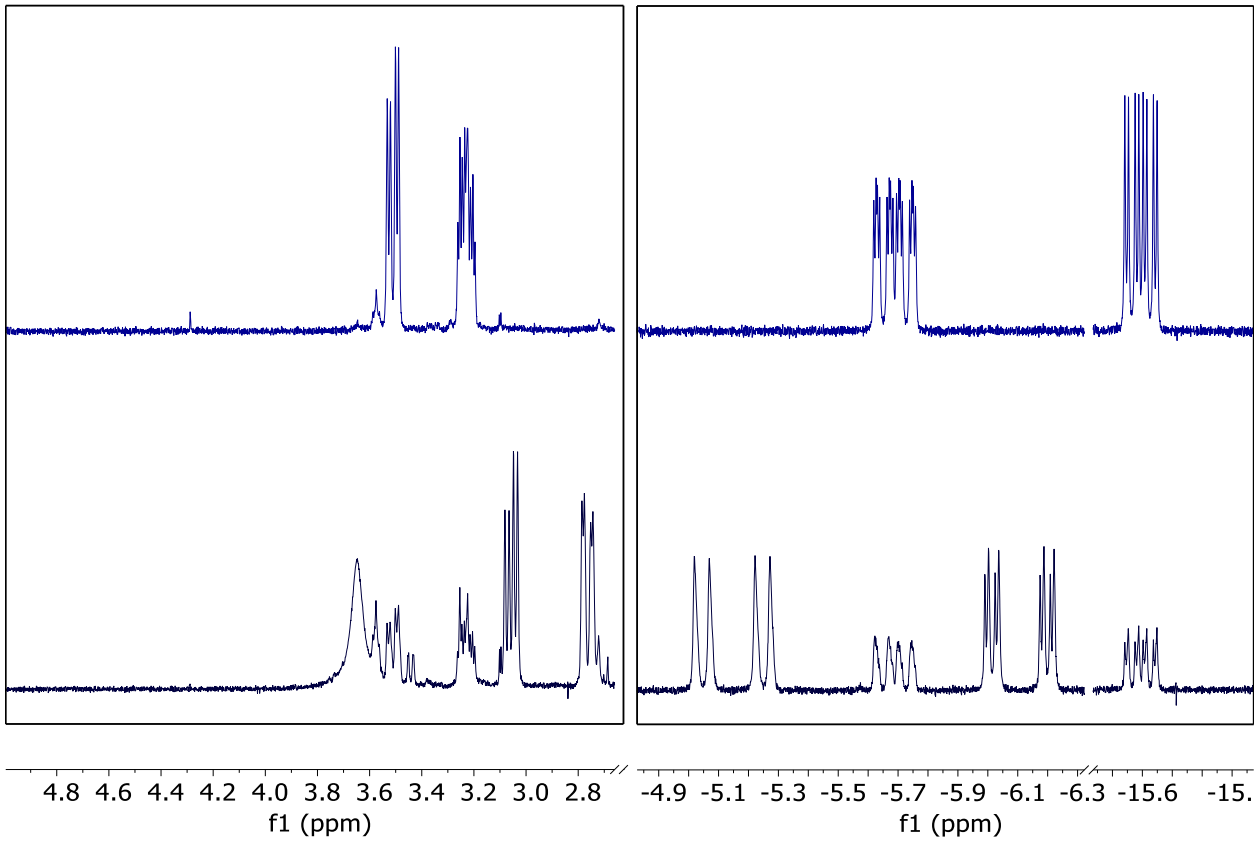

Figure S44. (top) 500 MHz ^{1}H NMR spectrum of a solution of **3** in C_6D_6 and 2-propanol-d_8. (bottom) The same solution after 1.5 h of broadband irradiation at 23 °C. (left) Zoomed in on the H_2, HD, and δ_{CH2} regions. (right) Zoomed in on the hydride region.

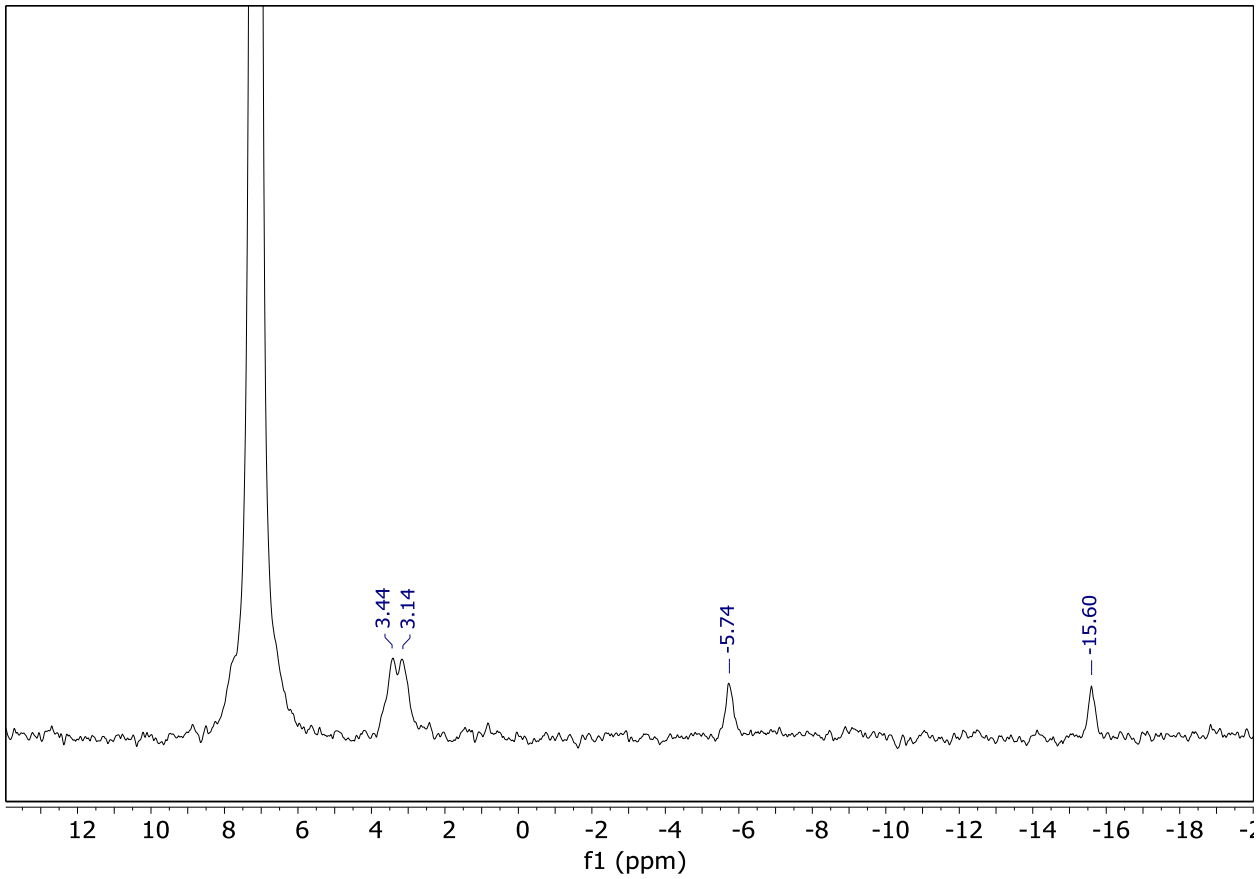

Figure S45. 500 MHz ^{2}H NMR spectrum of a solution of **3** in C_6H_6 (spiked with C_6D_6) and 2-propanol-d_8 after 1.5 h of broadband irradiation at 23 °C.

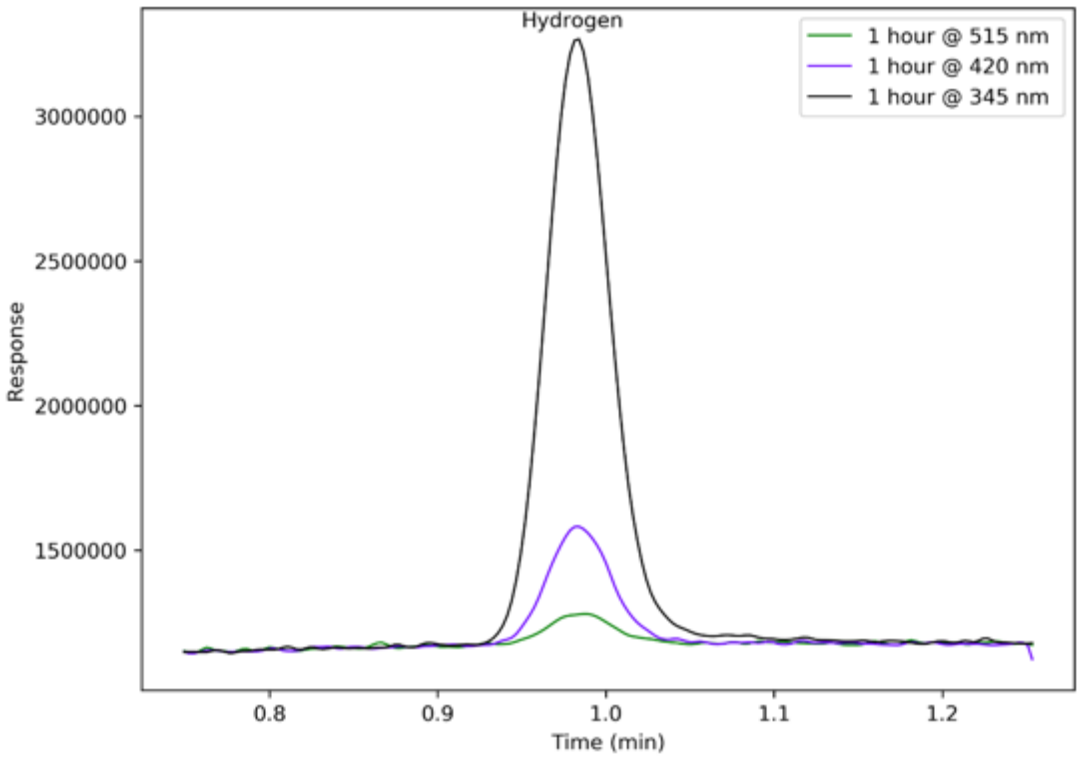

Figure S46. GC trace (zoomed in on the H_2 region) of the headspace samplings of a solution of **3** in 2-propanol after 1 h of irradiation at 23 °C with a 345 nm (black), 420 (blue), or 515 nm (green) cutoff filter.

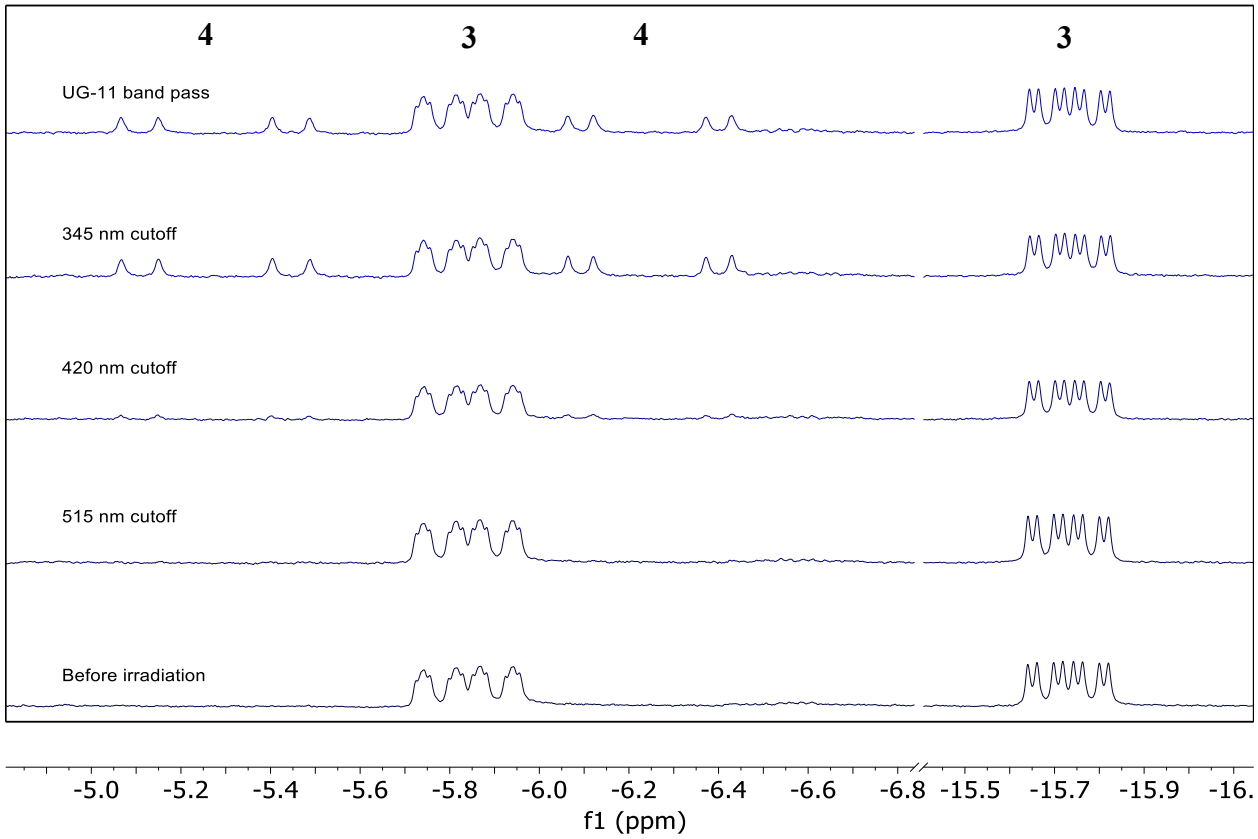

Figure S47. 300 MHz ^{1}H NMR of a solution of **3** in C_6D_6 before irradiation (bottom) and after 1 min of irradiation at 23 °C with a 515 nm cutoff, 420 nm cutoff, 345 nm cutoff, and UV band pass filter.

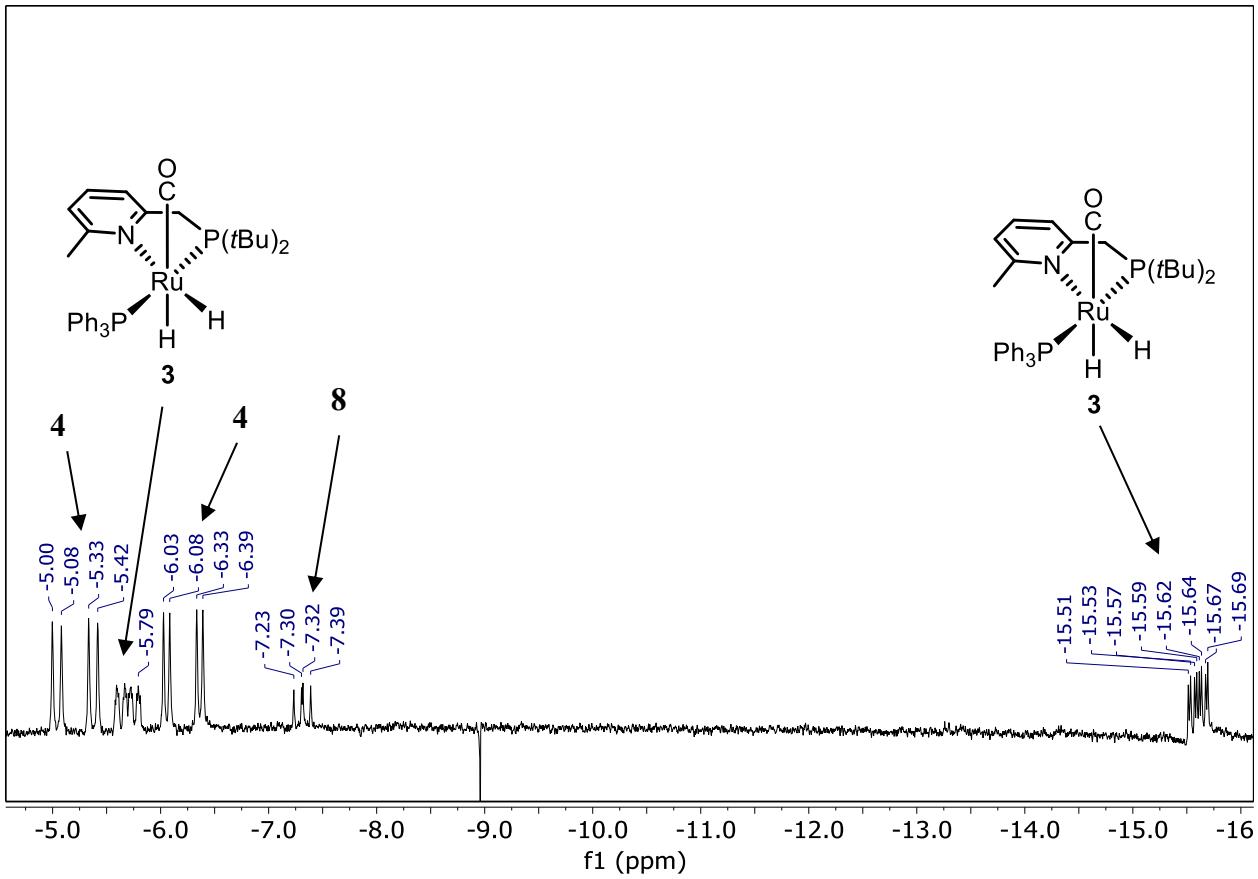

Figure S48. 300 MHz ^{1}H NMR spectrum of a solution of **3** and ethanol in C_6D_6 after 4.5 h of irradiation with a 345 nm cutoff filter zoomed in on the hydride region. The same species were observed for 2-propanol and 1-phenylethanol; note for methanol, these species were not observed and **8** was the major species.

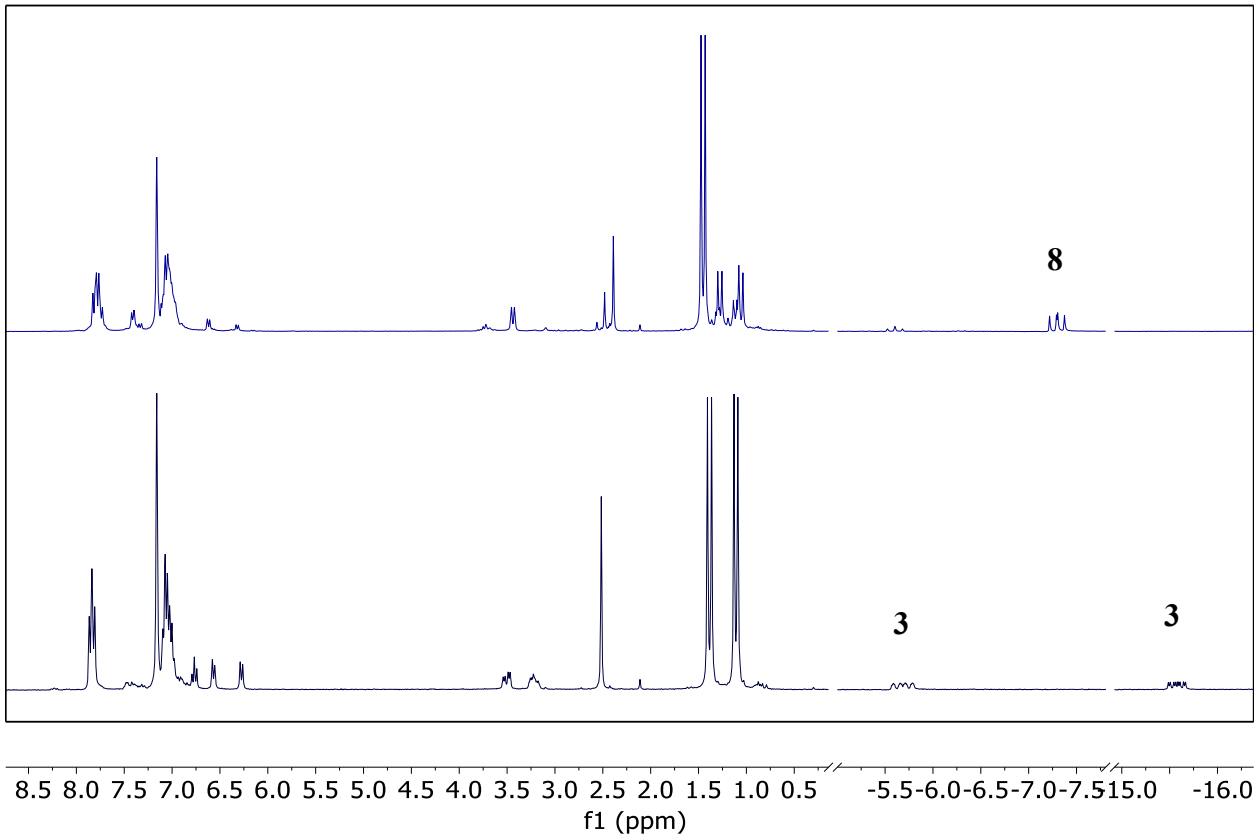

Figure S49. 300 MHz ^{1}H NMR spectrum of a solution of **3** under an atmosphere of $N_{2(g)}$ (bottom), and $CO_{(g)}$ (top) in C_6D_6 after 1 h of broadband irradiation (e.g., solution containing **8**).

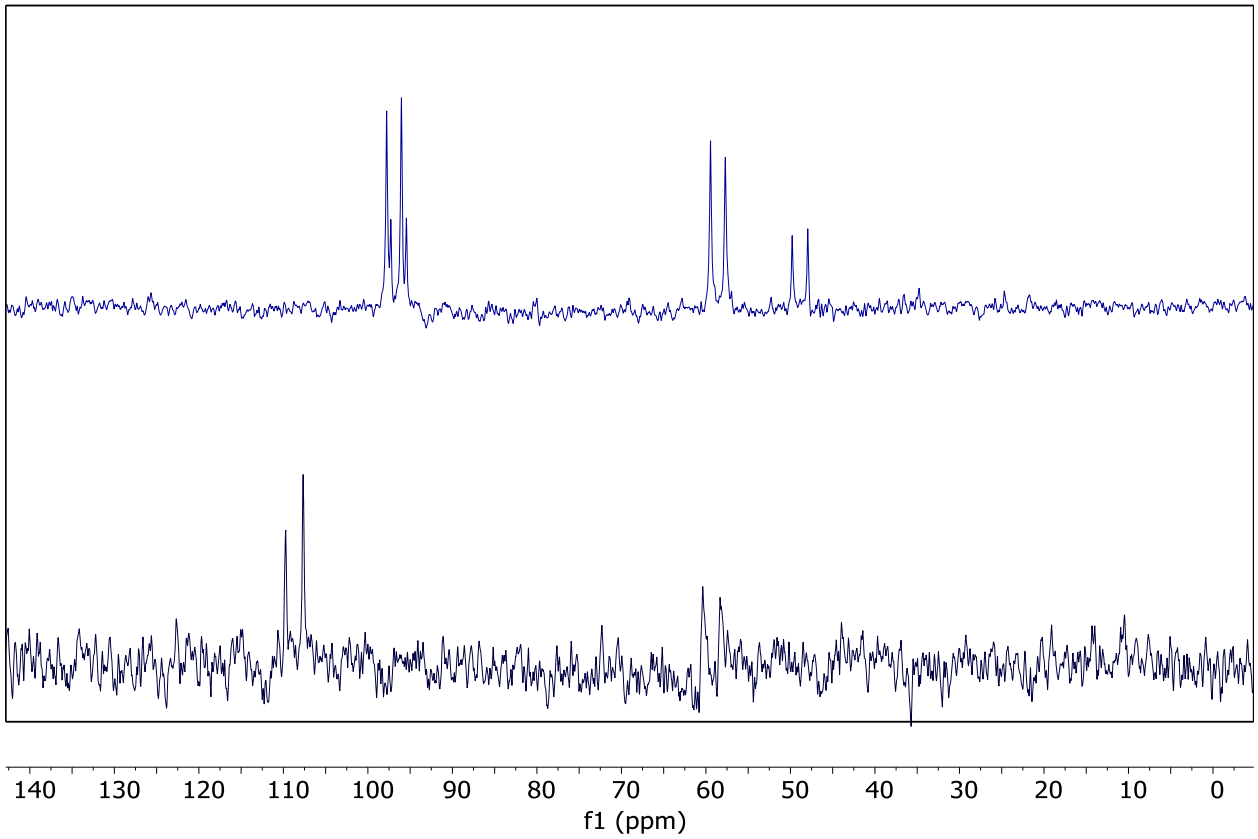

Figure S50. 121 MHz ^{31}P NMR spectrum of a solution of **3** under an atmosphere of N_2 (bottom), and CO (top) in C_6D_6 after 1 h of broadband irradiation (e.g., solution containing **8**).

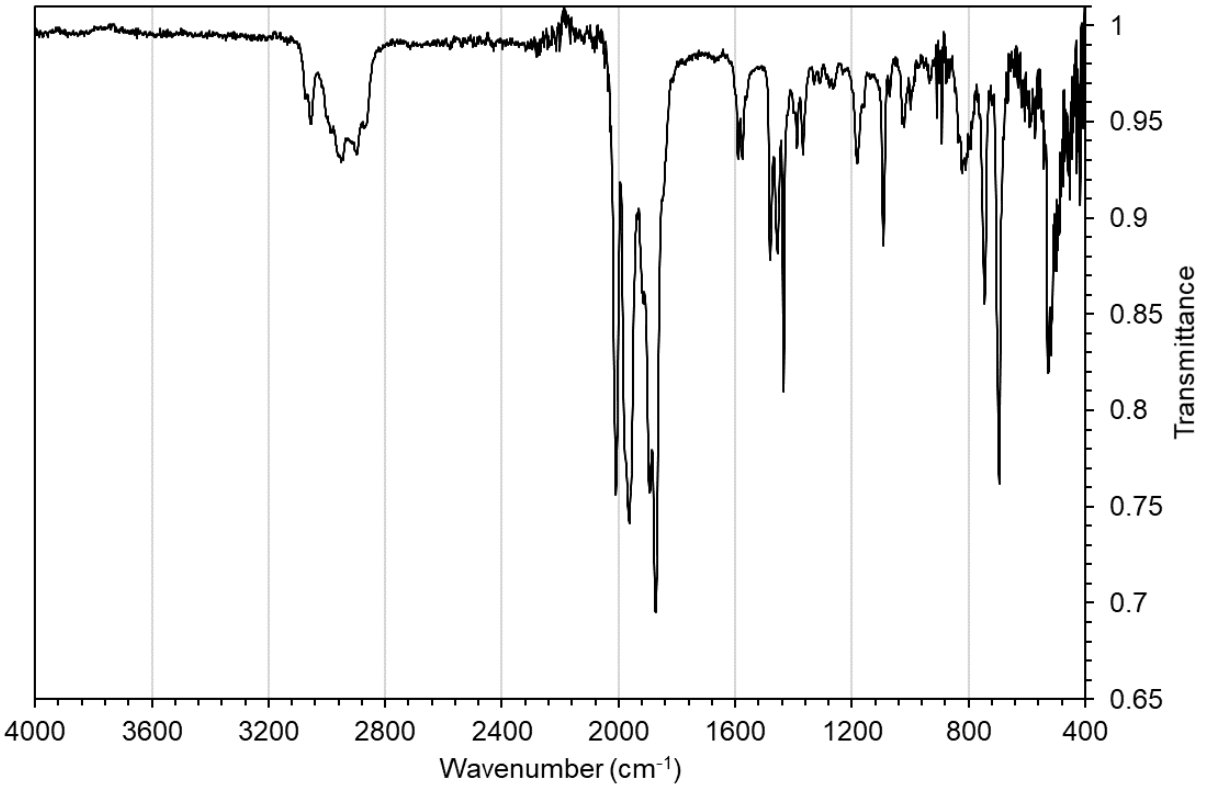

Figure S51. Drop-cast FTIR-ATR spectrum of **3** under $CO_{(g)}$ after 1 h of broadband irradiation (spectrum of solution containing **8**).

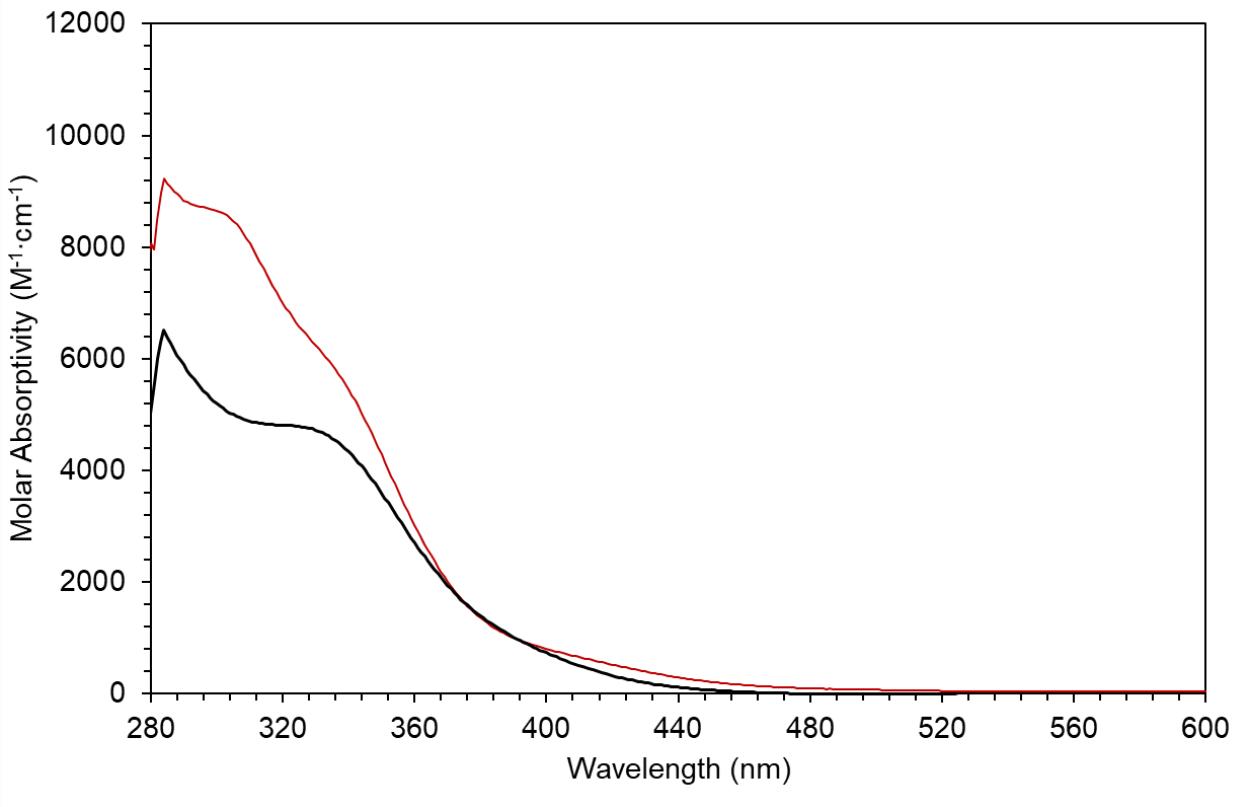

Figure S52. Overlayed UV-*vis* spectra of complex 0.182 mM **2** (red) and 0.25 mM **3** (black). Beer's law plots were obtained for complexes **2** and **3**. Molar absorptivity of **2** at 410 nm is 770 $M^{-1}\cdot cm^{-1}$. Molar absorptivity of **3** at 320 nm is 4,800 $M^{-1}\cdot cm^{-1}$.

Table S1. Crystal data and structure refinements for 2 and 3.

Complex	**2**	**3**
Identification code	rlacy87_abs	rlacy86_abs
Empirical Formula	$C_{34}H_{41}NOP_2Ru$	$C_{40}H_{49}NOP_2Ru$
Formula weight	642.69	722.81
Temperature	104(7) K	100.0(4) K
Wavelength	1.54184 Å	0.71073 Å
Crystal system	Triclinic	Triclinic
Space group	P -1	P -1
Unit cell dimensions	a = 9.2220(2) Å a = 75.095(2) Å	a = 10.67863(16) Å α = 86.746(2) Å
	b = 11.9881(3) Å b = 80.973(2) Å	b = 13.6063(2) Å β = 72.851(2) Å
	c = 15.2279(3) Å c = 74.316(2) Å	c = 14.2941(2) Å γ = 73.019(2) Å
Volume	1559.37(6) $Å^3$	1817.97(5) $Å^3$
Z	2	2
Density (calculated)	1.369 Mg/m^3	1.320 Mg/m^3
Absorption coefficient	5.235 mm^{-1}	0.550 mm^{-1}
F(000)	668	756
Crystal size	0.251 x 0.043 x 0.018 mm^3	0.202 x 0.15 x 0.111 mm^3
Theta range for data collection	3.016 to 77.088°	2.864 to 27.101°
Index ranges	-9<=h<=11, -15<=k<=15, -19<=l<=19	-13<=h<=13, -16<=k<=17, -18<=l<=18
Reflections collected	33481	40381
Independent reflections	6554 [R(int) = 0.0585]	8026 [R(int) = 0.0411]
Completeness to theta	99.9% (theta = 67.684°)	99.9% (theta = 25.242°)
Absorption correction	Gaussian	Gaussian
Max. and min. transmission	1.000 and 0.519	1.000 and 0.485
Refinement method	Full-matrix least-square on F^2	Full-matrix least-square on F^2
Data / restraints / parameters	6554 / 0 / 362	8026 / 0 / 419
GooF on F^2	1.076	1.054
Final R indices [I>2sigma(I)]	R1 = 0.0348, wR2 = 0.0918	R1 = 0.0245, wR2 = 0.0604
R indices (all data)	R1 = 0.0373. wR2 = 0.0935	R1 = 0.0309. wR2 = 0.0630
Extinction coefficient	n/a	n/a
Largest diff. peak and hole	0.891 and -1.347 $e.Å^{-3}$	0.555 and -0.551 $e.Å^{-3}$

References

1. Fanara, P. M.; MacMillan, S. N.; Lacy, D. C. *Organometallics* **2020**, *39*, 3628-3644.
2. Otsuka, T. Ishili, A.; Dub, P. A.; Ikariya, T. *J. Am. Chem. Soc.* **2013**, *135*, 9600-9603.
3. (a) Zhang, J.; Leitus, G.; Ben-David, Y.; Milstein, D. *J. Am. Chem. Soc.* **2005**, *127*, 10840-10841. (b) Gusev, D. Revised mechanisms of the catalytic alcohol dehydrogenation and ester reduction with the Milstein PNN complex of ruthenium. *Organometallics* **2020**, *39*, 258-270.
4. D. G. Hamilton, R. H. Crabtree *J. Am. Chem. Soc.* **1988**, *110*, 4126.
5. *CrysAlisPro*; Rigaku OD, The Woodlands, TX, 2015
6. Sheldrick, *G. M. Acta Cryst.* **2015**, A71, 3-8.
7. Sheldrick, *G.M. Acta Cryst.* **2008**, A64, 112-122.
8. Müller, P. *Crystallography Reviews* **2009**, 15, 57-83.